National Aeronautics and
Space Administration

Document No. TR-833-001
Date March 15, 1996

Test Report

Chemical Characterization and Reactivity Testing of Fuel-Oxidizer Reaction Product

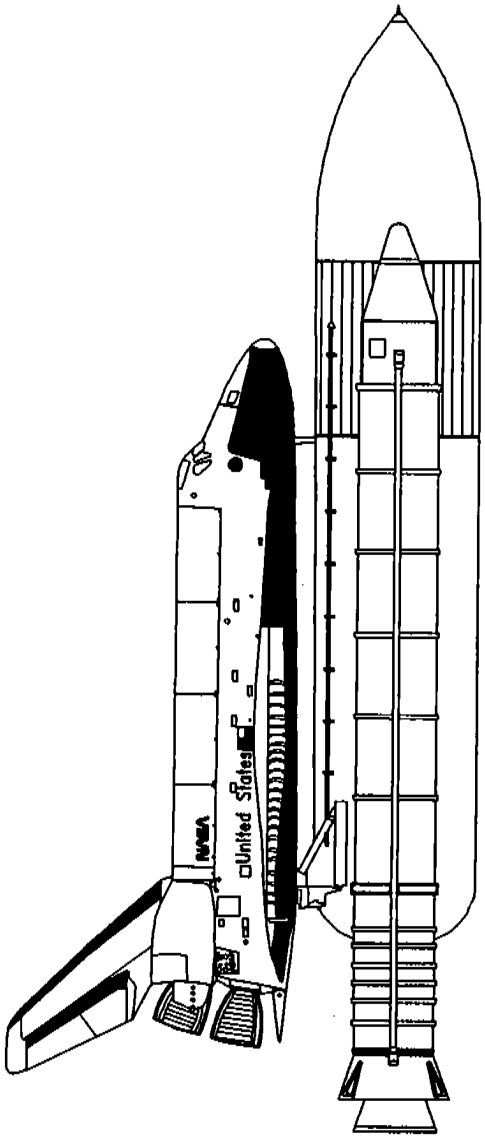

Lyndon B. Johnson Space Center
White Sands Test Facility
P. O. Drawer MM
Las Cruces, NM 88004
(505) 524-5011

Test Report

Chemical Characterization and Reactivity Testing of Fuel-Oxidizer Reaction Product

Issued By
National Aeronautics and Space Administration
Johnson Space Center
White Sands Test Facility
Laboratories Office

Prepared By: _____
Dennis D. Davis
AlliedSignal Technical Services Corp. Team

Prepared By: _____
Louis A. Dee
AlliedSignal Technical Services Corp. Team

Reviewed by: _____
Kristin A. Gillis
AlliedSignal Technical Services Corp. Team

Reviewed By: _____
Harold D. Beeson
NASA Laboratories Office

Approved By: _____
Harry T. Johnson, Chief
NASA Laboratories Office

Abstract

The product of incomplete reaction of monomethylhydrazine (MMH) and nitrogen tetroxide (NTO) propellants, or fuel-oxidizer reaction product (FORP), has been hypothesized as a contributory cause of an anomaly which occurred in the chamber pressure (P_c) transducer tube on the Reaction Control Subsystem (RCS) aft thruster 467 on flight STS-51. A small hole was found in the titanium-alloy P_c tube at the first bend below the pressure transducer. It was surmised that the hole may have been caused by heat and pressure resulting from ignition of FORP. The NASA Johnson Space Center (JSC) White Sands Test Facility (WSTF) was requested to define the chemical characteristics of FORP, characterize its reactivity, and simulate the events in a controlled environment which may have lead to the P_c-tube failure.

Samples of FORP were obtained from the gas-phase reaction of MMH with NTO under laboratory conditions, the pulsed firings of RCS thrusters with modified P_c tubes using varied oxidizer or fuel lead times, and the nominal RCS thruster firings at WSTF and Kaiser-Marquardt.

Fourier transform infrared spectroscopy (FTIR), differential scanning calorimetry (DSC), accelerating rate calorimetry (ARC), ion chromatography (IC), inductively coupled plasma (ICP) spectrometry, thermogravimetric analysis (TGA) coupled to FTIR (TGA/FTIR), and mechanical impact testing were used to qualitatively and quantitatively characterize the chemical, thermal, and ignition properties of FORP. These studies showed that the composition of FORP is variable but falls within a limited range of compositions that depends on the fuel/oxidizer ratio at the time of formation, composition of the post-formation atmosphere (reducing or oxidizing), and reaction or postreaction temperature. A typical composition contains methylhydrazinium nitrate (MMHN), ammonium nitrate (AN), methylammonium nitrate (MAN), and trace amounts of hydrazinium nitrate and 1,1-dimethylhydrazinium nitrate.

The thermal-decomposition reactions of FORP compositions used in this study were unremarkable. Neither the various compositions of FORP, the pure major components of FORP, nor mixtures of FORP with propellant-system corrosion products showed any unusual thermal activity when decomposed under laboratory conditions.

Off-limit thruster operations were simulated by rapid mixing of liquid MMH and liquid NTO in a confined space. The test hardware was constructed with pressure- and temperature-measurement devices to determine if the expected fuel/oxidizer reaction would result in increased energy release when FORP, FORP constituents, or propellant-system corrosion products were present. These tests demonstrated that FORP, MMHN, AN, or Inconel® corrosion products can induce a mixture of MMH and NTO to produce component-damaging energies. The simulation-test program was not extensive enough to provide statistical probabilities for these events but did show that such events can occur. Damaging events required FORP or metal salts to be present at the initial mixing of MMH and NTO.

Based on the results of these studies, it is suggested that removal or mitigation of a buildup of these materials may decrease the incidence of these high-energy, potentially damaging events.

Contents

Tables

Figures

Figures (continued)

Figures (continued)

Figures (continued)

Figures (continued)

1.0 Introduction

NASA Johnson Space Center (JSC) Propulsion and Power Division and the Rockwell Space Systems Division requested the White Sands Test Facility (WSTF) to assist in an investigation of an anomaly that occurred in the chamber pressure (P_c) transducer tube on the Reaction Control Subsystem (RCS) aft thruster S/N 467 on Flight STS-51.

A small hole was found in the titanium-alloy P_c tube at the first bend below the pressure transducer. Figure 1 shows the assembly and location of the hole. It was surmised that the hole may have been caused by heat and pressure resulting from ignition of Fuel-Oxidizer Reaction Product (FORP).

2.0 Objective

The purpose of this study was to define the chemical characteristics of FORP, characterize its reactivity, and simulate the events in a controlled environment which may have lead to the P_c-tube failure.

3.0 Background

It has been recognized since the early 1960's that some hypergolic propellant engines exhibited unique combustion phenomena such as hard start, pressure spiking, plume contamination, or partially oxidized residue accumulation. These phenomena became significant when hypergolic propellants were used in small engines operated in pulsed mode at subambient pressures (Takimoto and Denault 1969).

Hard starts were observed during simulated high-altitude testing of Apollo RCS engines, and as a result, the Manned Spacecraft Center requested the Bureau of Mines to investigate this problem (Purlee et al. 1967). 1,1-Dimethylhydrazine (UDMH), monomethylhydrazine (MMH), hydrazine, Aerozine-50 (50 percent by weight each UDMH and hydrazine), and nitrogen tetroxide (NTO) were the propellants used in these studies. Experimental efforts were primarily directed toward combustion characteristics of the propellants, identification of preignition reaction products, and definition of the physical and combustion properties of these products with respect to their presence in RCS engines. Nitrate salts of hydrazine and methylhydrazines were identified as constituents of the residues that remained in the RCS engines after each pulse. Tests with these materials showed that films as thin as 0.025 cm that contain hydrazinium nitrate would support a stable detonation. Engine damage potential was related not only to the quantity of residue present in the engine but also to its location (Purlee et al. 1967).

Steady-state firings of small (22 lb and 1 lb) MMH/NTO engines under vacuum resulted in the formation of ammonium nitrate (AN) engine residues; however, the possibility of methylhydrazinium nitrate (MMHN) formation was not excluded. The residues collected from pulsed firings were identified as primarily MMHN with some methylammonium nitrate (MAN). In spite of qualitative analysis correlations with synthesized standards, differential thermal analysis (DTA) data of the pulsed engines residues did not agree with that of pure standards. The pulsed engine residue had a DTA exotherm at ~160 °C that was not present

in laboratory-synthesized MMHN. Although not verified, it was suggested that a small amount of more unstable material such as methylhydrazinium dinitrate (MMHDN) might have been present in the engine residue. It was also theorized that, because higher chamber temperatures are achieved with steady-state firings, only the more thermally stable AN survived for collection (Takimoto and Denault 1969).

Low-pressure, gas-, and liquid-phase reactions in hypergolic bipropellant thrusters were studied with various propellant combinations using a gas-flow reactor and a simulated 2-D engine (Miron and Perlee 1974a,b). The condensed phase energetic products were nitrate salts whose composition depended on the fuel and the fuel/oxidizer ratio. Tests involving mixtures of hydrazines and NTO at subambient temperatures consistently resulted in violent explosions when the temperature of the mixtures was raised to -55 °C. Hydrazinium nitrate was often recovered from these experiments but was not considered the species responsible for the reaction. Miron and Perlee did conclude from these low-temperature tests that accumulation of condensed or frozen propellants in the engine should always be avoided (1974a,b).

4.0 Approach

Only a small quantity of FORP generated during RCS thruster firings was available for this study. Therefore, an approach was developed that involved the laboratory synthesis of FORP and its components to provide sufficient material for comparison to engine residues and to allow the determination of the chemical and physical characteristics of FORP.

The detailed approach was to:

- Develop a procedure to synthesize FORP by the gas-phase reaction of MMH with NTO to provide a supply of FORP for comparison and characterization studies
- Obtain the pure components of FORP such as the nitrate salts of ammonia, methyl amine, methylhydrazine, and 1,1-dimethylhydrazine
- Produce FORP from pulsed firings of RCS thrusters with modified P_c tubes using various oxidizer or fuel lead times for comparison to laboratory-synthesized FORP
- Obtain FORP samples from other RCS thruster firings at WSTF and Kaiser-Marquardt
- Use state-of-the-art chemical techniques to qualitatively and quantitatively characterize the composition, thermal, and ignition properties of FORP and its components; Fourier transform infrared spectroscopy (FTIR), differential scanning calorimetry (DSC), accelerating rate calorimetry (ARC), ion chromatography (IC), inductively coupled plasma (ICP) spectrometry, and thermogravimetric analysis (TGA) coupled to FTIR (TGA/FTIR) were selected as primary laboratory characterization tools
- Analyze water flush samples from P_c tubes of RCS thrusters located at Kennedy Space Center (KSC), WSTF, and Kaiser-Marquardt for FORP components and metal corrosion products to develop a database for contamination buildup and to aid in the determination of possible long-term P_c tube flush requirements

- Simulate off-limit thruster operation by rapid mixing of liquid MMH and liquid NTO to determine if the fuel/oxidizer reaction would result in an increased energy release when FORP was present

- Characterize the reactions of laboratory FORP, FORP components, and mixtures of FORP containing metal corrosion products (from Inconel® 718 and titanium) under conditions involving rapid mixing of MMH and NTO

5.0 Experimental

5.1 Procedures

The following paragraphs describe the procedures, conditions, and instrumentation used for the analysis and characterization of FORP and FORP components.

5.1.1 Fourier Transform Infrared Spectroscopy

A Nicolet FTIR Model 5SXC equipped with a mercury/cadmium telluride detector was used to gather FTIR spectral data. Spectra were obtained in the transmission mode from solvent-evaporated films deposited on 13-mm-dia. Irtran 2 (ZnS) discs. Irtran 2 was selected for its compatibility with hydrazines, amines, and nitric acid (HNO_3).

5.1.2 Differential Scanning Calorimetry

The calorimeter was an Omnitherm® Model 700 equipped with Omnitherm® thermal analysis software. Uncovered aluminum pans were referenced to an empty pan. Normal sample sizes ranged from 1 to 10 mg. Two temperature programs were used for acquisition of DSC data:

Program I 25 to 300 °C @ 5 °C/min/N_2 or air (25 mL/min)

Program II 25 to 500 °C @ 50 °C/min/air (25 mL/min)

Program I was used primarily for characterization of the laboratory-synthesized FORP ingredients where reliable thermochemical data were required. Program II was used to simulate the rapid temperature rises expected on RCS start-up. The DSC instrument was calibrated for temperature and heat flow using indium and tin standards provided by the manufacturer.

5.1.3 Ion Chromatography

A Dionex Model 4000i ion chromatograph equipped with pulsed amperometric (PA) and conductometric detectors was used for determination of aqueous ionic species. The detector output signals were digitized and processed using commercially available Turbochrom® software.

Analysis of the hydrazine fuels was accomplished using a Dionex HPIC-CS3A column connected to the PA detector. The eluent was 0.05 M HCl. The cations Li^+, Na^+, K^+, and NH_4^+ were analyzed using an Ionpak® CS14 column and the conductometric detector. The eluent was 10 mM methanesulfonic acid. The anions HCO_3^{1-}, PO_4^{3-}, Br^-, SO_4^{2-}, CO_3^{2-}, NO_2^-,

NO_3^-, Cl^-, and F^- were separated using a Dionex HPIC-AS4A column and were detected conductometrically. The eluent was a 1.7-mM carbonate/bicarbonate buffer at pH 10.0.

Blanks and standard solutions were used to construct calibration curves daily. Samples were determined in duplicate, and the results were averaged. Every eleventh sample was a check standard.

5.1.4 Inductively Coupled Plasma Spectrometry

Aqueous samples were prepared for metals determination by acidifying with HNO_3 and the appropriate dilution in distilled water. The ICP analyses were conducted using a Jobin Yvon Model 38 Plus ICP spectrometer in optical emission mode with an argon plasma. The metals determined were Ni, Fe, Ti, Cr, Al, V, Mo, Nb, and Ta. Blanks and standard solutions were used to construct calibration curves daily. Samples were determined in triplicate, and the results were averaged. Every eleventh sample was a check standard.

5.1.5 Thermogravimetric Analysis/Fourier Transform Infrared Spectroscopy

The TGA/FTIR analyses were conducted using an Omnitherm® Model 1500 thermogravimetric analyzer connected to a Nicolet Model 5SXC FTIR spectrometer. A heated 10-cm pathlength gas cell was used. Both Nicolet FTIR and Omnitherm® software packages were used for processing data. A typical test protocol involved heating a 3- to 10-mg sample from ambient to 500 °C at 10 °C/min in air free from carbon dioxide and moisture. FTIR spectra of the effluent gases were collected at approximately one second intervals.

5.1.6 Accelerating Rate Calorimetry

ARC tests on MMHN were performed in both isothermal and adiabatic modes using a calorimeter manufactured by Columbia Scientific Instruments, Austin, TX. The reaction vessels were 2.54-cm-dia. spheres fabricated from commercially pure titanium. Samples of MMHN weighing approximately 0.25 g under one atmosphere of NTO were monitored for exothermic events from 80 to 300 °C. Isothermal ARC tests were performed at 230 and 300 °C. The isothermal test at 300 °C was conducted with a small strip of polished Ti-6Al-4V alloy placed in the vessel before addition of the MMHN and NTO. Posttest analysis included sectioning and examining the vessel and contents.

5.1.7 Mechanical Impact Tests

Tests were conducted on FORP, MMHN, and FORP spiked with excess HNO_3 using an Army Ballistic Missile Agency (ABMA) tester (ASTM D2512-82, 1991). The tester uses a 20-lb weight which free-falls inside guide rails from preset heights onto a steel striker pin resting on the sample contained in an aluminum cup. The tester used in these studies was set at 81.3 ft-lb.

5.1.8 Fuel-Oxidizer Rapid Mixing Tests

Test hardware, designed and constructed at WSTF, was used to study the energy release and pressures generated during the rapid mixing of MMH and NTO in the presence of FORP. The FORP Reaction Test system consisted of a GN_2 pressurization subsystem, accumulator, gas heater, fast-opening valve, vacuum subsystem, and instrumentation to measure temperature and pressure (Figure 2). The piezoelectric pressure transducer had a 1-μsec rise time with a 20-μsec sampling rate. The thermocouple was a Type S with a 0.05-sec response time. A photograph of the fuel/oxidizer injector apparatus and test assembly is shown in Figure 3. The general test procedure was to load the liquid fuel, oxidizer, and FORP or other reactant into the injector apparatus and then connect the injector apparatus and test article to the Reaction Test System. The accumulator was then pressurized with GN_2, and the test assembly was evacuated to a pressure of less than 5 torr. After isolating the test assembly from the vacuum system, the fast-opening valve was actuated, driving the MMH and NTO liquid columns through the Teflon® diaphragms into the test assembly. Pressure and temperature data were recorded, the system was vented, and the test assembly was removed. Posttest analyses of the contents of the test assembly included IC analyses for nonmetallic ions and ICP analyses for metallic constituents.

5.2 Materials

Fluids used in the laboratory and propulsion procedures described conformed to current MIL or NASA specifications. All other reagents and solvents were reagent grade and used as supplied.

5.2.1 Ammonium Nitrate

AN was J. T. Baker ACS Reagent material used as supplied. The FTIR spectrum of AN is relatively simple with primary absorption bands at 3200 cm^{-1} and at 1380 cm^{-1} representing N-H and nitrate vibrations (Figure 4). DSC results (Figure 5) depict phase changes at 51, 124, and 170 °C, and a decomposition endotherm at 260 °C.

5.2.2 Methylammonium Nitrate

The synthesis of MAN was accomplished by slowly adding HNO_3 (0.03 mole, J. T. Baker) to a slight excess (0.0323 mole) of 40 percent aqueous methyl amine (Eastman). White crystals formed when the solution was evaporated on a hotplate at less than 60 °C under a stream of dry nitrogen. The melting range of the product was 101 to 103 °C. The literature value is reported to be 99 to 100 °C (Harris 1965). Using DSC Program I, two sharp endotherms at 79 and 108 °C followed by large merged endotherms at 245 and 269 °C were detected (Figure 6). The discrepancy between the melting point observation and the DSC endotherms may be caused by heat transfer rate differences between the two techniques. The first endotherm observed in the DSC may be a phase change that was not visually detectable when the crystals were observed in a Fisher-Johns melting point apparatus. The onset of the second DSC endotherm at 105 °C is quite close to the visual melting point. The FTIR spectrum of MAN (Figure 7) shows major absorptions at 3200 cm^{-1} and 1380 cm^{-1} with additional strong bands at 2900 cm^{-1} and 930 cm^{-1}.

5.2.3 Methylhydrazinium Nitrate

MMHN was prepared by a displacement reaction of MMH and AN. A 5-percent excess of MMH (Mil-P-27404B) was added rapidly to 0.0125 mole of powdered AN with stirring. Ammonia gas was evolved. The resulting wet crystals were dried at ambient temperature under a stream of dry nitrogen, heated to melting at approximately 50 °C under nitrogen, flushed with nitrogen for two hours, then allowed to cool to room temperature. White, needle-like crystals formed with a melting range of 39 to 41 °C. A DSC of the crystals using Program I (Figure 8) shows an endotherm at 40 °C and a sharp exotherm at 206 °C on the shoulder of a broad endotherm at about 150 to 240 °C. Lawton and Moran (1984) prepared MMHN by neutralization of MMH with HNO_3 and report a melting range of 37.5 to 40.5 °C, a DSC endotherm at 34 to 41 °C, and an exotherm at 208 °C on the shoulder of a broad endotherm starting at 140 °C.

The FTIR spectrum of MMHN (Figure 9) displays overlapping bands at 1330 cm^{-1} and 1379 cm^{-1} (nitrate), two broad, weak bands at 3324 cm^{-1} and 3080 cm^{-1} (N-H), and a weak band near 1600 cm^{-1} also indicative of the N-H moiety.

IC analysis showed a 1:1 mole ratio of methylhydrazinium to nitrate ions. Assuming a molecular formula of $MMH \cdot HNO_3$, the IC results showed a recovery of 99 percent. TGA results illustrated in Figure 10 show a single mass-loss transition centered at 238 °C. FTIR analysis of the effluent gases (Figure 11) indicates the presence of N_2O, a nitrate ester, possibly some HNO_3, and traces of H_2O, NH_3, and CO_2.

5.2.4 Methylhydrazinium Dinitrate

MMHN, prepared as above (0.1 g), was added to a slight excess of 7 M nitric acid. White crystals were formed on evaporation. Using DSC Program II (Figure 12), an endotherm at 91 °C, a small broad exotherm at 159 °C, and a sharp exotherm at 266 °C were detected. IC analysis of this product, assuming the molecular formula for $MMH \cdot 2HNO_3$, resulted in a 93 percent recovery.

The FTIR (Figure 13) displays a strong broad band at 3111 cm^{-1} and a strong overlapped bands at 1380 cm^{-1} and 1327 cm^{-1}. Minor spectral bands did not match those of MMHN. Others have reported the infrared spectrum of MMHDN appeared to be the same as that of MMHN (Takimoto and Denault 1969).

The TGA data (Figure 14) shows two weight-loss regions centered at 94 °C and 218 °C. The FTIR spectrum of the gases evolved at the start of the weight loss (Figure 15) corresponds to a mixture of HNO_3, NO_2, and trace CO_2. As the weight loss progressed, N_2O, water, and a hydrocarbon (possibly ethane) were evolved (Figure 16). The second weight-loss region in the TGA shows continued weight loss caused by the evolution of N_2O, H_2O, traces of CO_2, NH_3, and a nitrate ester (Figure 17). This second weight-loss region produced effluent gases that were the same as those from the decomposition of MMHN.

5.2.5 1,1-Dimethylhydrazinium Nitrate

A slight excess of 1,1-dimethylhydrazine (Mil-P-25604D) was rapidly added to 0.0125 mole of solid ammonium nitrate, and the solution was evaporated (< 60 °C, nitrogen). Yellow crystals with a melting range of 148 to 152 °C resulted. The DSC thermogram of these

crystals (Figure 18) displays weak endotherms at 50, 125, and 162 °C, and a broad endotherm at 235 °C. The onset of the endotherm centered at 162 °C occurs at 150 °C and likely corresponds to the melting point.

The FTIR spectrum (Figure 19) shows a pattern of overlapped bands at 3192, 3081, 2934, and 2855 cm^{-1}. Strong bands are also present at 1477, 1385, and 1330 cm^{-1}, which are typical of nitrate salts. Other minor bands did not match those shown by MMHN or MMHDN.

5.2.6 Formaldehyde Methylhydrazone

MMH (0.001 mole) was added to a stoichiometric amount of 37 percent aqueous formaldehyde (Aldrich). The mixture was evaporated (< 60 °C, nitrogen) to form what was expected to be formaldehyde methylhydrazone. The product sublimed at 97 °C with no exothermic DSC features.

5.2.7 Inconel® Nitrate

The simulated corrosion product of Inconel® 718 (60Ni/20Fe/20Cr) was prepared by dissolving a mixture of 3.0 g of nickel(II) nitrate hexahydrate, 0.95 g of iron(III) nitrate nonahydrate, and 1.05 g of chromium(III) nitrate nonahydrate in a minimum of water and heating to 110 °C until the brown-colored solid appeared to be dry.

5.2.8 Laboratory-Synthesized FORP

Laboratory-synthesized FORP was prepared using a procedure and apparatus developed at WSTF. The apparatus is shown in Figure 20. The essential components are an MMH vapor generator, an NTO vapor generator, and a reaction flask cooled to 0 °C. The entire apparatus was evacuated to less than 0.7 Pa, and the three chambers were isolated from each other. A syringe was used to introduce 0.1 to 0.4 mL of liquid MMH into the MMH vapor generator. The NTO vapor generator was filled to ambient pressure by adding a small amount of liquid NTO to the chamber and venting the excess vapor. MMH vapor was transferred to the mixing chamber by opening the connecting stopcock for five to 10 seconds. NTO vapor was then introduced into the reaction flask in the same manner. When the brown NTO vapor disappeared, more was introduced. A negative pressure, relative to the vapor generator flasks, was maintained in the reaction flask. When the MMH in the reaction flask was consumed as indicated by the persistence of the NTO vapor, the reaction flask was evacuated and the MMH/NTO addition sequence was repeated. The reaction flask gradually became coated with yellow-orange droplets. The addition sequences were repeated for 7 hr. At the end of the procedure, the reaction flask was evacuated overnight at ambient temperature followed by rinsing with 5 mL of methanol (MeOH). The nonvolatile residue from the MeOH rinses was isolated by evaporation (< 60 °C, nitrogen). A typical yield was 100 to 150 mg of a yellow-orange oil that occasionally contained needle-like crystals. This preparative procedure was repeated 19 times, and only one unusual occurrence, a small flash of light during the mixing sequence, was observed.

The FTIR spectra of different batches of FORP were similar, showing strong bands above 3000 cm^{-1} caused by N-H bonds and absorptions near 1380 cm^{-1} caused by the NO_3^- ion. DSC results varied depending on whether the oily or the crystalline portion was sampled. Variations were minimized by evaporating combined MeOH rinses.

5.2.9 WSTF RCS Engine FORP's

Residues were obtained from two series of RCS engine firings in which the engine had modified P_c-tube assemblies. RCS engine (S/N 208) with various diameter holes drilled in the P_c tube was fired. Samples of residue were obtained after each test firing. Residues were recovered from the P_c-transducer assembly by physical removal or rinsing with a minimum amount of isopropyl alcohol (IPA). The residues were analyzed by FTIR and IC. The quantity of residue produced by these firings was insufficient for DSC analysis.

RCS thruster S/N 467 was modified by replacing the P_c tube with a detachable assembly consisting of two tubes, one attached to the chamber (T_c) and one attached to the transducer (T_t), connected together through a 0.040-in.-dia. orifice. A series of multipulse firings was conducted in which either the fuel or oxidizer lead times were varied. The assembly was removed from the thruster after the firing series, and the residue was recovered by MeOH rinses. The weight of recovered FORP, FTIR spectra, and in some cases DSC data, was then acquired.

5.2.10 Kaiser-Marquardt FORP

Engine residue samples were also provided by Kaiser-Marquardt. The history of these samples is not known, but they were apparently obtained in a manner similar to those used at WSTF. The engine is not believed to have been an RCS thruster.

5.2.11 Water Flush Samples

Water flush samples from the RCS thrusters on OV-102 following STS-58 and OV-105 were analyzed for anions, cations, and selected metals identified as potential engine corrosion products. Separate data reports, WSTF Nos. 94-28652, 94-28653, and 94-28654, are available. A summary of major findings is presented in Section 6.1.5.

6.0 Results and Discussion

6.1 Characterization of FORP's From Different Sources

6.1.1 Laboratory-Synthesized FORP

IC analyses shown in Table 1 indicate that WSTF laboratory-synthesized FORP consisted of varying mixtures of ammonium, methylated ammonium, hydrazinium, and methylated hydrazinium cations with nitrate as the counter anion. A trace of nitrite ion was detected only once.

The DSC behavior of the FORP batches appeared to fall into two families. The first displayed a single sharp exotherm above 230 °C (Figures 21 and 22). The corresponding FTIR spectra are shown in Figures 23 and 24. The second family exhibits two DSC exotherms at ~200 and ~230 °C (Figures 25 through 27). Corresponding FTIR spectra for these FORP's are shown in Figures 28 through 30.

A synthetic mixture of pure ingredients, based on typical IC results for laboratory-synthesized FORP, was prepared (10 percent AN, 40 percent MMHN, and 50 percent MAN). The

Table 1
Ion Chromatographic Analysis of Laboratory FORP and FORP Components

Analyte	(wt. %)							
	MMHN	MMHDN	FORP 9[a]	FORP 14	FORP 15	FORP 16	FORP 17/18	FORP 19
MMH_2^+	44	27	20	6.6	ND	8.7	3.1	7.6
$N_2H_5^+$	ND	0.7	0.3	ND	ND	0.5	0.03	1.0
$UDMH_2^+$	ND	ND	0.7	1.3	ND	1.2	0.5	ND
NH_4^+	0.3	0.4	2.0	3.3	7.4	2.2	3.3	1.3
$CH_3NH_3^+$	ND	1.8	22	26	33	27	33	37
$(CH_3)_2NH_2^+$	ND	ND	2.6	ND	ND	2.5	2.5	1.8
NO_3^-	55	71	53	62	59	58	58	51
NO_2^-	ND	ND	ND	ND	ND	ND	ND	0.06
F^-	ND	ND	ND	ND	ND	ND	ND	ND
Cl^-	0.9	ND	ND	ND	ND	0.5	0.5	0.5

[a] Numbers in this row indicate a batch identifier.
Note: ND = Not detected

infrared spectrum (Figure 31) of this mixture is similar to many of the laboratory-synthesized FORP batches.

A TGA/FTIR scan of FORP 13 (Figure 32) showed traces of water and N_2O early in the heating scan followed by increased amounts of N_2O and a nitrate ester. At approximately 225 °C, CO_2 and water were the most prominent effluent gases. These products persisted for the remainder of the weight loss, (Figures 33 through 35). The TGA/FTIR analysis was repeated with FORP 19 with somewhat different results. The TGA plot for FORP 19 is shown in Figure 36. It shows an onset of 215 °C which is slightly lower than FORP 13. The sequential FTIR spectra of the evolved gases are shown in Figures 37 through 43. Early in the run, the gases were primarily water and N_2O followed by evolution of a nitrate ester, possibly ethyl nitrate. As the decomposition proceeded, CO_2 and water became the major evolved gases. Unlike FORP 13 no ammonia was formed, and oxidation processes seemed to predominate in the decomposition of FORP 19.

6.1.2 Kaiser-Marquardt Engine FORP

Figures 44 and 45 show the FTIR spectra of two Kaiser-Marquardt FORP samples, KM44 and KM45. KM44 contained a substantial amount of nitrite ion as indicated by the strong absorption at ~1250 cm^{-1} (Figure 44). The nitrite-containing FORP appears to be similar to that recovered from RCS S/N 467 which was pulsed with a 10-msec fuel lead (Figure 46). The FTIR spectrum of a third sample, KM47, is shown in Figure 47. DSC scans of KM44 and KM47 are depicted in Figures 48 and 49. Unlike the laboratory-synthesized FORP which had one or two large exotherms above 220 °C, there was only a series of small exotherms between 50 and 300 °C in the KM samples. The only cation detected by IC analysis of KM47 was ammonium, suggesting that the engine which provided the samples was fired in a

continuous mode.

6.1.3 RCS Thruster FORP

RCS thruster firings were conducted at WSTF to assess the performance impact of different size holes in the P_c-transducer tube of thruster S/N 208. Either neat- or solvent-rinse samples were taken from external surfaces or inside the transducer components and the P_c tube. Samples were also obtained from thrusters S/N 332, S/N 413, S/N 224, and S/N 327, all of which had intact P_c tubes. Analysis of most of the rinses involved only nitrate ion determinations which showed nitrate invariably was present. Some IC analyses for both cations and anions were performed, and the results are shown in Table 2. The compositions of these thruster samples are very similar to those gathered by water flushing of orbiter P_c tubes (Sec. 6.1.5).

Figure 50 is the FTIR spectrum of the nonvolatile residue from a MeOH rinse of the inside of the S/N 208 P_c tube. Figure 51 is an FTIR spectrum of a sample taken from thruster S/N 413. The strong bands near 1380 cm^{-1} and 1600 cm^{-1} are ascribed to nitrate ion and aliphatic amines, hydrazines, or their salts, respectively. The similarity in band locations and variation in band intensities indicates that similar materials are present in the samples in varying amounts. FTIR and IC analysis results of samples from thruster S/N 208 and other thrusters showed large quantities of nitrate ion, and FTIR spectra indicated the presence of MAN, some AN, and possibly MMHN. The presence of ammonium, methylammonium, nitrate, and the general absence of detectable nitrite ion was confirmed by IC analyses (Table 2).

Samples taken from the transducer side of the P_c tubes and several from the external surface of the S/N 208 P_c tube showed the presence of an additional compound with an FTIR absorption at 2000 cm^{-1}. Figure 52 is the FTIR spectrum of FORP removed from the outside surface of the P_c tube near the hole of RCS thruster S/N 208. Note the prominent band near 2000 cm^{-1}. Absorptions between 2250 cm^{-1} and 2000 cm^{-1} usually are ascribed to moieties with multiple nitrogen-nitrogen or carbon-nitrogen bonds (i.e., -C≡N, -N=N-, >C=N-, -N-

Table 2
Ion Chromatographic Analyses of FORP From WSTF RCS Engine Firings

Analyte	(wt. %)		
	S/N 332[a]	S/N 208	KM47
MMH_2^+	ND	ND	ND
$N_2H_5^+$	ND	ND	ND
$UDMH_2^+$	ND	ND	ND
NH_4^+	11	4	18
$CH_3NH_3^+$	19	8	ND
NO_3^-	70	88	82
NO_2^-	ND	ND	ND

[a] S/N refers to a batch identifier.
Note: ND = Not detected

N=N) or amine salts (RNH_3^+, $R_2NH_2^+$). These types of bonds might be possible from structural rearrangements of MMH and/or its thermal decomposition and reaction products. Based on the ratios of the 1600 cm^{-1} and 1300 cm^{-1} bands, the FORP taken from the outside of the P_c tubes has less fuel (R_nN-H) than that taken from the inside. This result is not surprising because hydrazines are less stable in air.

6.1.4 WSTF RCS Thruster FORP: Fuel and Oxidizer Lead Studies

Thruster S/N 467 with a modified P_c tube was pulse fired using either an oxidizer lead, no lead, or a fuel lead. Samples of FORP were quantitatively removed from the P_c tube collection assembly with MeOH, and the amount recovered was determined. Table 3 shows the quantities of FORP recovered for each test sequence. FTIR spectra for a 10-ms NTO lead, a 5-ms NTO lead, a 5-ms MMH lead, and a 10-ms MMH lead are represented by Figures 53, 54, and 55. Note the growth in the band at ~2000 cm^{-1} and the changes in the relative ratio of the ~1380 cm^{-1} and 1600 cm^{-1} bands with respect to the propellant and the lead time (Table 4). The 1380 cm^{-1} bands are indicative of the presence of NO_3^- whereas the 1600 cm^{-1} bands indicate a fuel-rich product. From the FTIR spectra it appears that the quantity of nitrate ion formed is directly proportional to the oxidizer lead time. The DSC scan (Figure 56), which represents FORP accumulated from pulsed firings using a 10-msec fuel lead, shows no exotherms. The absence of exotherms also indicates that no oxidizing moieties (i.e., NO_3^-) were present. It is also interesting to note that the total quantity of FORP collected approached a minimum as oxidizer lead time decreased. Takimoto and Denault also observed that oxidizer leads increased residue formation (1969).

DSC scans and FTIR spectra were gathered from FORP samples isolated from thruster S/N 467 which was operated with a 10-ms MMH lead. Two of these FORP samples were exposed to either vapor or liquid NTO in the laboratory before removal from the P_c tube. Figure 57 is the FTIR spectrum of FORP after exposure to NTO vapor. Note the growth in the ~1380 cm^{-1} band, the decrease in the ~1640 cm^{-1} band, and the appearance of a band in the 2000 cm^{-1} region. The DSC data (Figure 58) shows two exotherms at 117 and 220 °C.

Table 3
FORP Recoveries From RCS S/N 467

Lead Propellant	Lead Time (msec)	T_c (mg)	T_t (mg)	Total (mg)
NTO	10	14.4	17.5	31.9
NTO	5	33.6	18.3	51.9
NTO	5	8.0	5.5	13.5
NTO	0	2.2	1.6	3.7
MMH	5	7.2	0	7.2
MMH	10	8.4	1.8	10.2
MMH	10	1.4	1.4	2.8
MMH	10	1.6	1.8	3.4
MMH	10	1.0	5.7	6.7

Data from the FORP sample exposed to liquid NTO (Figures 59 and 60) show only minor differences from the vapor-exposed material. The liquid oxidizer-exposed FORP only produced a single exotherm at 213 °C. Table 4 is a summary of the FTIR and DSC data.

The ratio of the band intensities for NO_3^- ($\sim$1380 cm^{-1}) and N-H ($\sim$1640 cm^{-1}) are largest for oxidizer-lead FORP and oxidized fuel-lead FORP, both of which are similar to the synthetic mixture of pure ingredients (10 percent AN, 40 percent MMHN, 50 percent MAN) described previously. FTIR spectra of actual P_c tube residues from RCS engines previously shown indicate nitrate/N-H band intensity ratios from 1.2 to 0.8, the lower values representing samples taken from inside the tube.

6.1.5 Water Flush Samples

Analysis of 37 samples taken from the thrusters on OV-102 after the STS 58 flight showed no methylhydrazinium or hydrazinium ions. Chloride was detected in all samples, and probably was an adventitious contaminant. The major nonmetallic cations were methylammonium and ammonium in the approximate weight ratio of 4:1. Nitrate ion was the predominant anion. Nitrite was noted in two samples and fluoride was noted in one. The metallic ions were predominantly nickel, iron, and chromium in the ratio of 68:16:16, with a wide variation. Inconel® 718 has these elements in the approximate ratio of 60:20:20. Titanium was detected in four samples, and aluminum was found in two samples.

Table 4
Properties of FORP Generated in RCS S/N 467

Lead Propellant	Lead Time (msec)	IR Absorption Ratio 1380:1640	Exo-therm (°C)	Endo-therm (°C)	Energy (mcal/mg)
NTO	10	4.9	ND	ND	ND
NTO	5	2.2	ND	ND	ND
MMH	10	ND	ND	ND	ND
No NTO	ND	0.4	ND	231	53
Vapor NTO	ND	2.7	117, 220	ND	-45, -98
Liq. NTO	ND	3.0	213	ND	-113
Syn. Mix	ND	4.0	ND	ND	ND

ND = Not determined

6.2 Comparison of FORP's

6.2.1 Compositional Variability

Both laboratory- and engine-generated FORP samples consisted of greater than 50 percent nitrate and usually greater than 20 percent methylammonium ion on a weight basis. Laboratory-synthesized FORP differed from engine FORP in that the 30-percent balance consisted of ammonium ion with up to 10 percent methylhydrazinium ion. Methylhydrazinium ion was never found in engine-generated FORP. Laboratory-synthesized FORP was prepared at 0 °C, and engine FORP presumably was produced at much higher temperatures leading to the decomposition of the unstable methylhydrazinium component. Others have observed similar composition variability in MMH engine residues that depended on the thermal history of the sample (Takimoto and Denault 1969). The reaction products from NTO and MMH are also subject to composition differences based on stoichiometry at initial mixing and subsequent exposure of the products to one of the reactants. This was demonstrated by exposure of fuel-rich, engine-generated FORP to NTO after the initial formation of FORP. Regardless of the conditions initially present for FORP formation, significant changes in the product composition can be effected by subsequent thermal and reactant exposure. Studies of MMH/NTO reaction products even under carefully controlled conditions have shown that complex mixtures normally result (Saad, Detweiler, and Sweeney 1972).

Differences in the decomposition products of FORP can be attributed to these compositional differences. A comparison of the TGA/FTIR results from FORP 13 and FORP 19 suggests an unique oxidative process was occurring in the later stages of FORP 19 thermal degradation. The DSC thermograms have not revealed any abnormally high energy releases (>400 mcal/mg) even though the thermal decomposition profiles indicated that the chemical process were dissimilar. The data in this report and that of others indicate that it is highly unlikely that one can exactly repeat a FORP composition in an engine or even in the laboratory. The overall complexity of the reactions that occur at first contact of MMH and NTO, post-contact reactions with excess MMH, NTO, or reaction intermediates, and the thermal history precludes specific predictability of all products. The common thread in all FORP's is that they are on a weight basis primarily nitrate, methylammonium, ammonium, and, if not exposed to high temperatures, methylhydrazinium ion. The thermal decomposition characteristics of all FORP's tested, regardless of source, are as expected for these compositions.

6.3 Reactivity of FORP

6.3.1 Thermal Reactivity of Laboratory-Synthesized FORP with Contaminants

The thermal reactivity of laboratory-synthesized FORP with suspected contaminants and potential corrosion products from a RCS engine was explored using DSC. It was necessary to use more than one batch of FORP for these tests because of the limited quantities available. Baseline DSC data for FORP batches 5, 7, 578 (a combination of batches 5, 7, and 8), and 19 were compared to the DSC data of these batches containing additives. Figure 61 shows the DSC data for FORP 19. Figure 62 shows the DSC data for the same FORP 19 mixed with 17 percent by weight titanium powder. The DSC scans were taken using Program II, which uses a high temperature-ramp rate. There are no significant differences in the DSC data.

FORP 5 was treated with sufficient nitric acid to ensure that any hydrazine nitrates present would be converted to dinitrate salts. The excess water and nitric acid were removed by drying. The DSC scan of this mixture of nitrated FORP 5 and 4 percent iron oxide (Fe_2O_3) is shown in Figure 63. With the exception of a small exotherm at 424 °C, the DSC scan is identical to the data for FORP 578 which was reacted with nitric acid in the same manner (Figure 64). Figure 65 shows the DSC scan for neat FORP 578. The neat FORP 578 had a small exotherm at 192 °C followed by a large one at 284 °C, whereas the HNO_3-treated FORP 578 has a medium exotherm at 120 °C, a small one at 168 °C, and a large one at 272 °C. In spite of these differences in appearance, the total energy released is not very different, 166 mcal/mg and 150 mcal/mg, respectively.

DSC scans of mixtures of nitrated FORP 578 with powdered Inconel® 718 (36 percent, fine filings) and nickel powder (28 percent) are displayed in Figures 66 and 67, respectively. The comparison of the differences in the total heat released in the DSC between the baseline nitrated FORP 578 and that with the two metal additives is significant. The baseline FORP released 149 mcal/mg while the Inconel® 718 and nickel released 232 and 208 mcal/mg, respectively. This energy difference could be attributed to reactions of the metals with the acidified FORP.

Mixtures of FORP 578 with 34 percent AN (Figure 68) or FORP 7 with 21 percent sodium nitrite ($NaNO_2$, J. T. Baker) (Figure 69) show no unusual reactions. The merged exotherm at 301 °C in the FORP/AN mixture is likely caused by the decomposition of AN itself. Table 5 is a summary of the FORP reactivity data discussed previously. From Table 5 it is apparent that the number of exotherms and their peak temperatures can change because of the presence of the additives, but large differences in total energy released do not occur.

6.3.2 Accelerating Rate Calorimetry (ARC) Tests

No exothermic events were detected when a sample of MMHN under NTO vapor in a titanium reaction vessel was investigated using the standard ARC wait-search routine over the temperature range 80 to 300 °C. An isothermal aging test of MMHN under NTO vapor for two hours at 230 °C gave no evidence of thermal activity. A similar test with an added strip of Ti-6Al-4V alloy was conducted at 300 °C, and no thermal activity was noted. The interior surface of the ARC vessel showed a dark deposit on the bottom, but no evidence of localized corrosion. The titanium alloy strip showed numerous dark deposits and oxidized regions, but the deposits could be removed with an alcohol swab. No localized corrosion was evident.

6.3.3 Mechanical Impact Tests

The Army Ballistic Missile Agency-type tester was operated at its maximum energy setting of 81.3 ft-lb. Five replicate tests of each were conducted with FORP, MMHN, and FORP dinitrate. No indication of an audible report, visible flash, or significant temperature rise occurred with any of these tests.

6.3.4 Rapid Mixing of MMH/MON-3

An extensive series of tests in which liquid MMH was rapidly mixed with vapor or liquid NTO in the presence of FORP, FORP constituents, or transducer corrosion products showed

Table 5
DSC Behavior of Laboratory-Synthesized FORP with Additives

FORP (Batch #)	Additive	Exotherm Event at (°C)	Heat Released (mcal/mg)
19	None	300	289
19	17% Ti	301	236
5	None	142	22
		199, 267	192
5	HNO_3 + 4% Fe_2O_3	127	23
		270	87
		424	33
578	None	192	21
		284	145
578	34% AN	203	14
		284, 301	130
578	HNO_3	120	30
		168	7
		272	112
578	HNO_3 + 36% Inc.718	265	232
578	HNO_3 + 28% Ni	102	30
		198	30
		284	103
		371	45
7	None	137	35
		263	127
7	21% $NaNO_3$	134	21
		176	9
		223	133

that unusual and/or damaging pressure excursions can occur. The apparatus used for the liquid/liquid tests is shown in Figure 2. Summaries of the results are shown in Tables 6 and 7.

Examples of pressure vs time traces are shown in Figures 70 through 77. The first test (Test 1) exhibited large noise spikes presumably caused by liquid fuel or oxidizer droplets striking the PCB face. Perforated disks designed to act as droplet filters were installed in front of the PCB transducers and were used for all subsequent testing. Check-outs verified that the perforated disks did not affect the pressurization rates of the test articles. Lower noise levels and less spiking were seen in subsequent tests.

Table 6
Rapid Mixing of MMH and NTO:[a] Effect of FORP

Test No.	FORP[b] (mg)	ΔT[c] (°C)	ΔP (psi)	Result	Cation Residue Analysis (wt. %) MMHN	HN	AN	MAN
1	0	ND	ND[d]	NVD	ND	ND	ND	ND
2	0	24	711	NVD	ND	ND	ND	ND
3	0	128	1660	NVD	ND	ND	ND	ND
4	0	31	700	NVD	71.2	4.4	1.1	23.2
5	0	113	750	NVD	5.3	.6	38.3	55.9
6	50	6	6370	NVD	79.4	3.2	1.6	15.9
7	50	17	1200	NVD	97.5	.6	.14	1.8
8	50	4	1520	NVD	74.8	3.0	1.5	20.7
9	50	4	507	NVD	76.7	2.5	.9	19.9
10	110	69	798	NVD	15.5	1.4	12.6	70.4
11	100	31	ND	Disk, PCB destroyed	54.8	2.9	6.0	36.3
12	100	ND	ND	Disk, PCB destroyed	81.9	0	8	17.3
13	100	90	ND	NVD	57.9	2.2	.7	39.3
14	100	96	[d, e]	Disk damaged	0	0	12.7	87.3
15	100	139	[d, e]	NVD	39.5	1.0	10.6	48.9
16	99	138	[e]	Disk damaged	59.8	0	1.3	39
17	100	2	485	NVD	66.4	2.9	1.0	29.8
18	100	13	910	NVD	66.2	2.0	0	31.7
19	100	17	2200	NVD	76.6	3.2	0	20.2
20	100	3	495	NVD	70.0	3.9	.4	25.8
21	100	6	1290	NVD	74.6	3.4	.6	21.5
22	100	31	[d]	NVD	68.7	3.4	.5	27.5

[a] MMH and NTO (0.5 mL each) pushed by 500 psi GN_2
[b] FORP film on interior wall of test article (2" of 1/4" OD × .035 wall 304 SS tube)
[c] Initial temperature 24 ± 6 °C
[d] Pressure spikes and noise caused by liquid droplet impingement of PCB face
[e] A titanium adapter was used in place of the SS adapter.
Note: NVD = No visible damage, ND = Not determined

Table 7
Rapid Mixing of MMH and NTO: Effects of Added Materials[a]

Test No.	FORP[b] (mg)	Material	Wt. Added (mg)	ΔT[c] (°C)	ΔP (psi)	Result	Cation Residue Analysis (wt. %) MMHN	HN	AN	MAN
23	0	MMHN	100	62	ND	Disk destroyed	72.7	2.6	2.1	22.6
24	0	MAN	100	0	477	NVD	77.9	1.8	0.8	19.5
25	0	MAN	100	53	ND	NVD	91.7	0.8	0	7.5
26	0	AN	100	31	ND	Disk destroyed	17.7	0	82.3	0
27	0	AN	102	52	620	NVD	89.0	1.9	0.9	8.2
28	0	$Ni(NO_3)_2$	100	ND	ND	NVD	77.2	3.2	0.6	19.0
29	0	$Ni(NO_3)_2$	100	47	1170	NVD	82.6	3.7	0.8	13.0
30	0	$Ni(NO_3)_2$	100	0	530	NVD	75.1	7.5	2.9	14.5
31	0	$Ni(NO_3)_2$	100	0	490	NVD	19.0	2.4	1.2	77.4
32	0	Ni·MMH[d]	100	64	NA	Disk destroyed, PCB damaged	28.9	2.2	31.1	37.8
33	0	Ni·MMH[d]	100	ND	8730	NVD	64.4	6.8	5.1	23.7
34	0	Ni·MMH[e]	100	1	483	NVD	53.2	3.6	0	43.2

[a] MMH and NTO (0.5 mL each) pushed by 500 psi GN_2

[b] FORP film on interior wall of test article (2" of 1/4" OD × .035 wall 304 SS tube)

[c] Initial temperature 24 ± 6 °C

[d] Nickel nitrate·MMH complex

[e] Nickel nitrate·MMH complex, no liquid MMH, oxidizer only

NOTE: ND = Not determined, NA = Not available, NVD = No visible damage

Table 7
Rapid Mixing of MMH and NTO: Effects of Added Materials[a] (continued)

Test No.	FORP[b] (mg)	Material	Wt. Added (mg)	ΔT[c] (°C)	ΔP (psi)	Result	Cation Residue Analysis (wt. %) MMHN	HN	AN	MAN
35	0	Ni·MMH[d]	100	1	903	NVD	14.7	.06	4.7	80.6
36	0	Inconel NO_3	100	ND	9400[e]	NVD	41.7	2.8	41.7	13.9
37	0	Inconel NO_3	100	54	1313	NVD	63.2	3.5	5.3	28.1
38	0	Inconel NO_3	297	38	550	NVD	38.5	7.7	23.1	30.8
39	0	Inconel NO_3	297	ND	9400[e]	NVD	25.0	0	75.0	0
40	0	Inconel NO_3	297[f]	30	1645	NVD	61.5	7.7	15.3	15.4
41	0	Inconel NO_3	297[f]	35	9390[e]	NVD	43.3	6.7	33.3	16.7
42	50	Inconel NO_3	50	2	4255	NVD	67.4	7.1	7.8	17.7
43	50	Inconel NO_3	50	2	752	NVD	48.9	2.2	10.9	38.0
44	100	Inconel NO_3	100	ND	2140	NVD	9.1	0.6	11.5	78.8
45	100	Inconel NO_3	100	11	480	NVD	14.7	0.06	4.7	80.6
46	100	Inconel NO_3	100	28	9390[e]	Disk damaged	74.2	2.9	5.3	17.5
47	100	Inconel NO_3	100	18	648	NVD	72.3	2.5	1.0	24.1

[a] MMH and NTO (0.5 mL each) pushed by 500 psi GN_2
[b] FORP film on interior wall of test article (2" of 1/4" OD × .035 wall 304 SS tube)
[c] Initial temperature 24 ± 6 °C
[d] Nickel nitrate·MMH complex, no liquid MMH, oxidizer only
[e] PCB overranged
[f] No oxidizer added
NOTE: ND = Not determined, NA = Not available, NVD = No visible damage

Tests 1 through 5 were baseline runs to determine the pressure, temperature, and damage levels associated with the rapid mixing of MMH and NTO alone. Moderate pressure rises of approximately 700 psi (200 psi above the push-gas pressure of 500 psi) were noted. The temperature changes were variable, and no visible damage to the perforated disk, PCB, or the rest of the test article was noted.

Tests 6 through 9 explored the effects of adding 50 mg of laboratory-synthesized FORP to the mixing event. Test 6 showed a high-pressure spike which is suspected not to be caused by droplets impinging. No visible damage was noted in this series of tests.

Tests 10 through 22 were performed with ~100 mg of added laboratory-synthesized FORP, and four instances of visual damage were noted. These events severely damaged the face of the pressure transducers, deposited slag on the adapter, and/or destroyed the stainless steel perforated disk as shown in Figures 78 through 84.

Temperature responses, measured on the outside of the test article, were inconsistent. A rapid and localized thermal event for which the thermal conductivity and soak time of the test-article controls the observed temperature responses may not provide meaningful data.

Chemical analyses of the residues left after the mixing are also included in Table 6. There is no obvious correlation between observed damage and composition of the residues. The rapid-mixing tests were performed with an NTO/MMH mass ratio of 1.6, which is considerably fuel-rich compared to the stoichiometric ratio of 2.5 or the commonly used thruster ratio of 2.3. With large variability, the average composition is 70/3/1/26 for MMHN/HN/AN/MAN. This composition is the average of the residue analyses of Tests 17 through 22 which were chronologically the latest of the set. The average composition of the added laboratory-synthesized FORP was approximately 21/1/8/69 for MMHN/HN/AN/MAN with small additional amounts of UDMHN and dimethylammonium nitrate. As expected, the fuel-rich, rapid-mixing test residues are higher in MMHN than for laboratory-synthesized FORP formed under more oxidizer-rich conditions.

The results of rapid-mixing experiments in which FORP constituents and/or suspected transducer corrosion products were added are summarized in Table 7. Pressure vs time plots for this series of tests are not shown; only the peak pressure recorded at the PCB is tabulated. Again, temperature changes were variable and noncorrelated to other observations.

General observations are listed below:

- ***MMH Nitrate, no FORP, Test 23***: One test was performed, and the reaction destroyed the stainless steel perforated disk. Pressure data were not acquired because of particle impingement on the PCB face.

- ***Methylammonium Nitrate, no FORP, Tests 24 through 25***: No damage was noted in two tests.

- ***Ammonium Nitrate, no FORP, Test 26 through 27***: The stainless steel perforated disk was destroyed in Test 26.

- ***Nickel Nitrate, no FORP, Tests 28 through 31***: This corrosion product appears to be benign showing low pressures and no apparent damage.

- ***MMH Complex of Nickel Nitrate, no FORP, Tests 32 through 35***: In Test 32 the disk and PCB were destroyed. The duplicate test, No. 33, showed no visual damage, but a suspected real pressure rise to 8730 psi was noted. When only oxidizer was injected (Tests 34 and 35), no apparent damage occurred, and pressure changes were normal.

- ***Inconel® Nitrate, 0-50 mg FORP, Tests 36 through 43***: No visual evidence of unusual reaction was noted; however, in three tests the PCB was overranged (> 9300 psi) and in a fourth test, a pressure increase to 4250 psi was noted. With one exception, larger than average amounts of AN were found in the posttest residues of Tests 36 through 41 (no FORP). The AN is formed at the expense of MMHN.

- ***Inconel® Nitrate, 100 mg FORP, Tests 44 through 47***: Disk damage and a PCB overrange indication were noted in Test 46.

The incidence and conditions for anomalous events are listed in Table 8. The criteria for an anomalous event occurring during the rapid mixing of MMH and NTO are:

- Observation of physical damage to the test article

  or

- Pressure increases of greater than 2000 psi.

For the latter criterion, a PCB overrange is taken as a positive indication of an anomalous result. Table 9 gives a high-level summary.

7.0 Conclusions

7.1 FORP Chemical Characteristics

The chemical and physical tests used to characterize FORP from various sources have demonstrated that the formation of exactly repeatable compositions either between or within sources is unlikely. However, these same tests have shown that FORP from all sources falls within a limited range of compositions that depends on the fuel/oxidizer ratio, composition of postformation atmosphere (reducing or oxidizing), and reaction or postreaction temperature. In an oxidizer-rich atmosphere, the principle FORP products are AN and MAN. If FORP is formed at a lower temperature, but still with sufficient oxidizer, up to 10 percent of the FORP consists of MMHN. If the FORP is produced in a fuel-rich environment, little or no nitrate anion is detected in the FORP. If the fuel-rich FORP is subsequently exposed to oxidizer, compositions similar to oxidizer-rich FORP or laboratory-synthesized FORP result.

It can be concluded that FORP composition is qualitatively predictable if reactant ratio, knowledge of the thermal history, and subsequent vapor exposures are known.

Table 8
Incidence of Anomalous Events in MMH/NTO Rapid Mixing Tests

FORP	Additive	No. of Anomalies	No. of Tests
None	None	0	5
50 mg	None	1	4
100 mg	None	5	13
None	100 mg MMHN	1	1
None	100 mg MAN	0	2
None	100 mg AN	1	2
None	100 mg Ni $(NO_3)_2$	0	4
None	100 mg Ni·MMH Complex	2	2
None	100 mg Ni·MMH Complex[a]	0	2
None	100 mg Inconel NO_3	1	2
None	300 mg Inconel NO_3	2	4
50 mg	50 mg Inconel NO_3	1	2
100 mg	100 mg Inconel NO_3	2	4
	Totals	16	47

[a] No liquid NTO added

Table 9
Summary of Anomalous Events

Conditions	No. of Anomalies	No. of Tests
No FORP	0	5
FORP alone	6	17
FORP and Additives	9	25
Additives alone	7	19

7.2 FORP Reactivity

No instances of FORP or mixtures of FORP with various additives showed any unusual thermal decomposition modes by DSC or other laboratory tests. FORP was not found to be sensitive to mechanical impact. However, configurational testing established that highly energetic reactions can occur when either FORP, MMHN, AN, or Inconel® corrosion products were present during rapid mixing of liquid MMH and NTO. Rapid mixing of MMH and NTO without these added ingredients did not produce high-energy events.

7.3 Damage Potential

This effort has demonstrated that FORP, MMHN, AN, or Inconel® corrosion products can induce a mixture of MMH and NTO to produce component-damaging energies. The test program was not extensive enough to provide statistical probabilities for these events, but did show that such events can occur. Damaging events required FORP or metal salts to be present at the initial mixing of MMH and NTO. Based on the results reported here, removal or mitigation of a buildup of these materials may decrease the incidence of these high-energy, potentially damaging events.

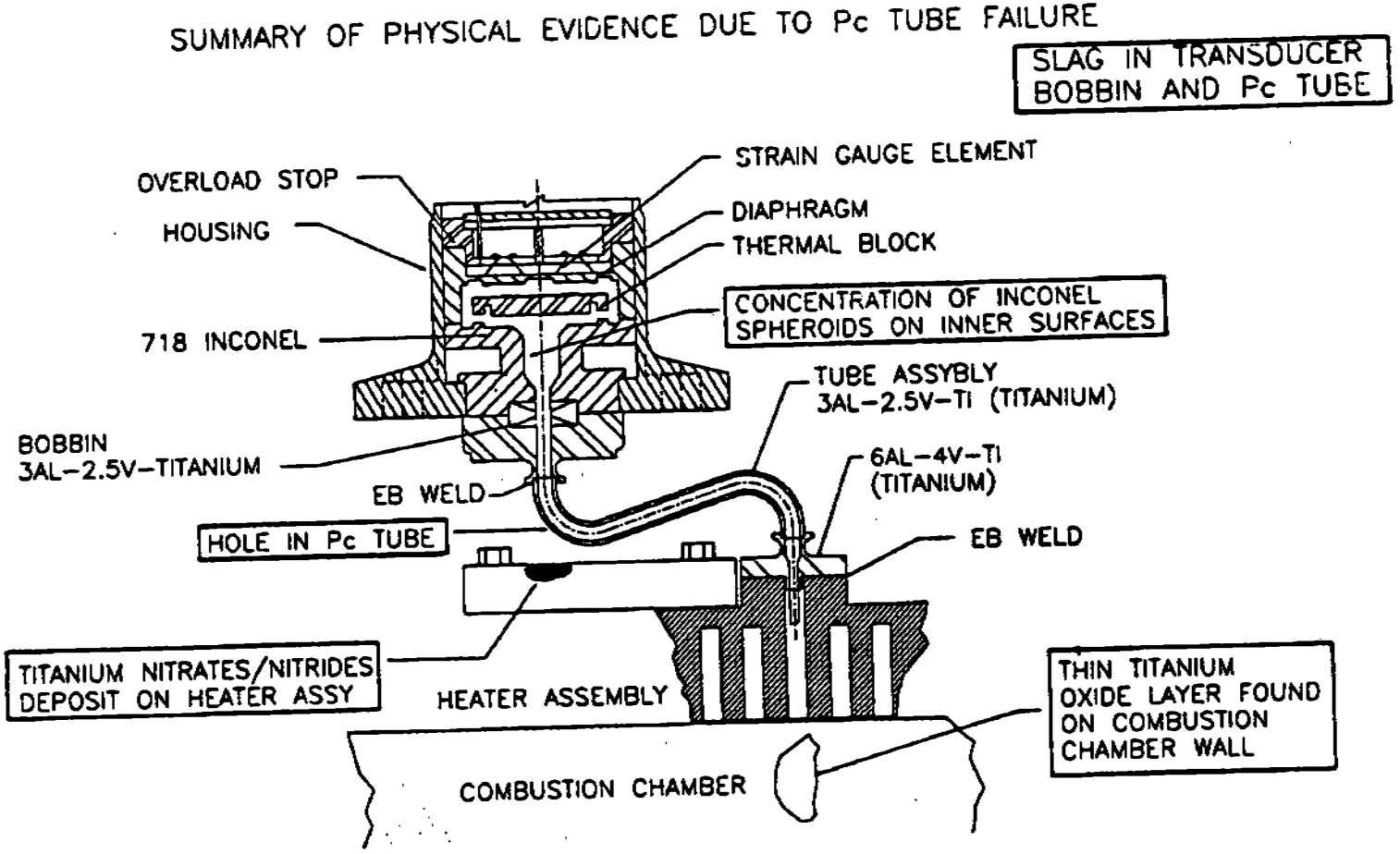

Figure 1
P_c Transducer and Assembly Showing the Location of the Failure

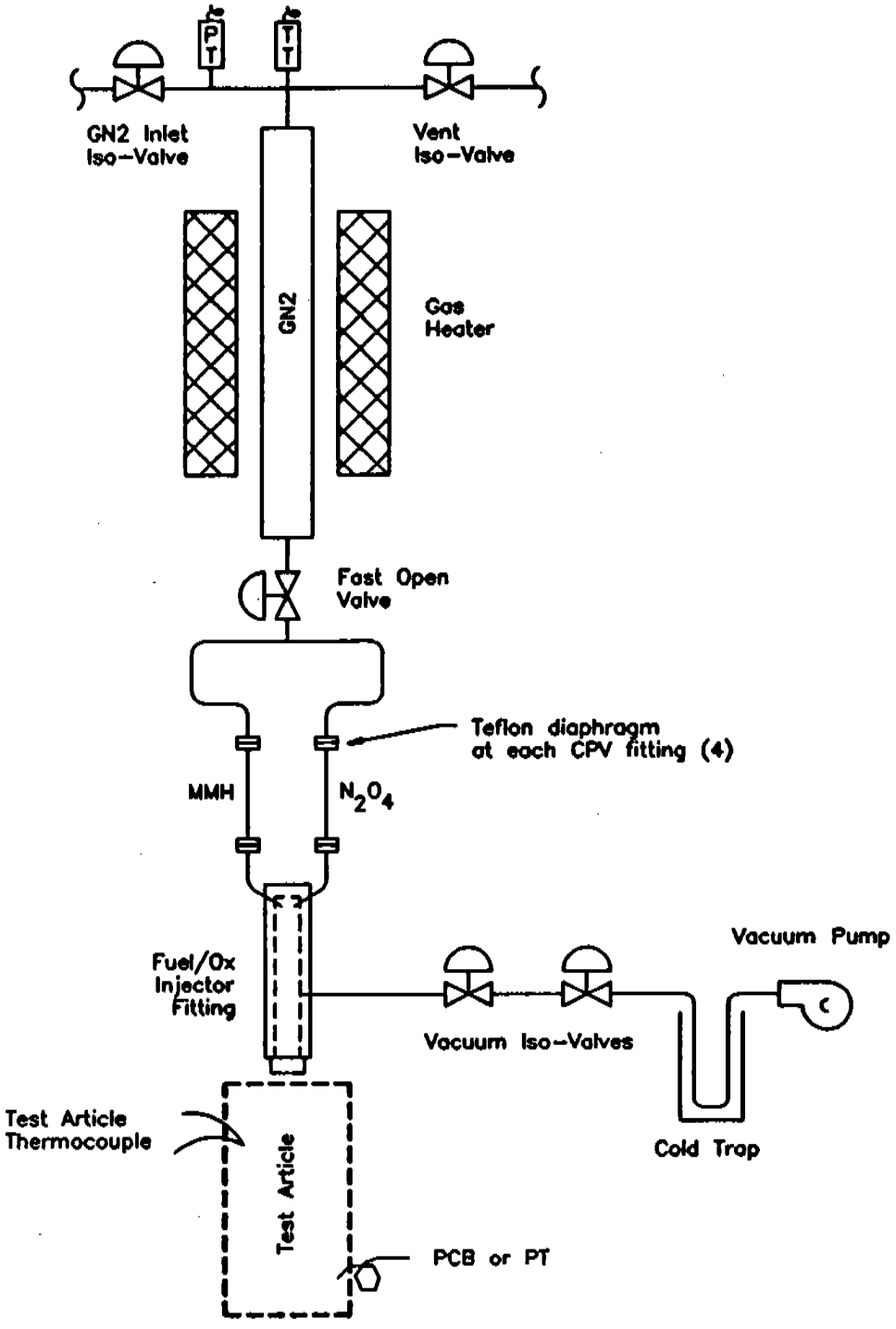

Figure 2
WSTF Fuel/Oxidizer/FORP Reaction System

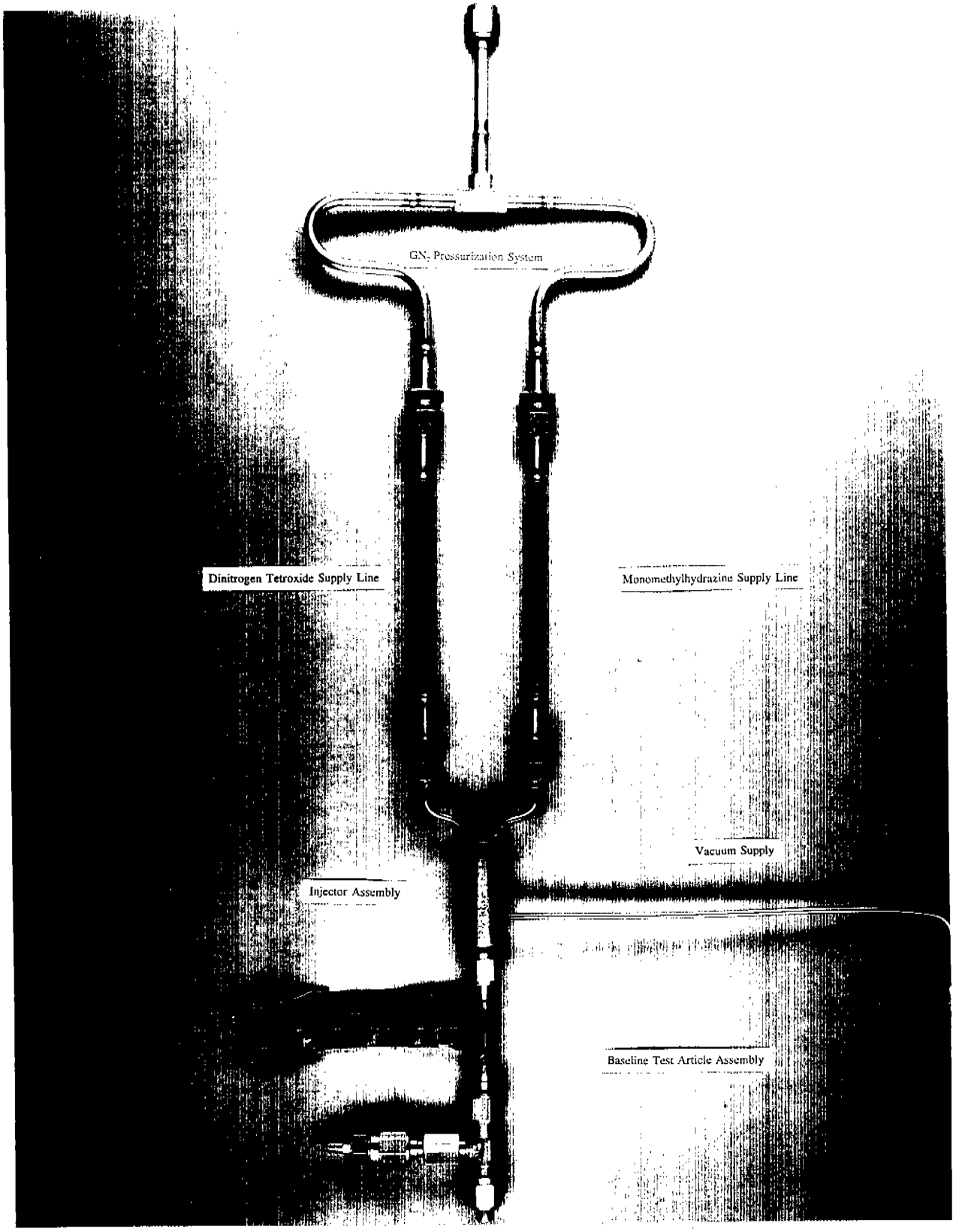

NASA-WSTF
0394-0448

Figure 3
Fuel/Oxidizer/FORP Injector Apparatus

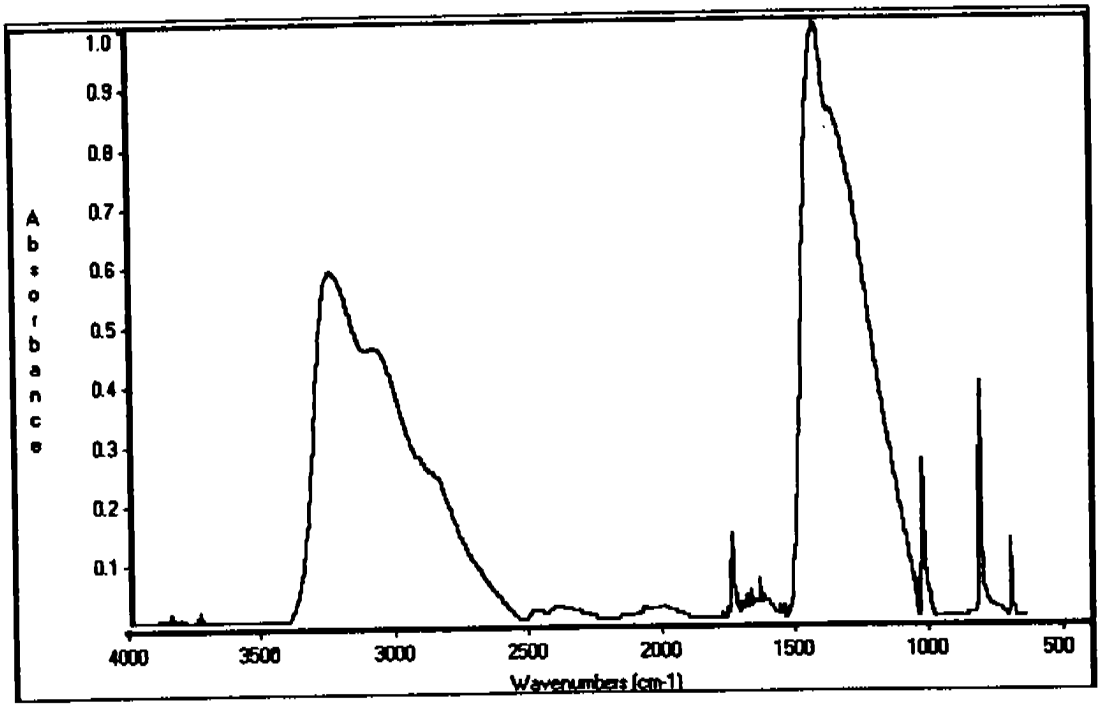

Figure 4
FTIR Spectrum of Ammonium Nitrate

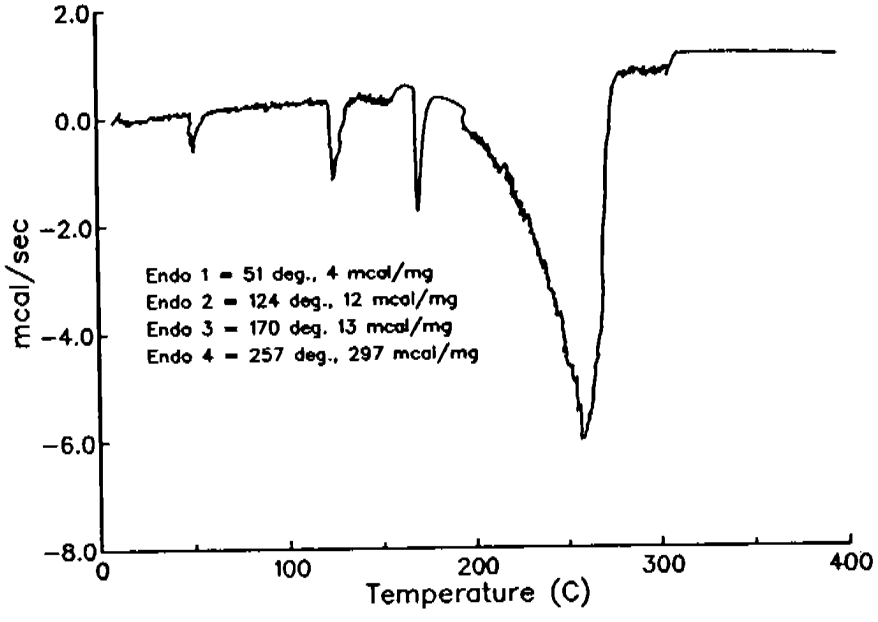

Figure 5
DSC of Ammonium Nitrate

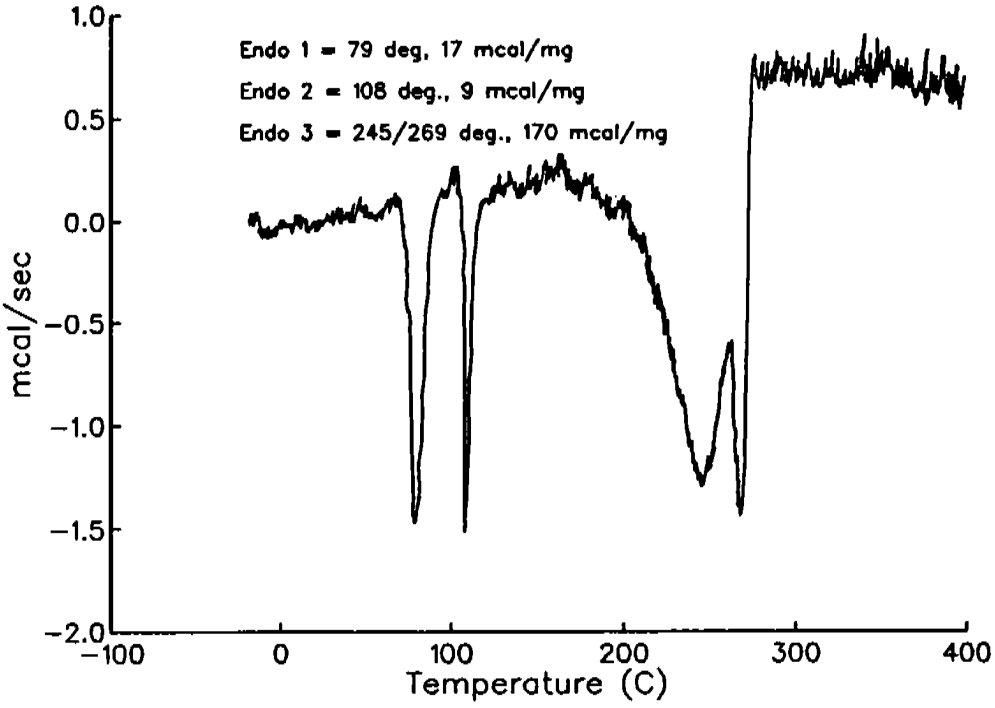

Figure 6
DSC of Methylammonium Nitrate

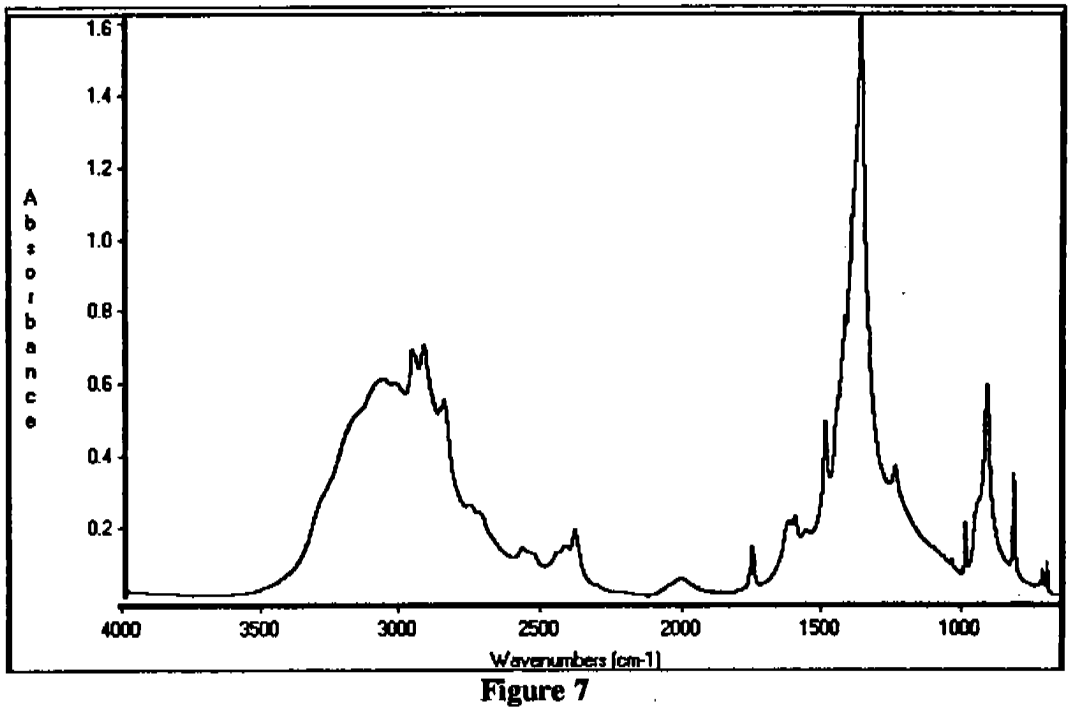

Figure 7
FTIR of Methylammonium Nitrate

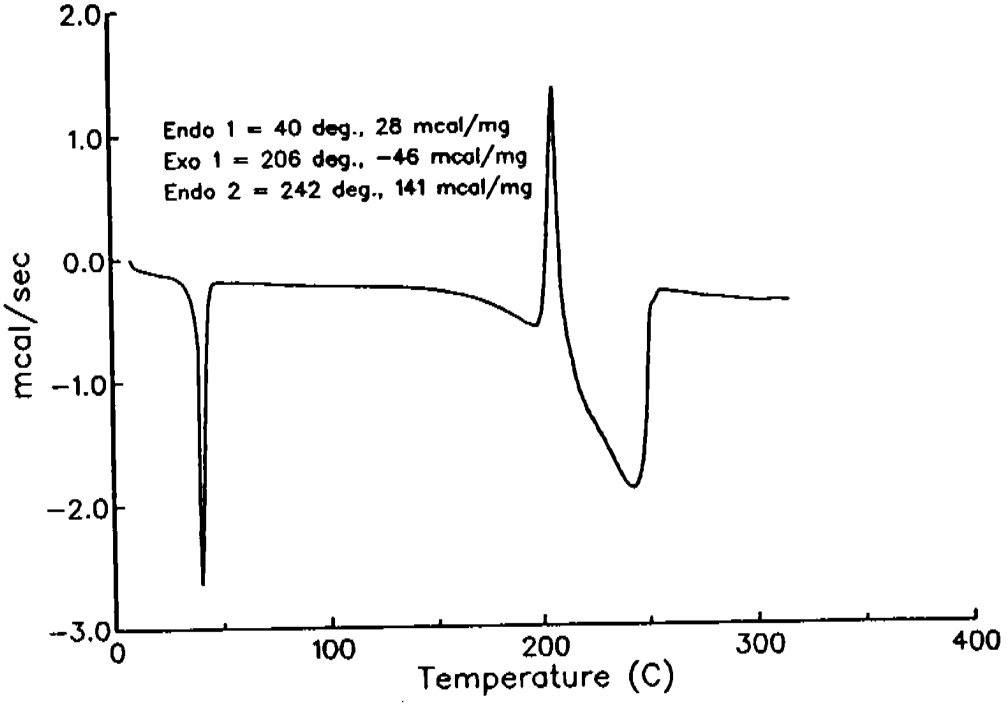

Figure 8
DSC of Methylhydrazinium Nitrate

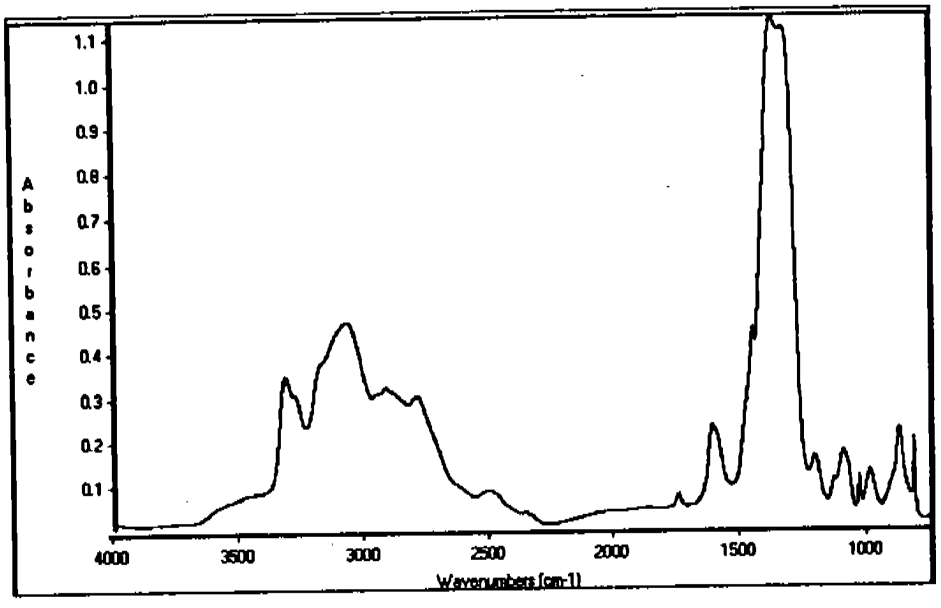

Figure 9
FTIR of Methylhydrazinium Nitrate

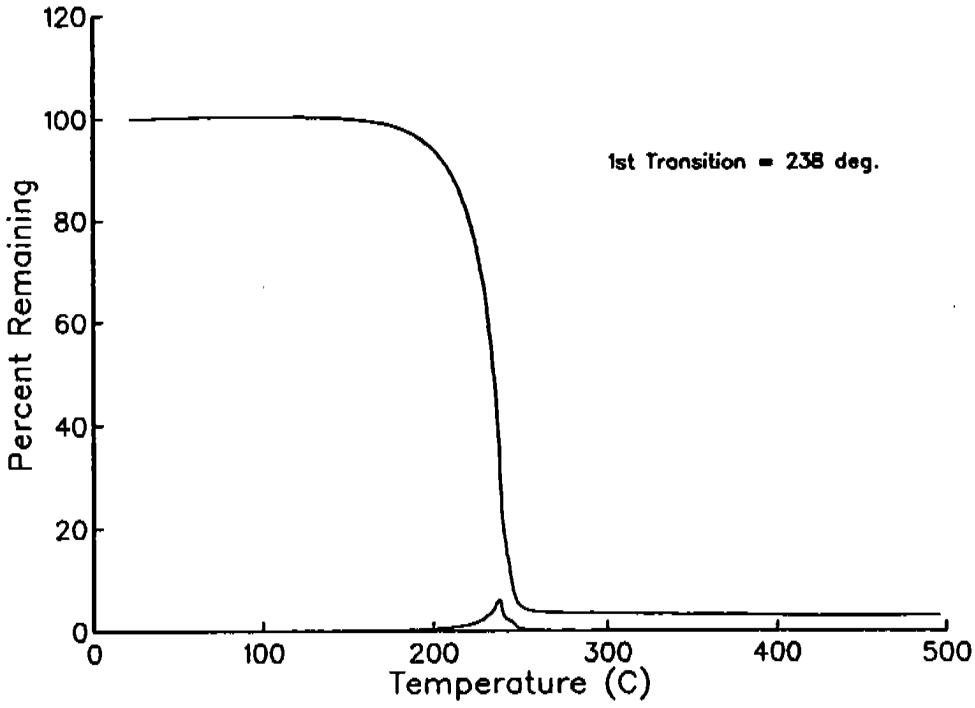

Figure 10
TGA of Methylhydrazinium Nitrate

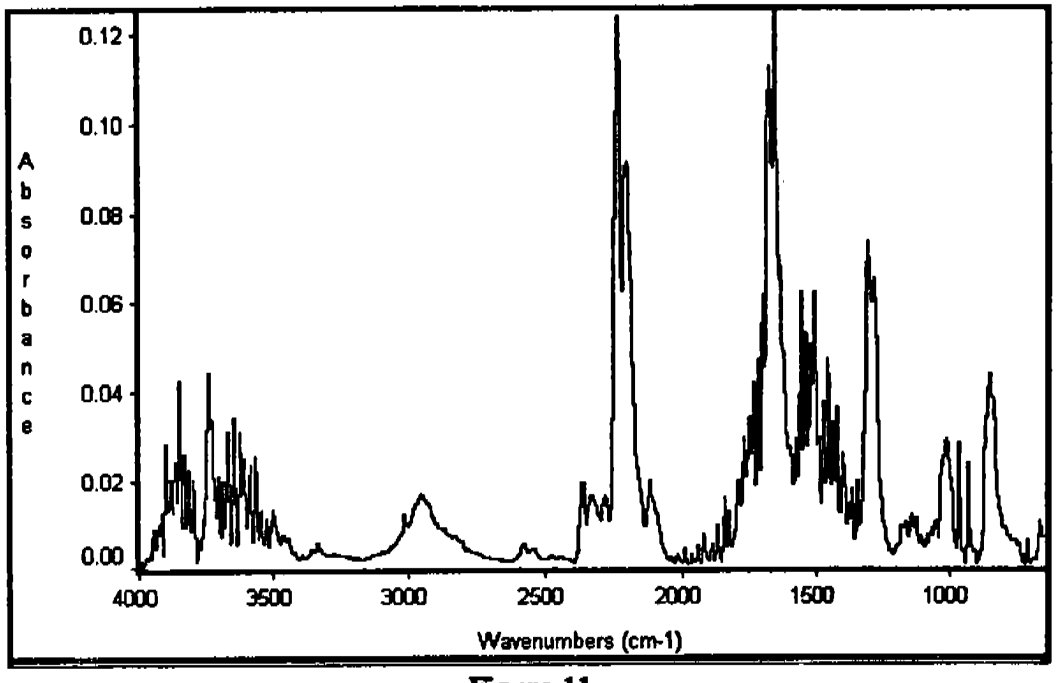

Figure 11
FTIR of TGA Effluent Gas from Methylhydrazinium Nitrate During First Transition

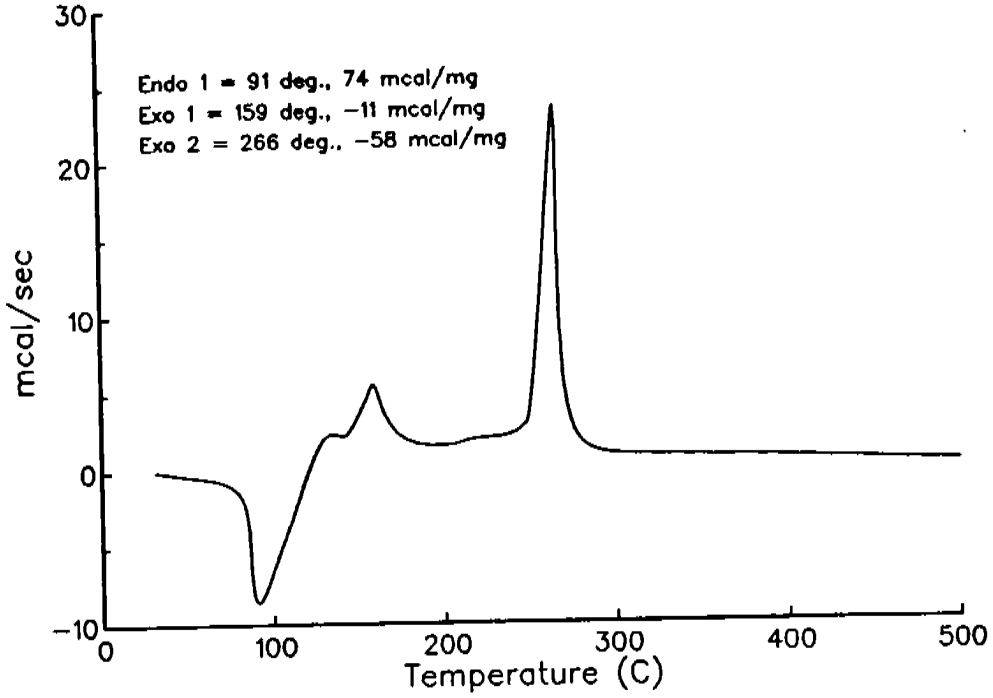

Figure 12
DSC of Methylhydrazinium Dinitrate

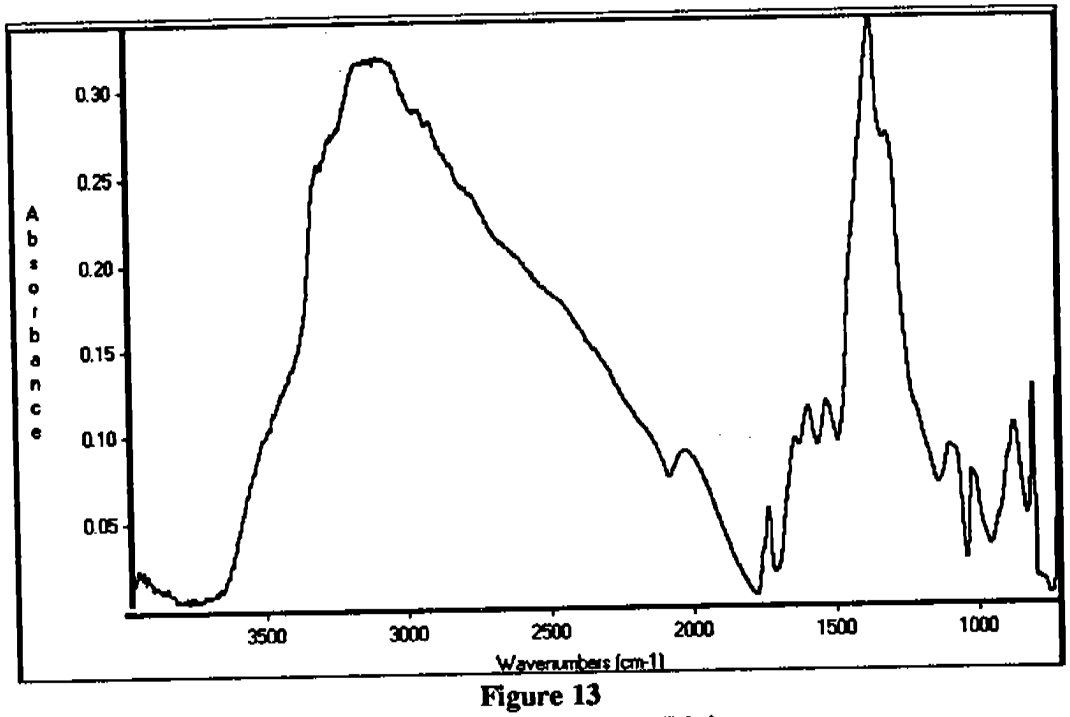

Figure 13
FTIR of Methylhydrazinium Dinitrate

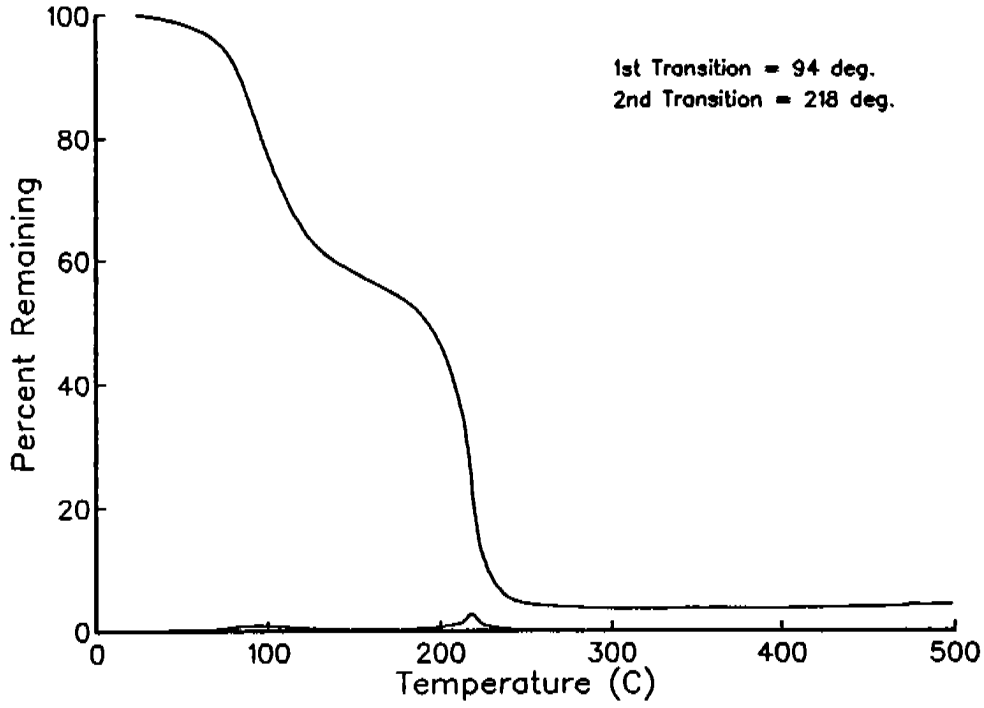

Figure 14
TGA of Methylhydrazinium Dinitrate

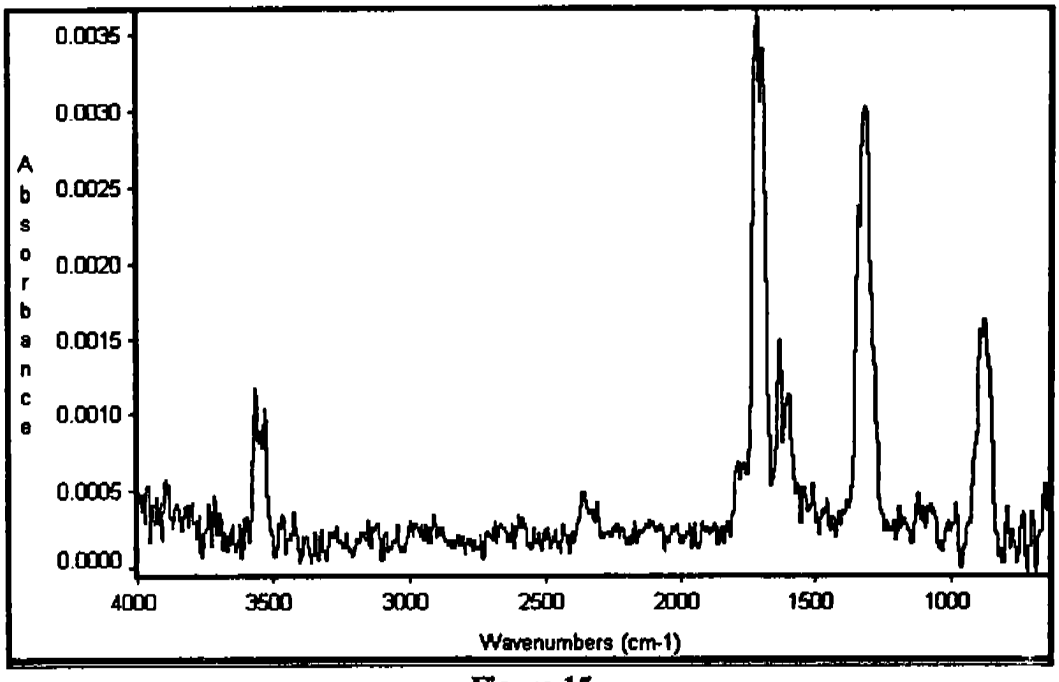

Figure 15
FTIR of TGA Effluent Gas from Methylhydrazinium Dinitrate Early During First Transition

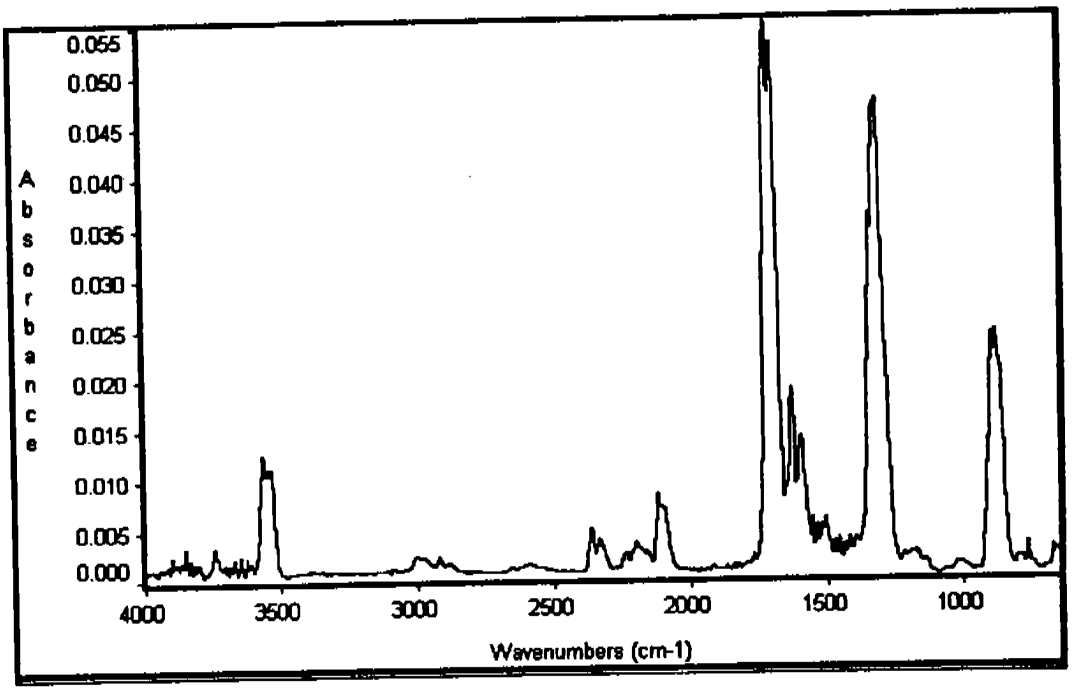

Figure 16
FTIR of TGA Effluent Gas from Methylhydrazinium Dinitrate Late During First Transition

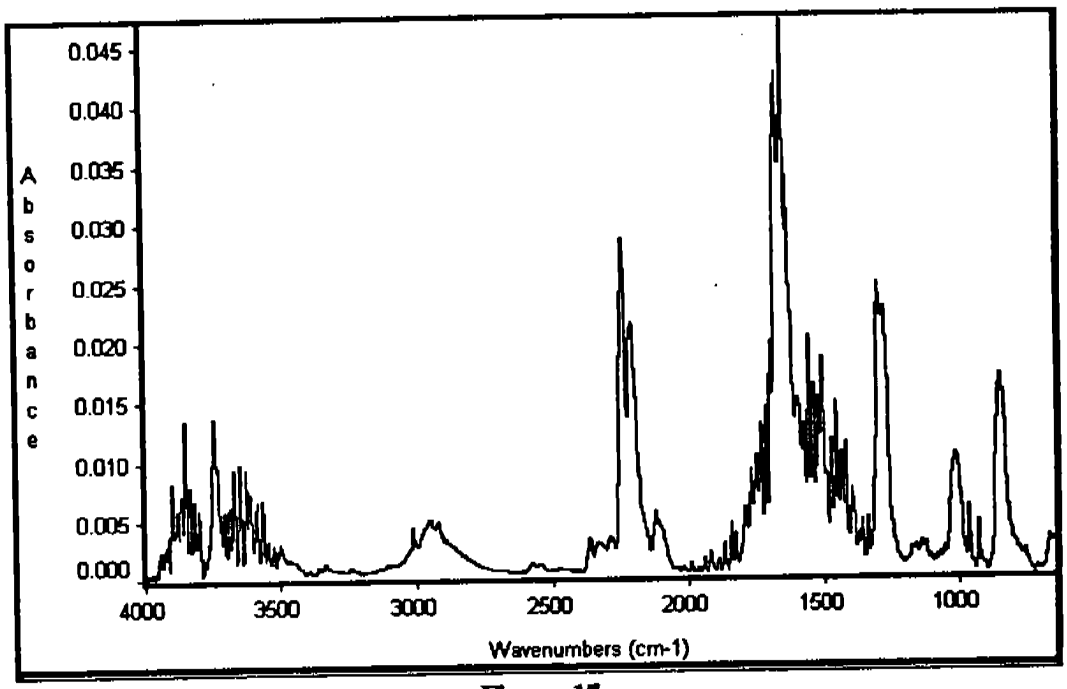

Figure 17
FTIR of TGA Effluent Gas from Methylhydrazinium Dinitrate At Second Transition

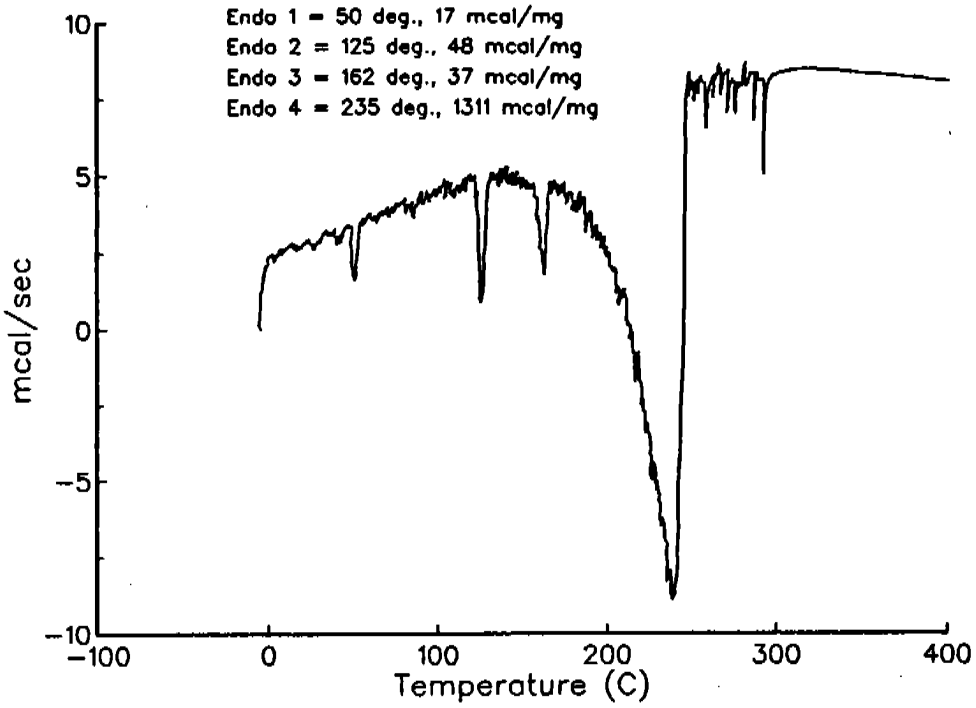

Figure 18
DSC of 1,1-Dimethylhydrazinium Nitrate

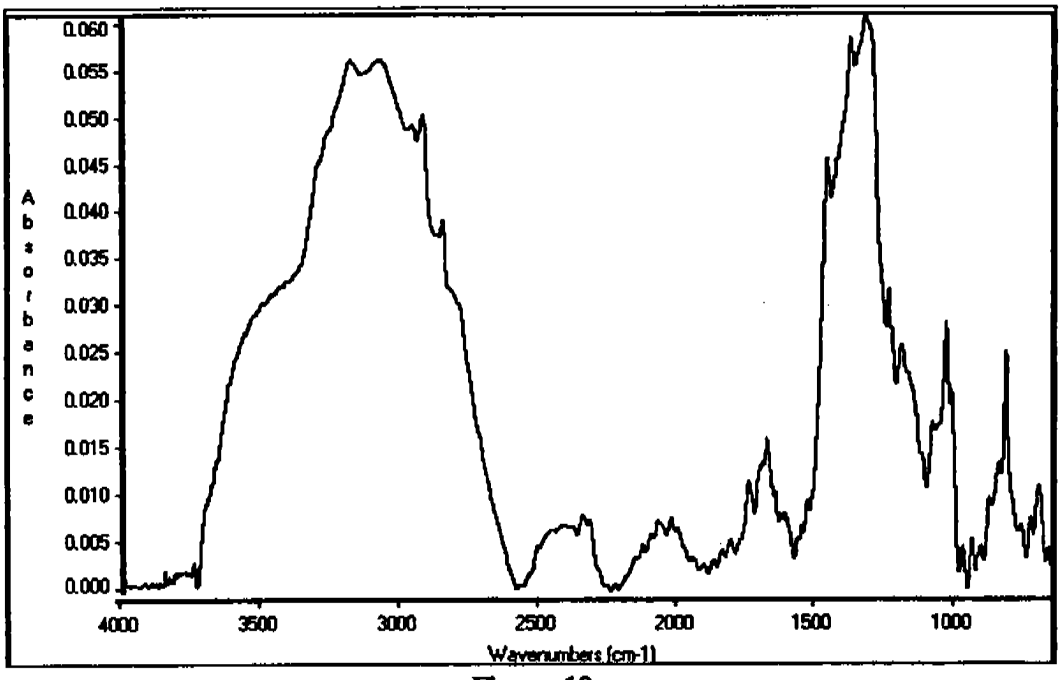

Figure 19
FTIR of 1,1-Dimethylhydrazinium Nitrate

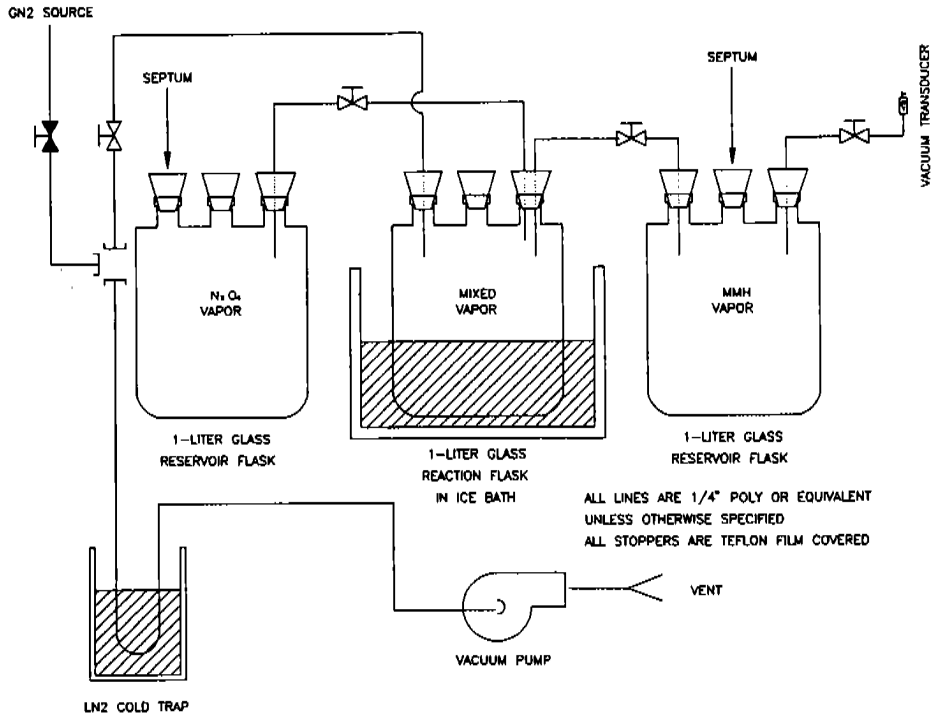

Figure 20
WSTF FORP Generation Apparatus

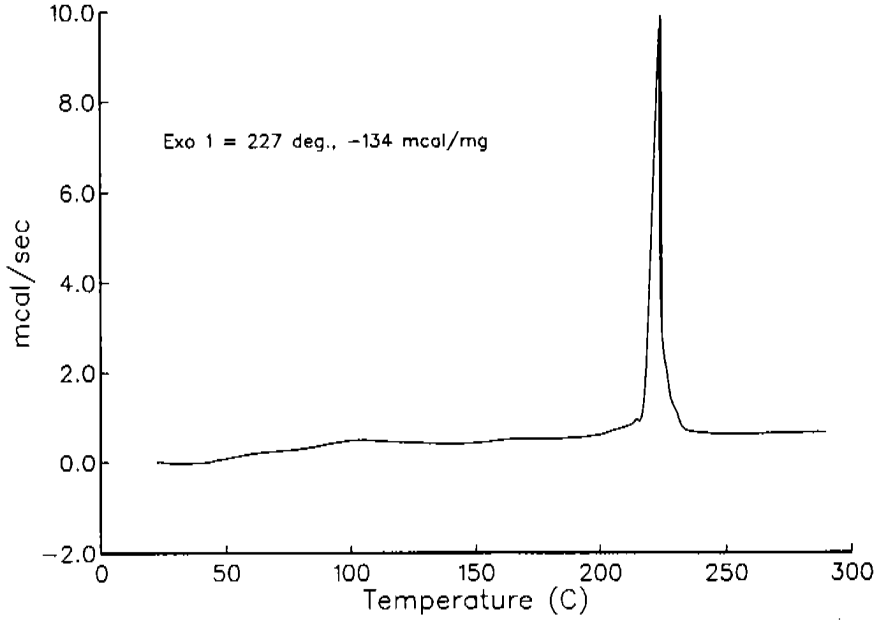

Figure 21
DSC of WSTF Laboratory-Synthesized FORP Batch 12

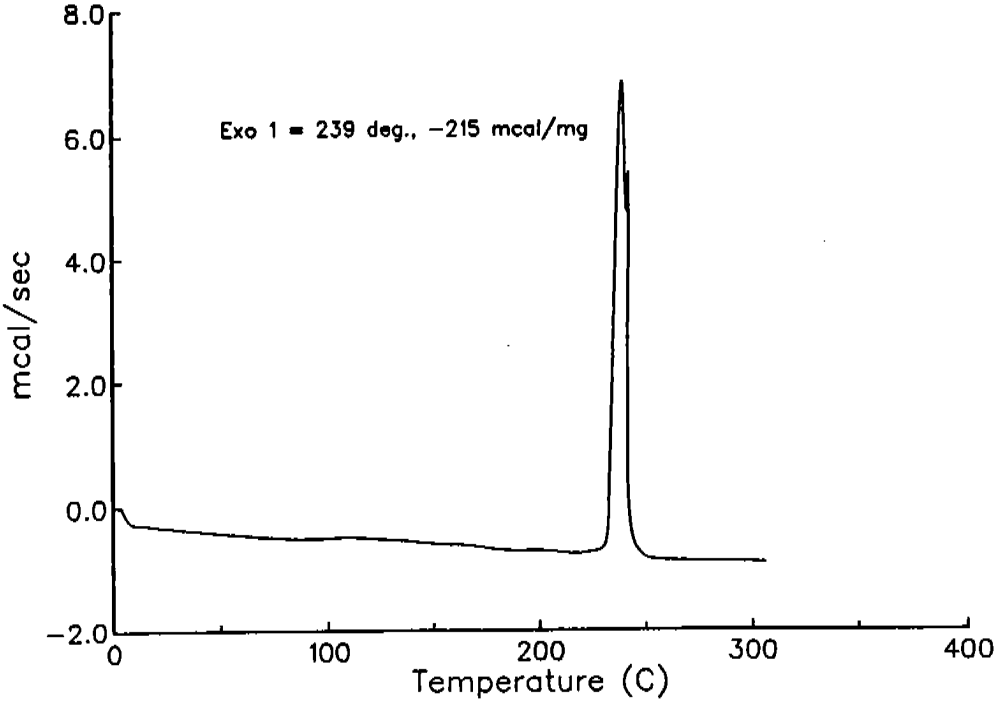

Figure 22
DSC of WSTF Laboratory-Synthesized FORP Batch 14

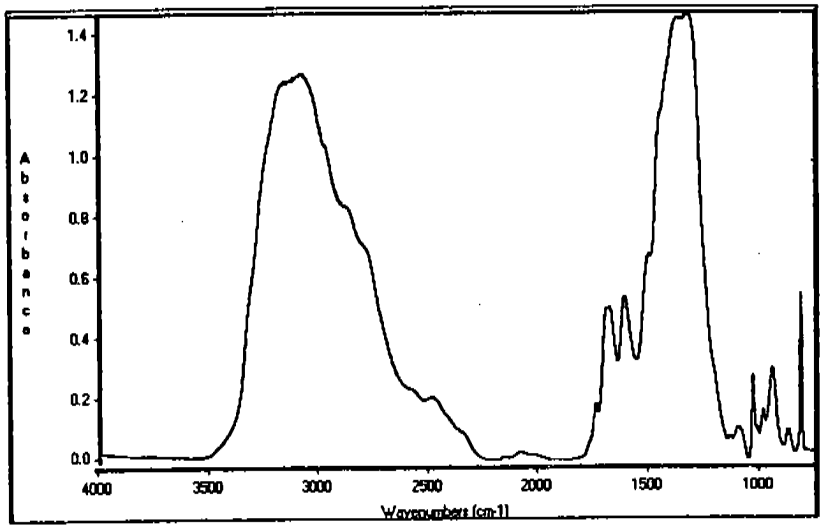

Figure 23
FTIR of WSTF Laboratory-Synthesized FORP Batch 12

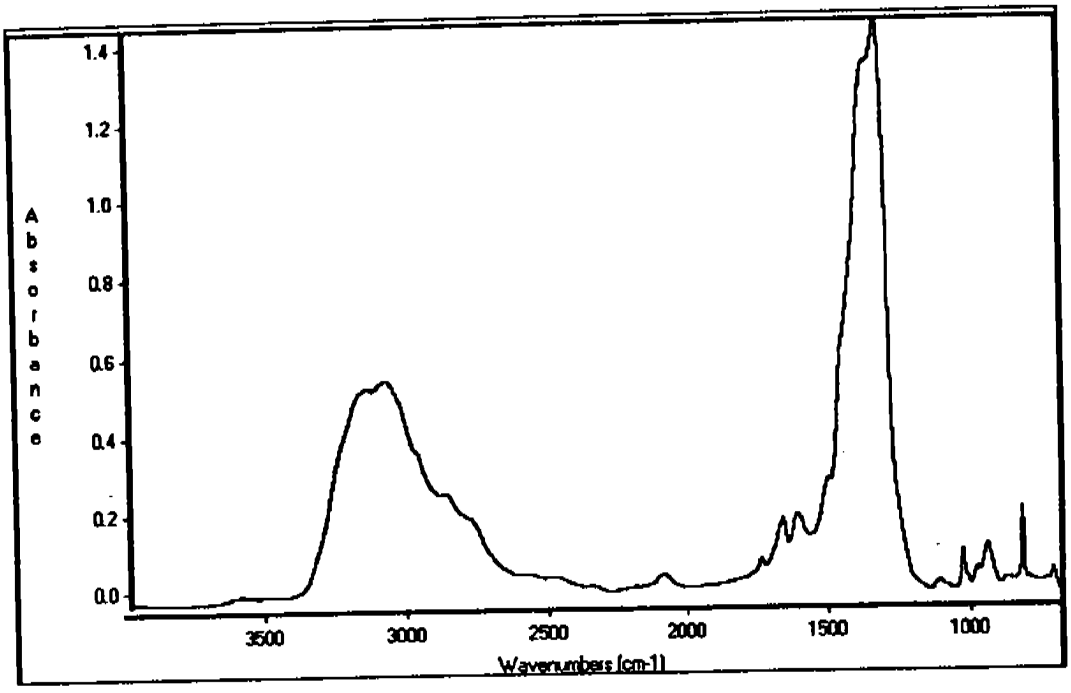

Figure 24
FTIR of WSTF Laboratory-Synthesized FORP Batch 14

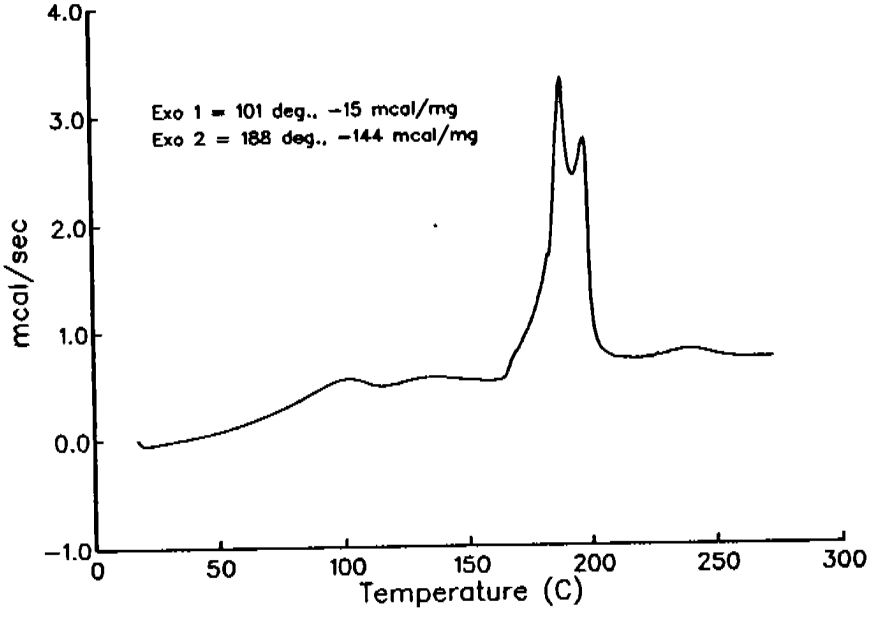

Figure 25
DSC of WSTF Laboratory-Synthesized FORP Batch 1

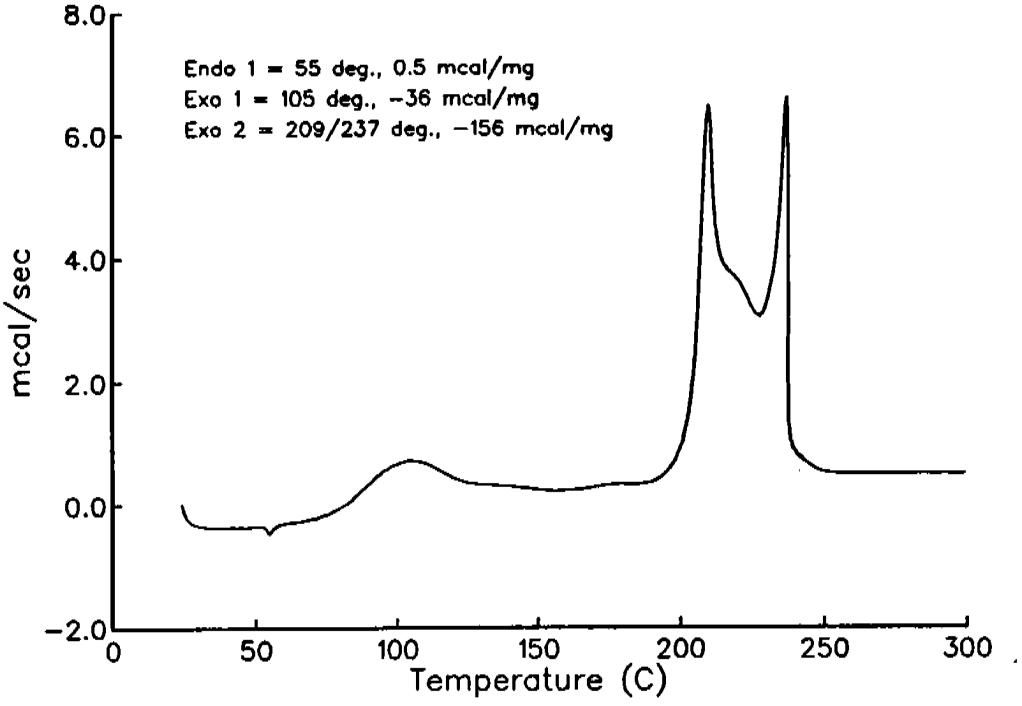

Figure 26
DSC of WSTF Laboratory-Synthesized FORP Batch 5, Vacuum Dried

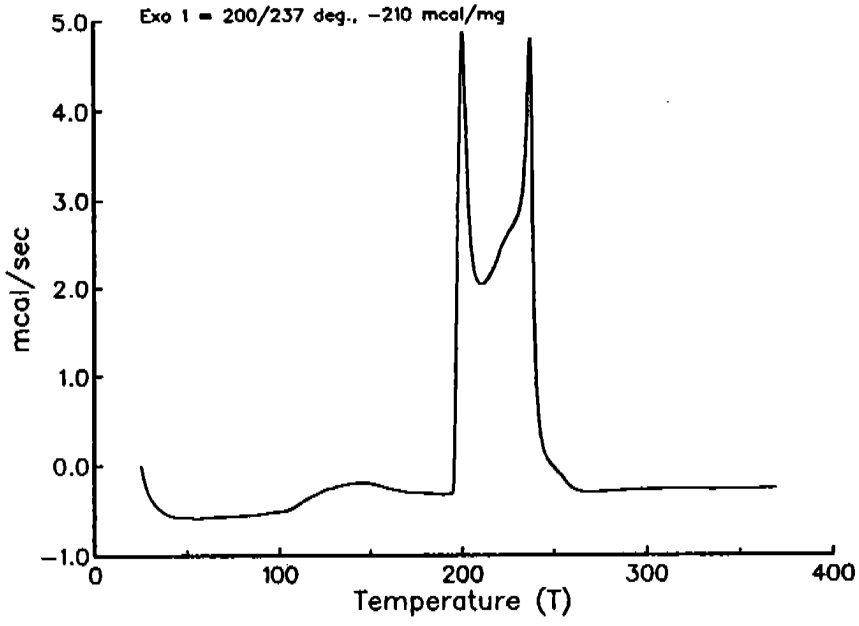

Figure 27
DSC of WSTF Laboratory-Synthesized FORP Batch 15

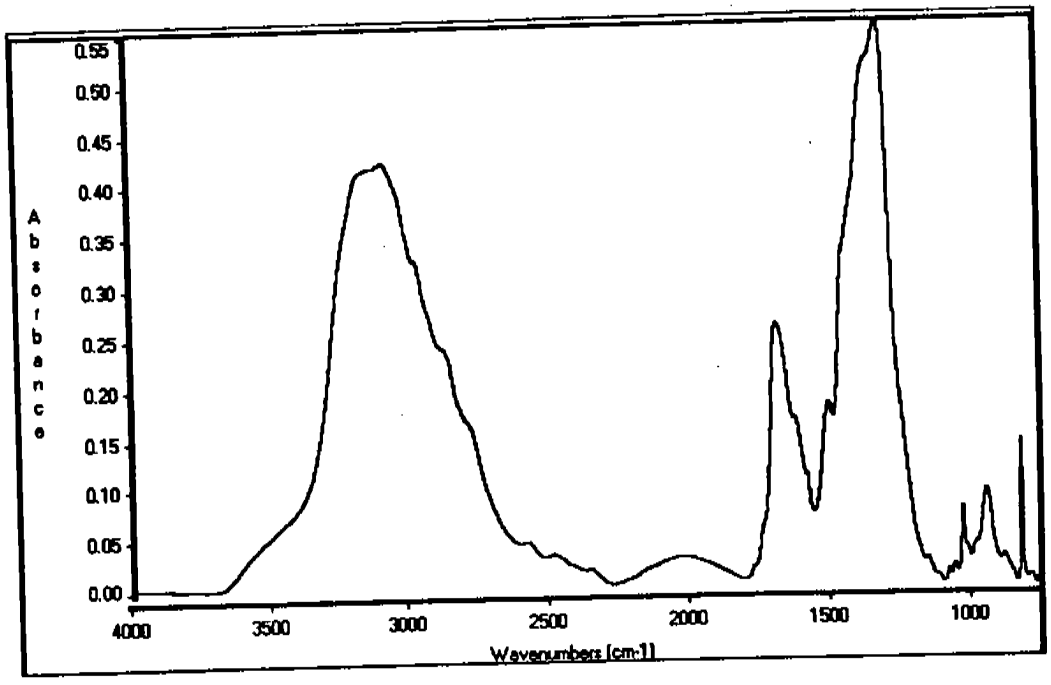

Figure 28
FTIR of WSTF Laboratory-Synthesized FORP Batch 1

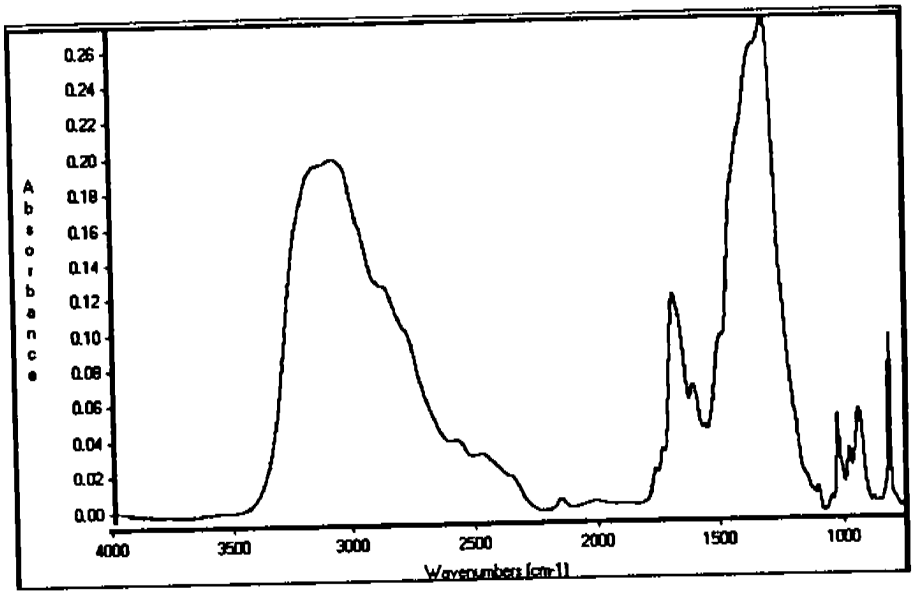

Figure 29
FTIR of WSTF Laboratory-Synthesized FORP Batch 5, Vacuum Dried

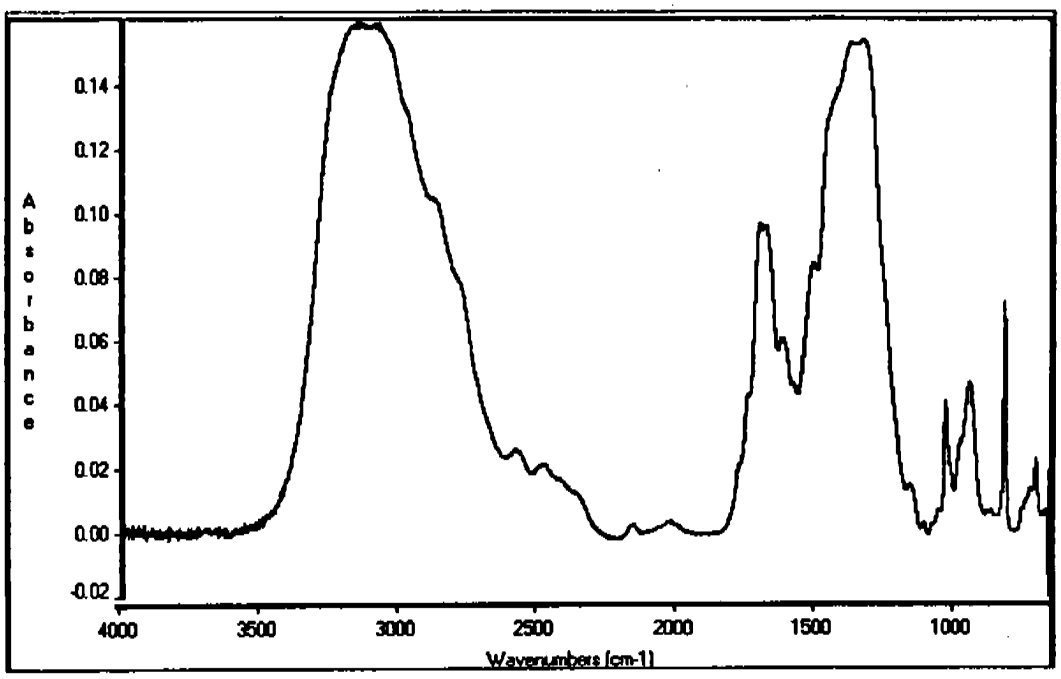

Figure 30
FTIR of WSTF Laboratory-Synthesized FORP Batch 15

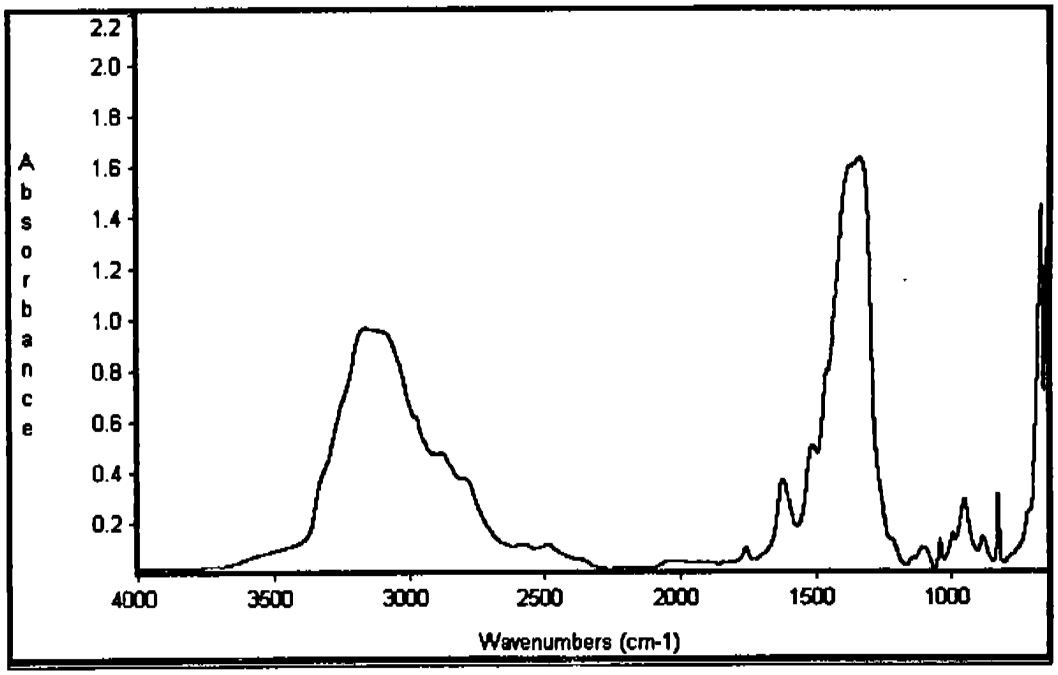

Figure 31
FTIR of Synthetic Mixture, 10% AN, 40% MMHN, 50% MAN

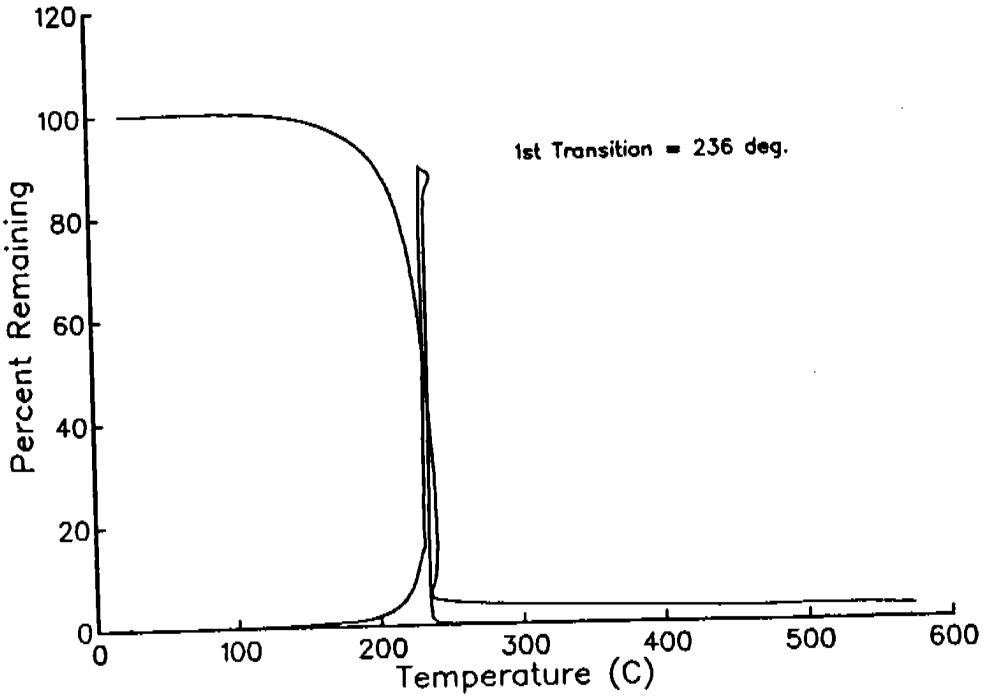

Figure 32
TGA of WSTF Laboratory-Synthesized FORP Batch 13

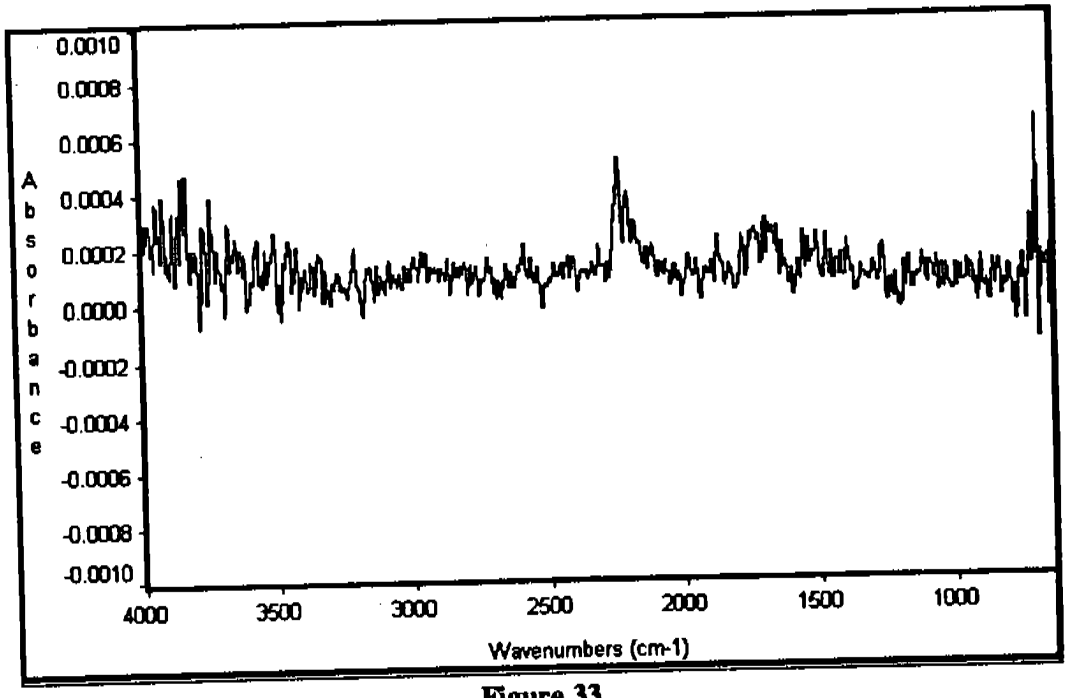

Figure 33
FTIR of TGA Effluent Gas from WSTF Laboratory-Synthesized FORP Batch 13, Early During Transition

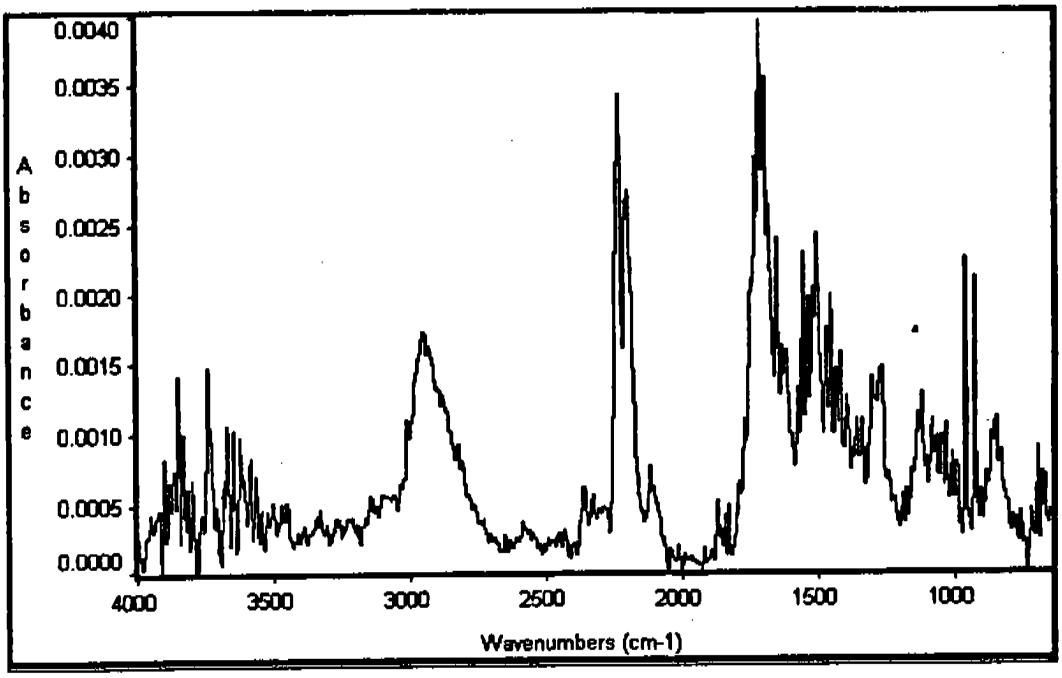

Figure 34
FTIR of TGA Effluent Gas from WSTF Laboratory-Synthesized FORP Batch 13,
At Peak of Transition

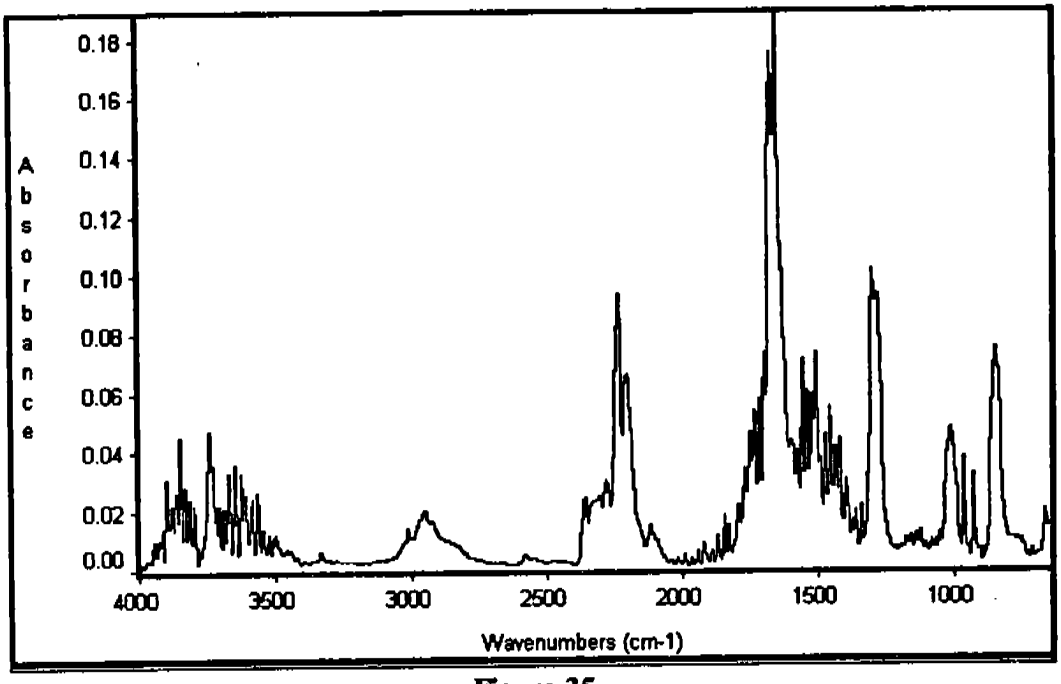

Figure 35
FTIR of TGA Effluent Gas from WSTF Laboratory-Synthesized FORP Batch 13,
Late in Transition

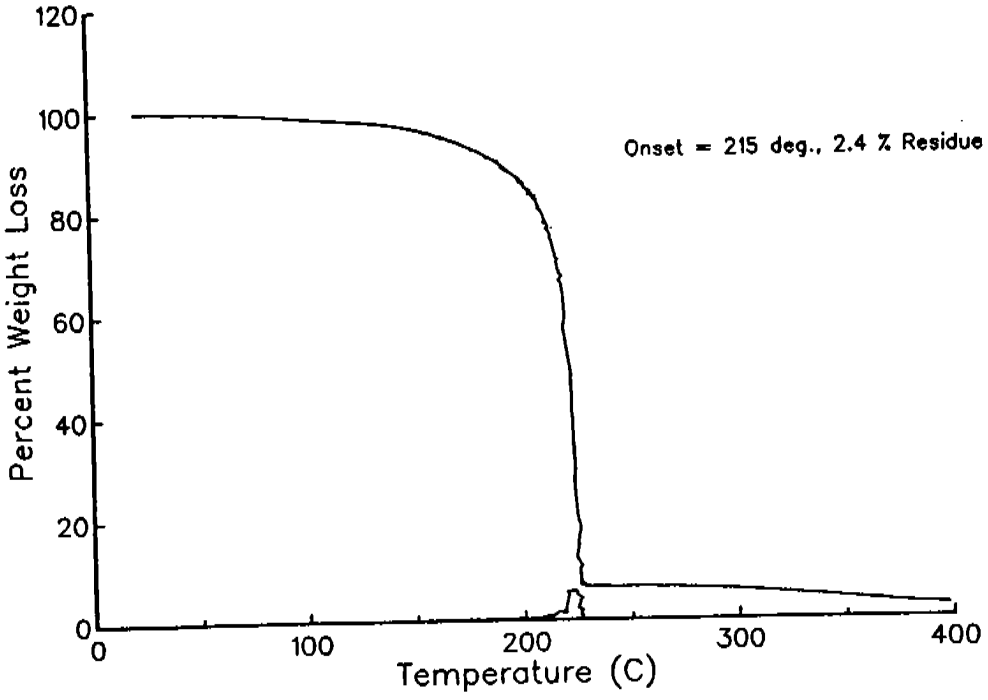

Figure 36
TGA of WSTF Laboratory-Synthesized FORP Batch 19

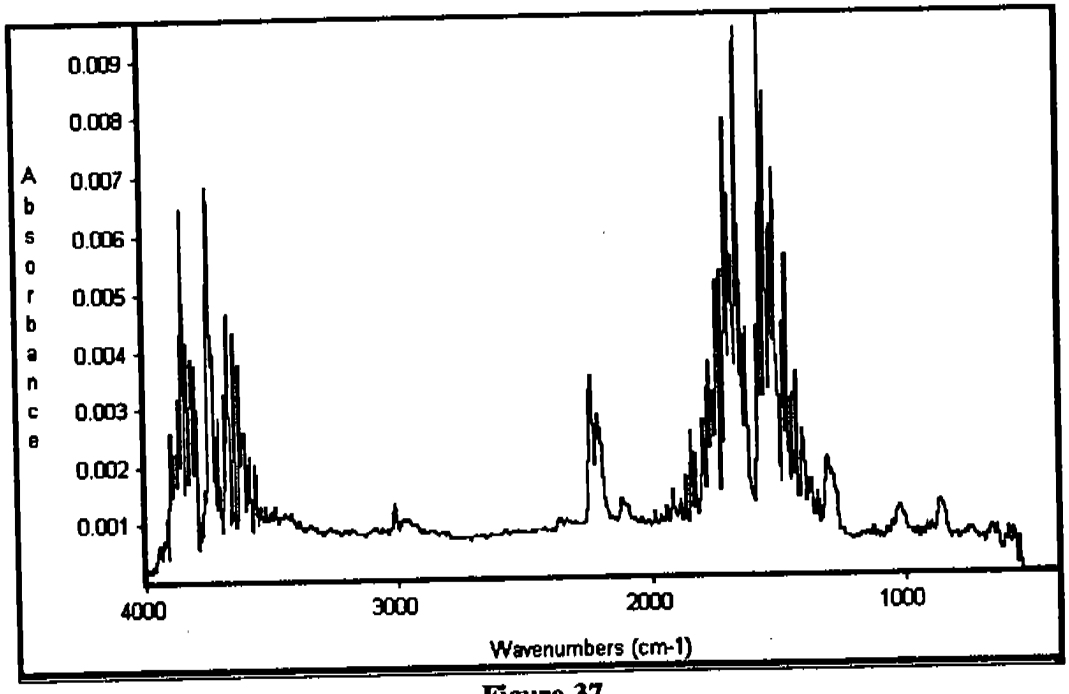

Figure 37
FTIR of TGA Effluent Gas from WSTF Laboratory-Synthesized FORP Batch 19, Very Early During Transition

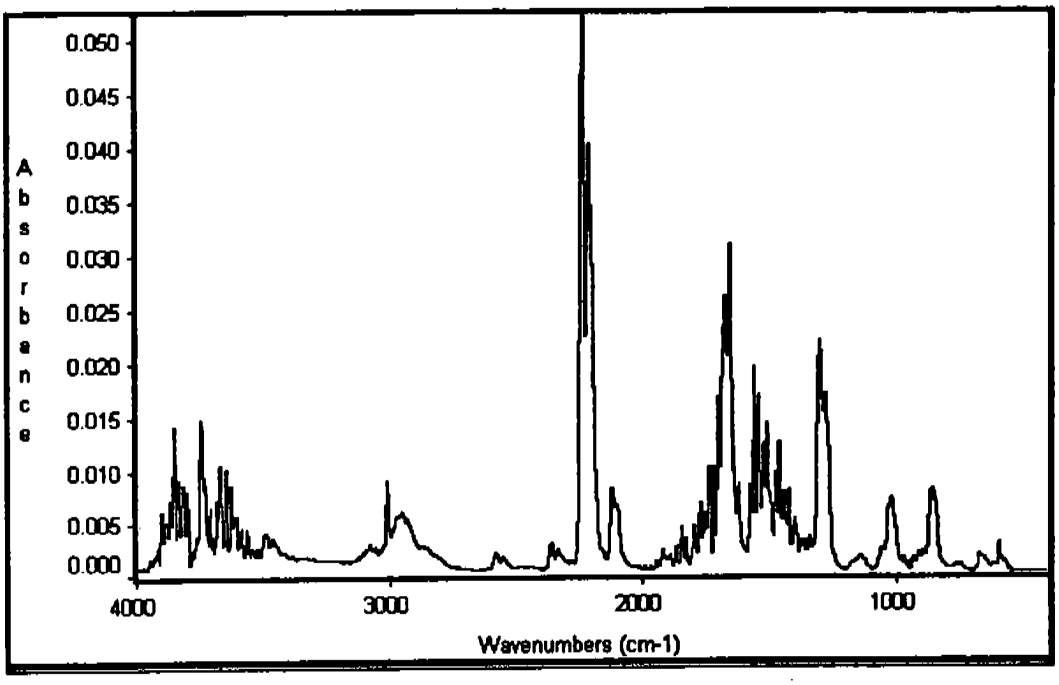

Figure 38
FTIR of TGA Effluent Gas from WSTF Laboratory-Synthesized FORP Batch 19, Early During Transition

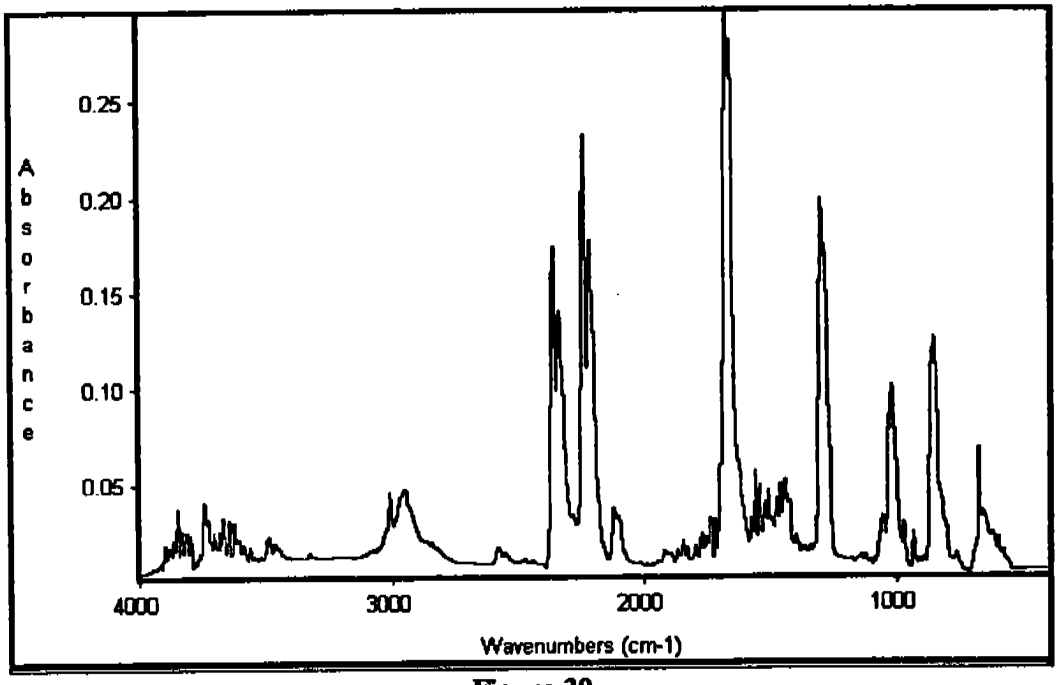

Figure 39
FTIR of TGA Effluent Gas from WSTF Laboratory-Synthesized FORP Batch 19, Before Peak of Transition

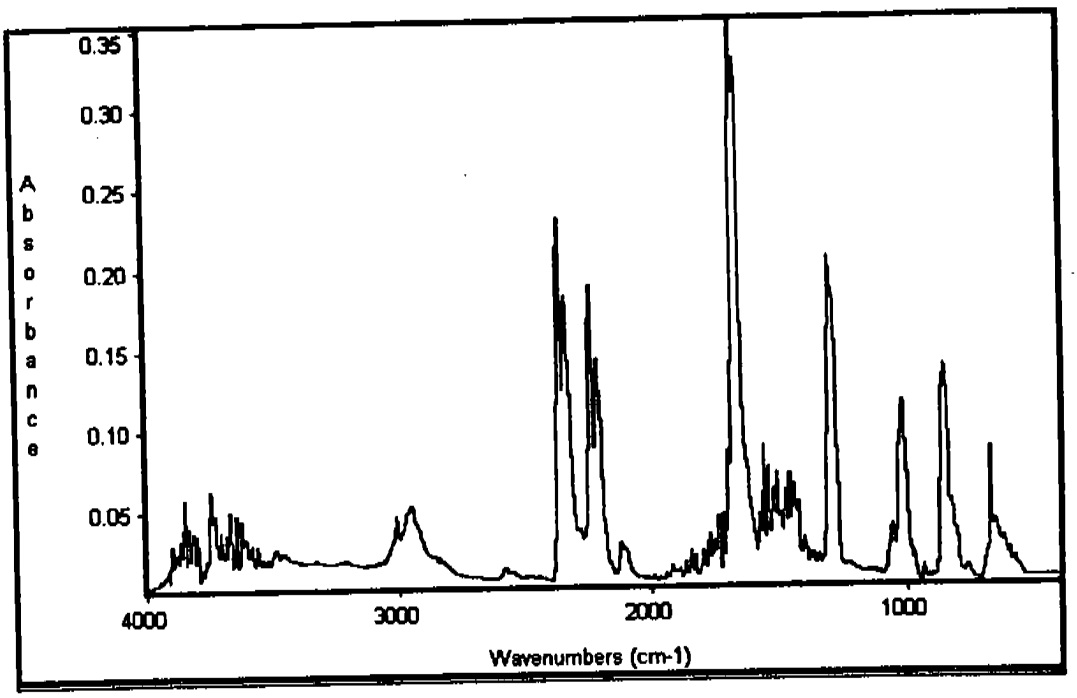

Figure 40
FTIR of TGA Effluent Gas from WSTF Laboratory-Synthesized FORP Batch 19, Slightly Before Peak of Transition

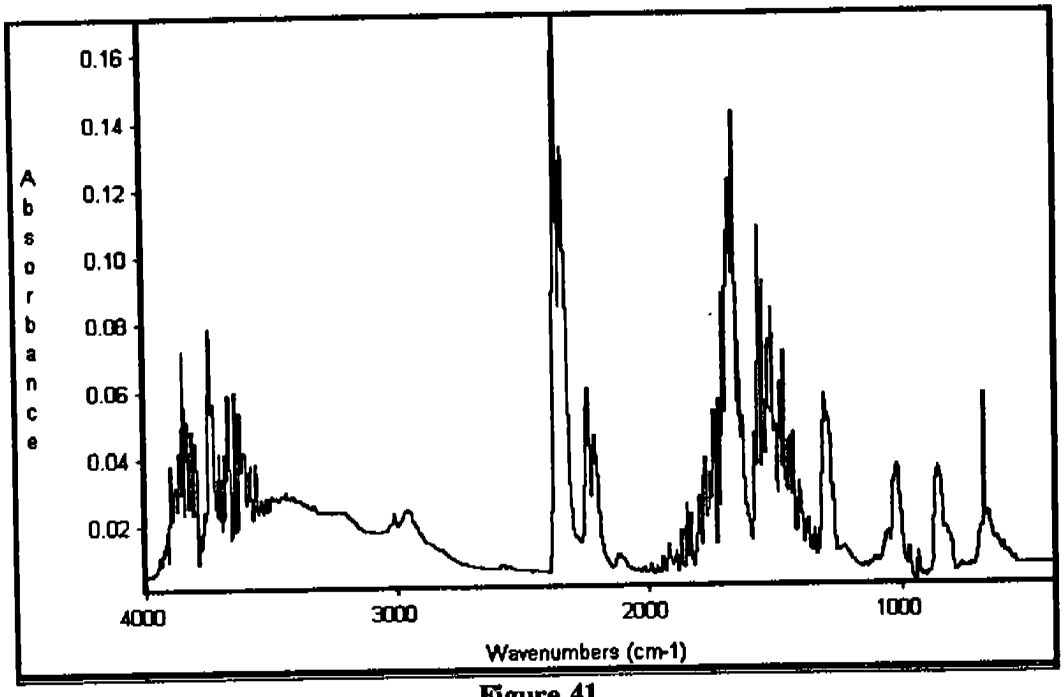

Figure 41
FTIR of TGA Effluent Gas from WSTF Laboratory-Synthesized FORP Batch 19, At Peak of Transition

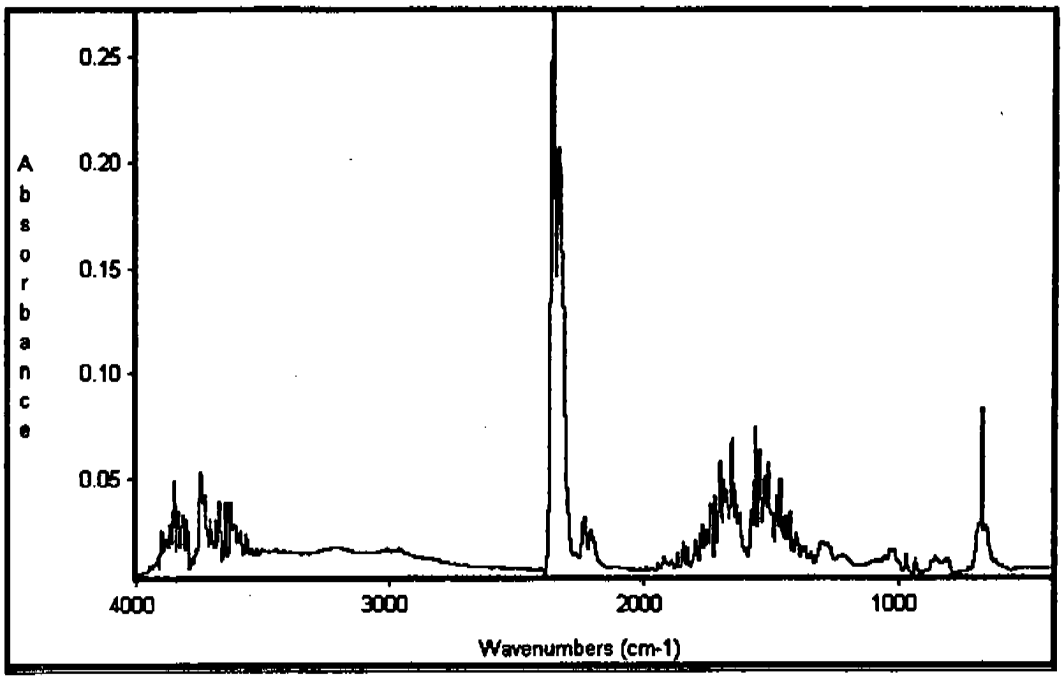

Figure 42
FTIR of TGA Effluent Gas from WSTF Laboratory-Synthesized FORP Batch 19, Near End of Transition

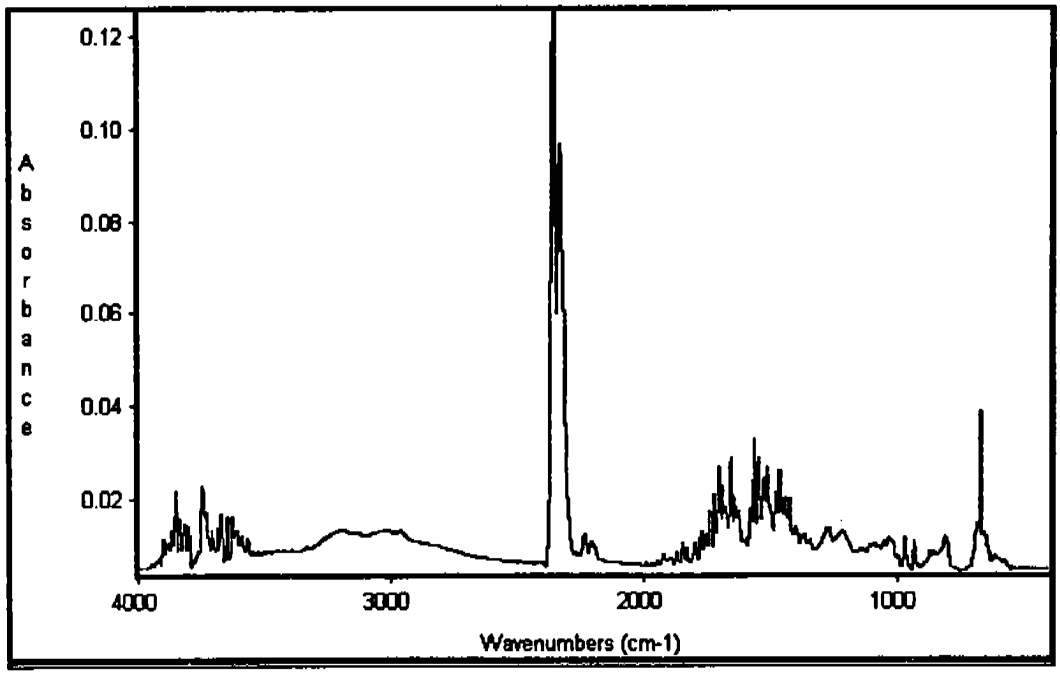

Figure 43
FTIR of TGA Effluent Gas from WSTF Laboratory-Synthesized FORP Batch 19, At End of Transition

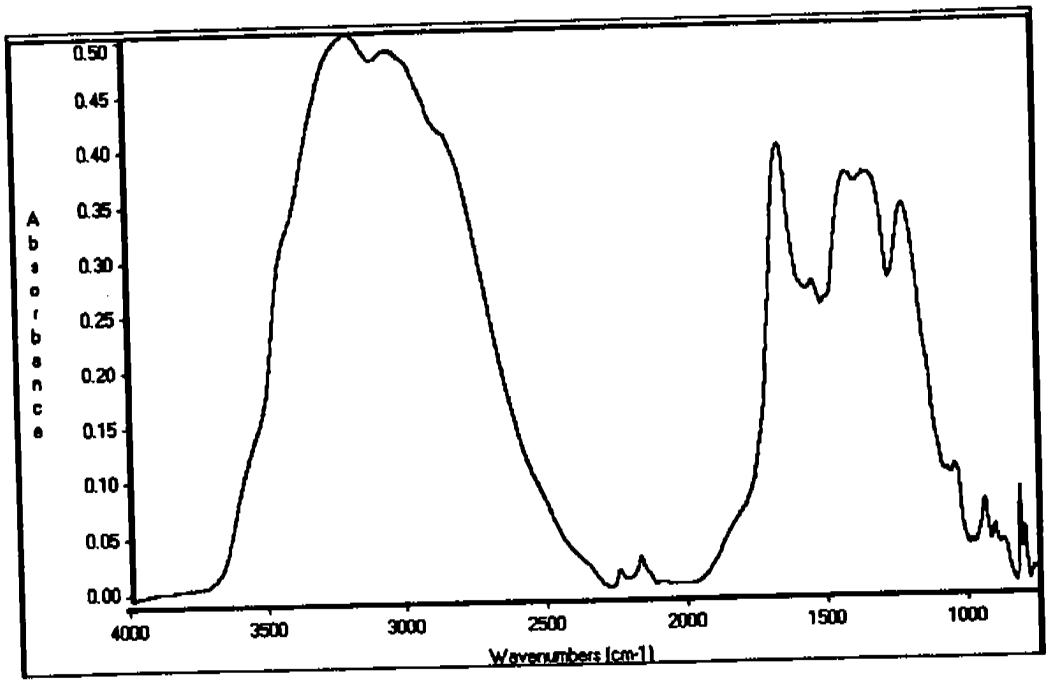

Figure 44
FTIR of Marquardt FORP, KM44

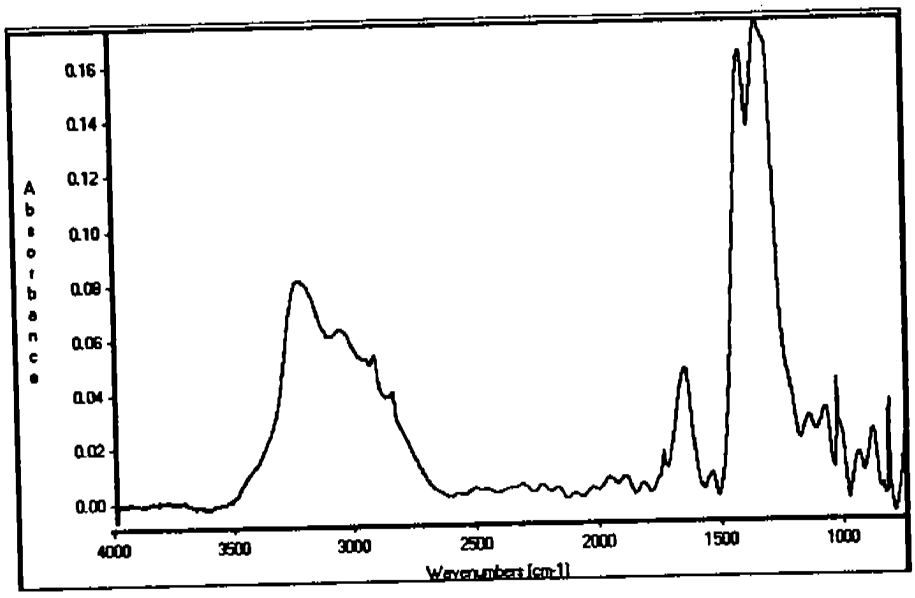

Figure 45
FTIR of Marquardt FORP, KM45

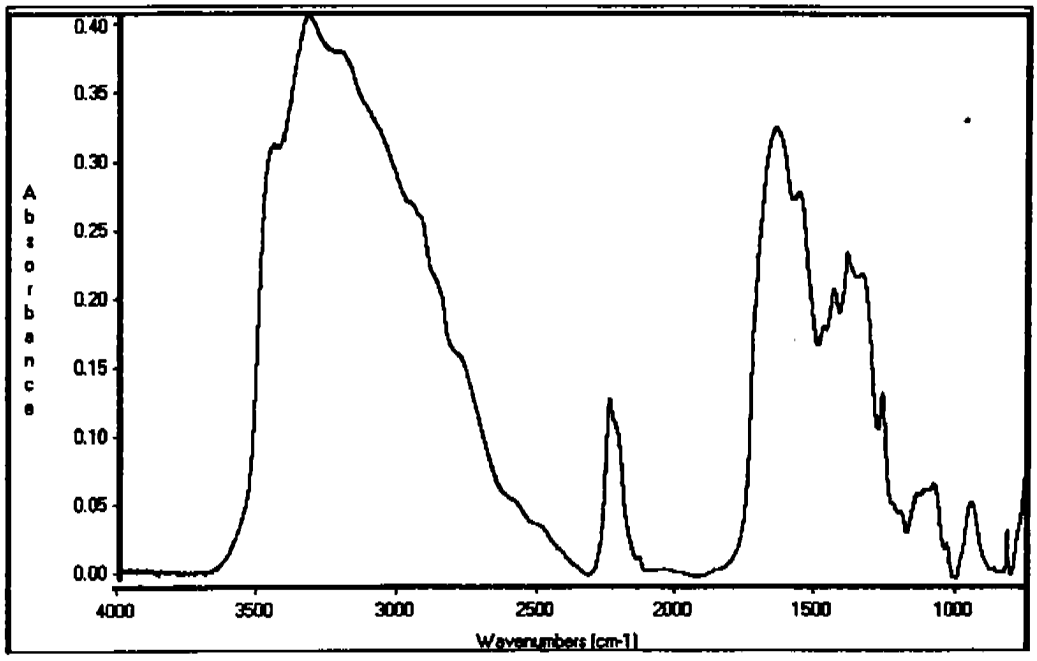

Figure 46
FTIR of Residue from Solvent Rinse of RCS S/N 467 P_c Tube, 10 msec Fuel Lead

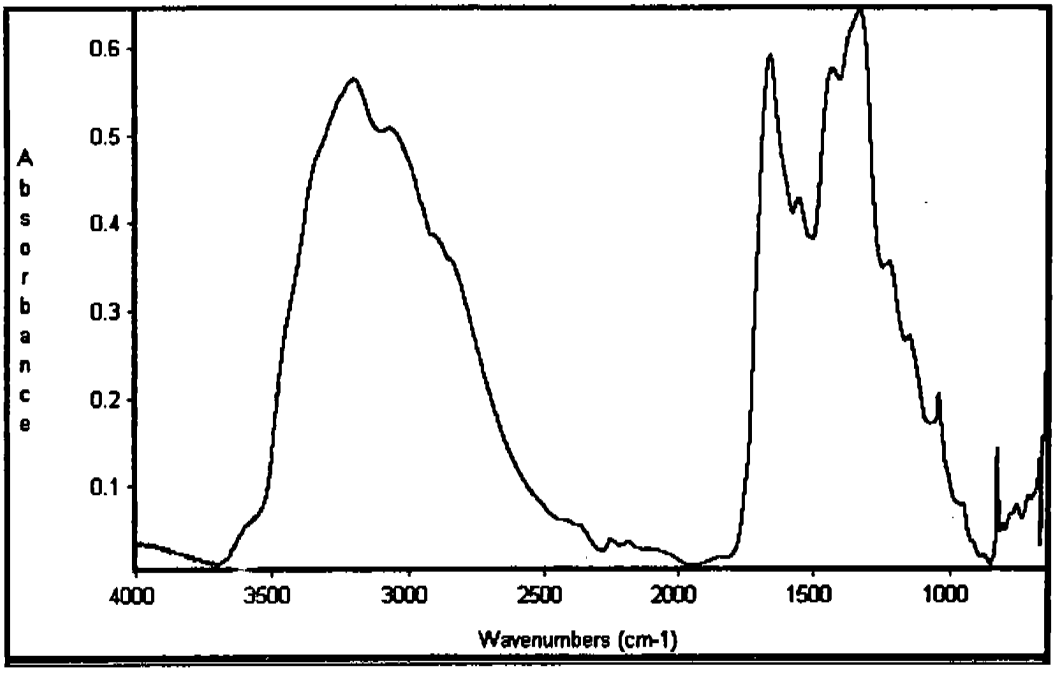

Figure 47
FTIR of Marquardt FORP, Batch 2

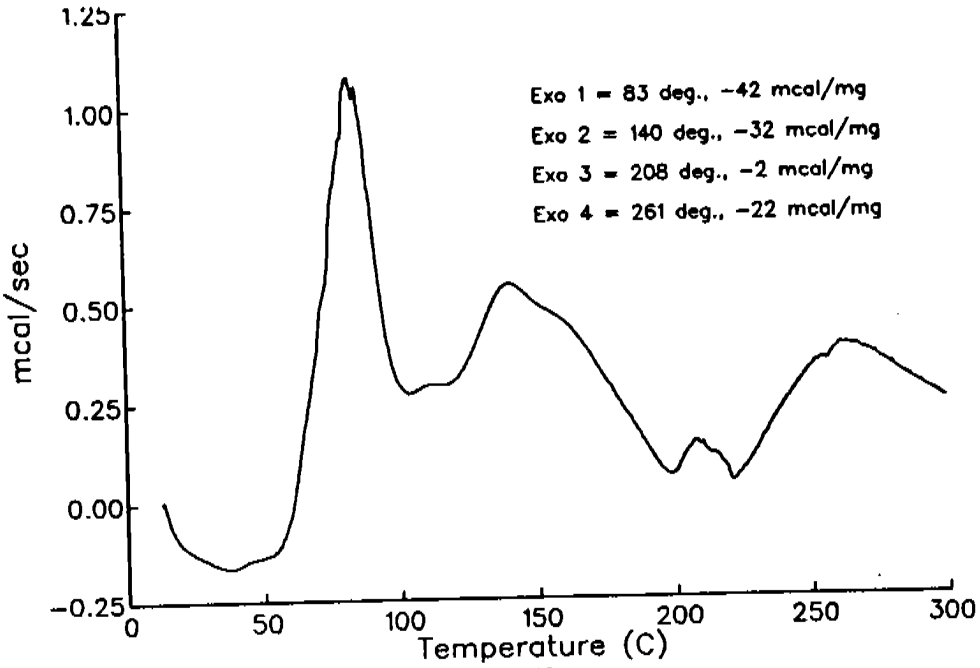

Figure 48
DSC of Marquardt FORP, Batch 1, KM44

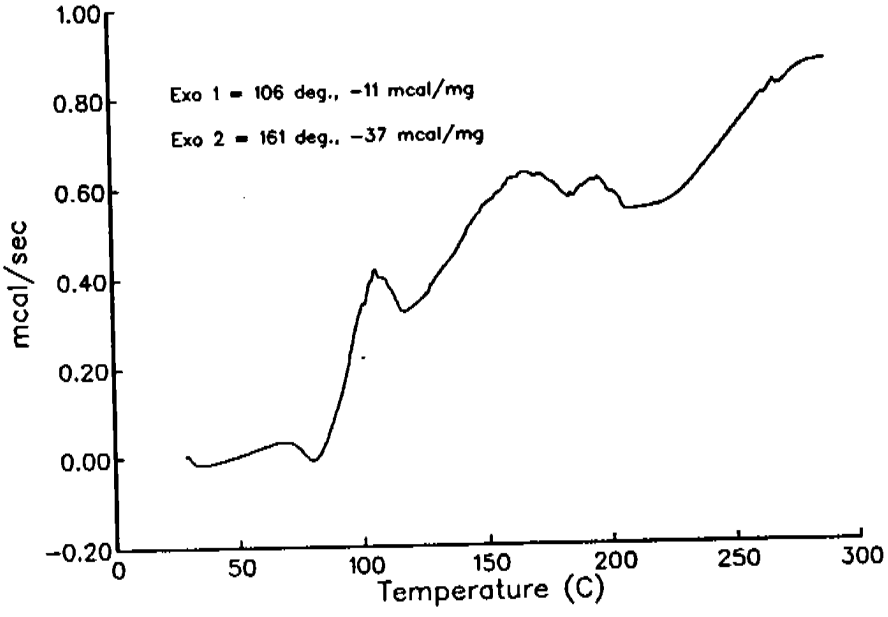

Figure 49
DSC of Marquardt FORP, KM47

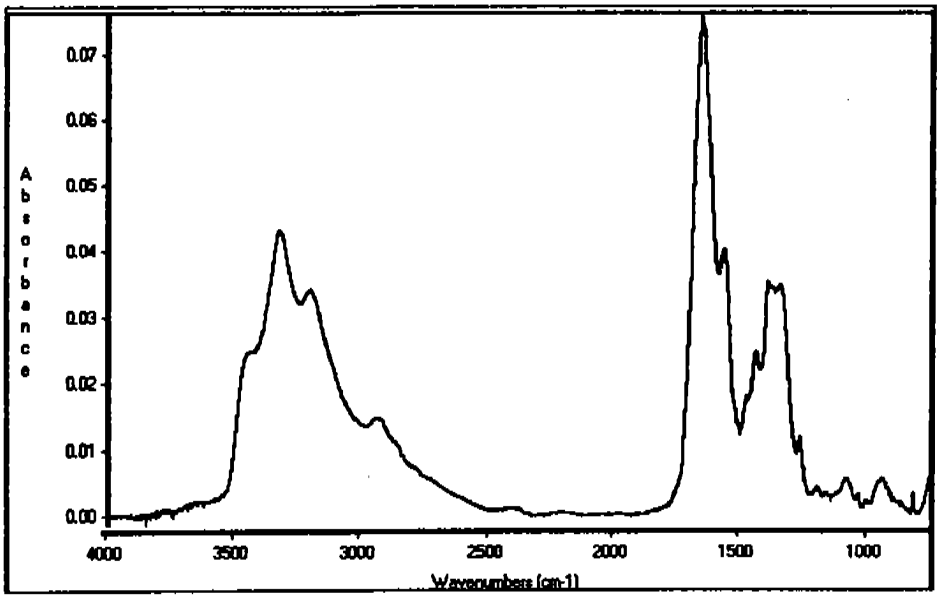

Figure 50
FTIR of Residue from Solvent Rinse of RCS S/N 208 P_e Tube

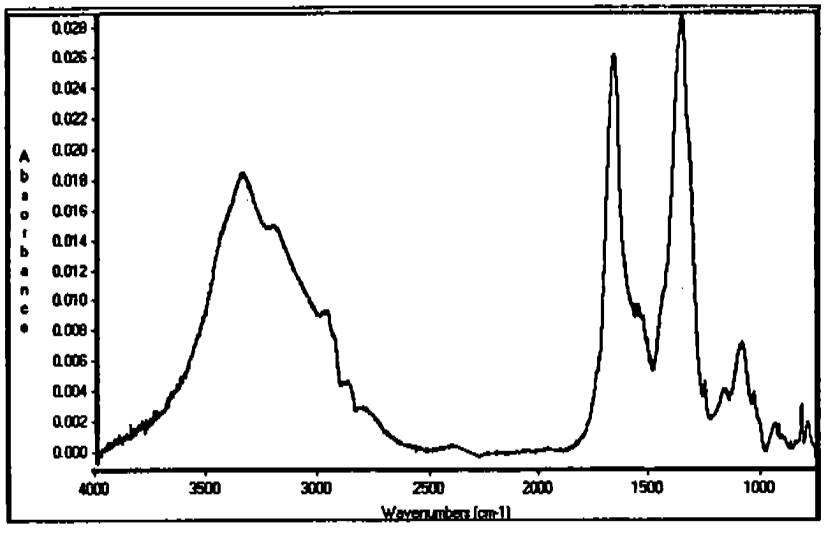

Figure 51
FTIR of Residue from Solvent Rinse of RCS S/N 413 P_e Tube

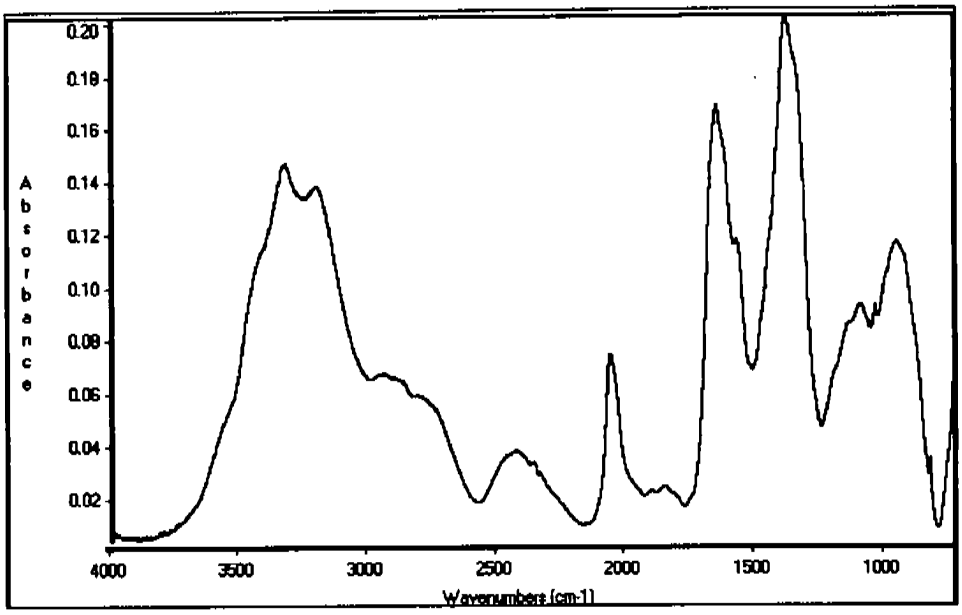

Figure 52
FTIR of Residue on External Surface of RCS S/N 208 P_c Tube

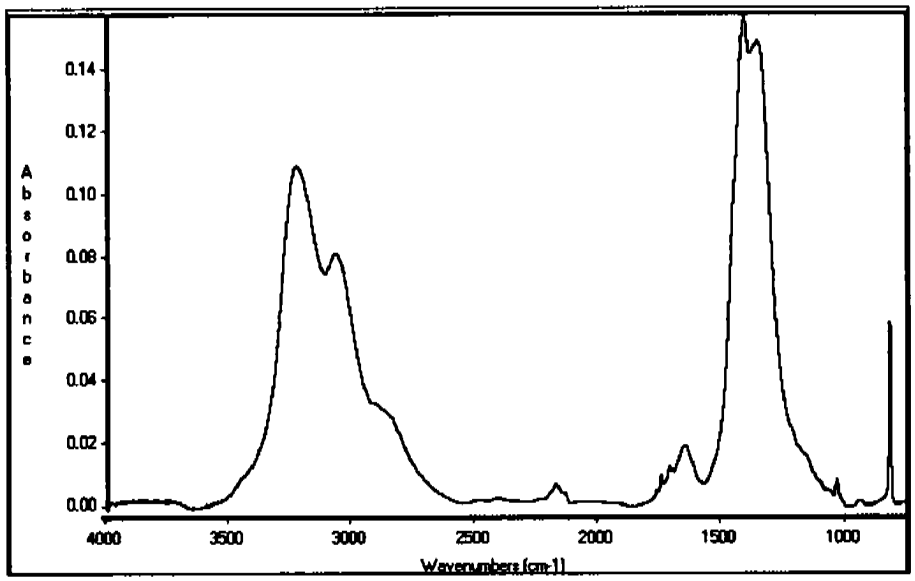

Figure 53
FTIR of Residue from Solvent Rinse of RCS S/N 467 P_c Tube,
10 msec Oxidizer Lead

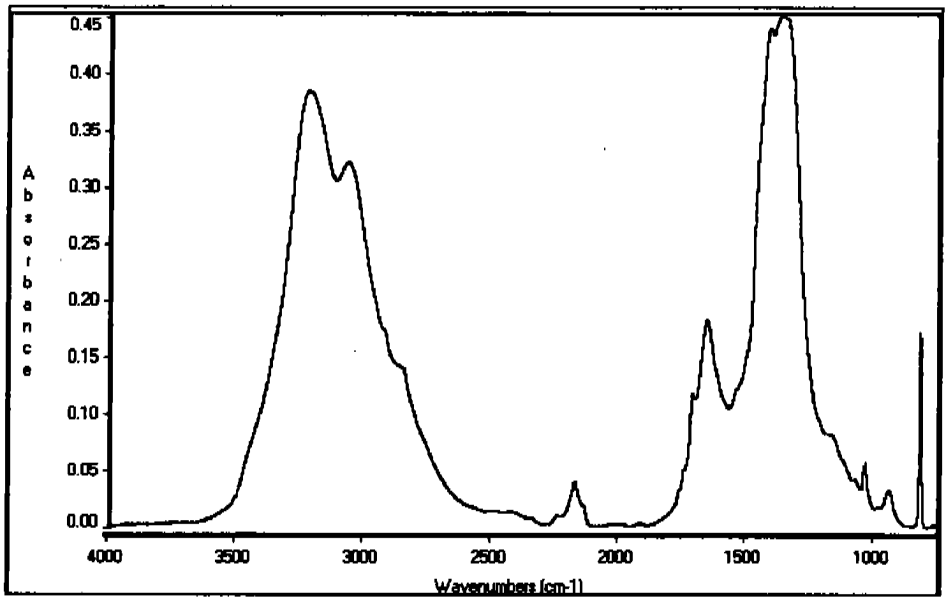

Figure 54
FTIR of Residue from Solvent Rinse of RCS S/N 467 P_c Tube,
5 msec Oxidizer Lead

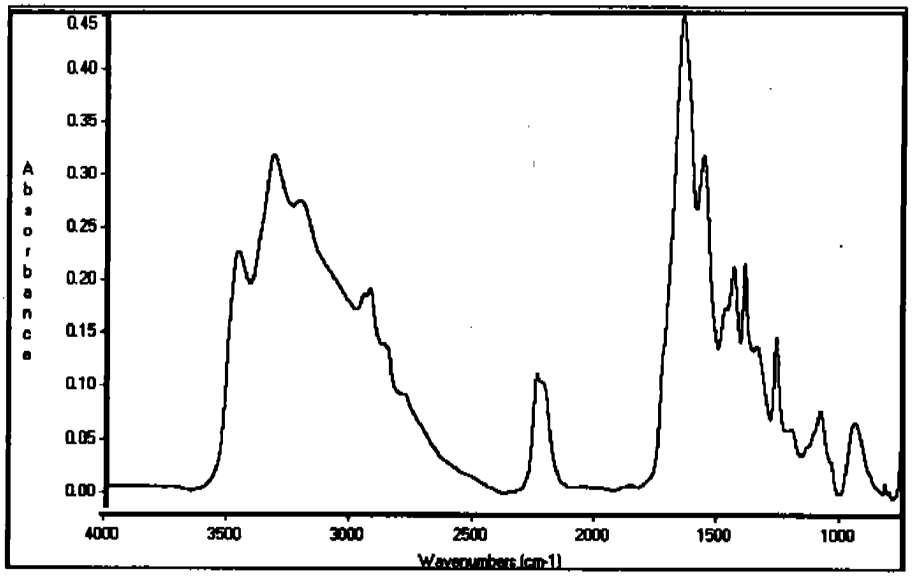

Figure 55
FTIR of Residue from Solvent Rinse of RCS S/N 467 P_c Tube, 5 msec Fuel Lead

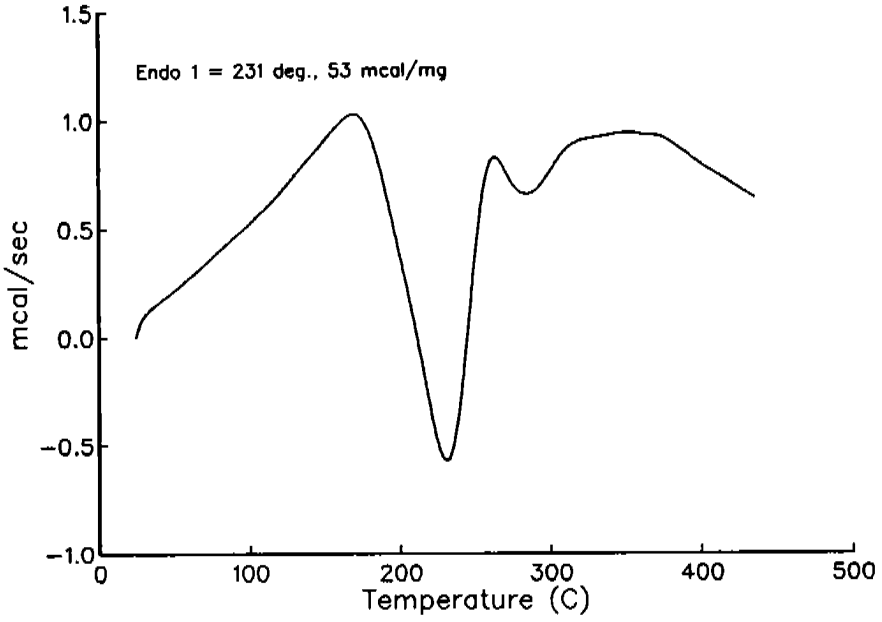

Figure 56
DSC of Residue from Solvent Rinse of RCS S/N 467 P_c Tube,
10 msec Fuel Lead, No NTO Exposure

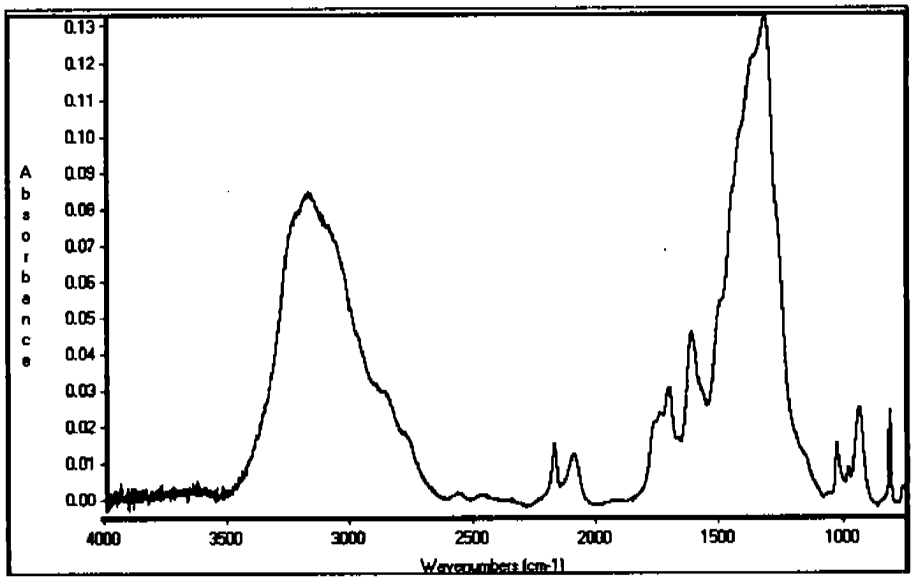

Figure 57
FTIR of Residue from Solvent Rinse of RCS S/N 467 P_c Tube, 10 msec Fuel Lead,
After Exposure to Gaseous NTO

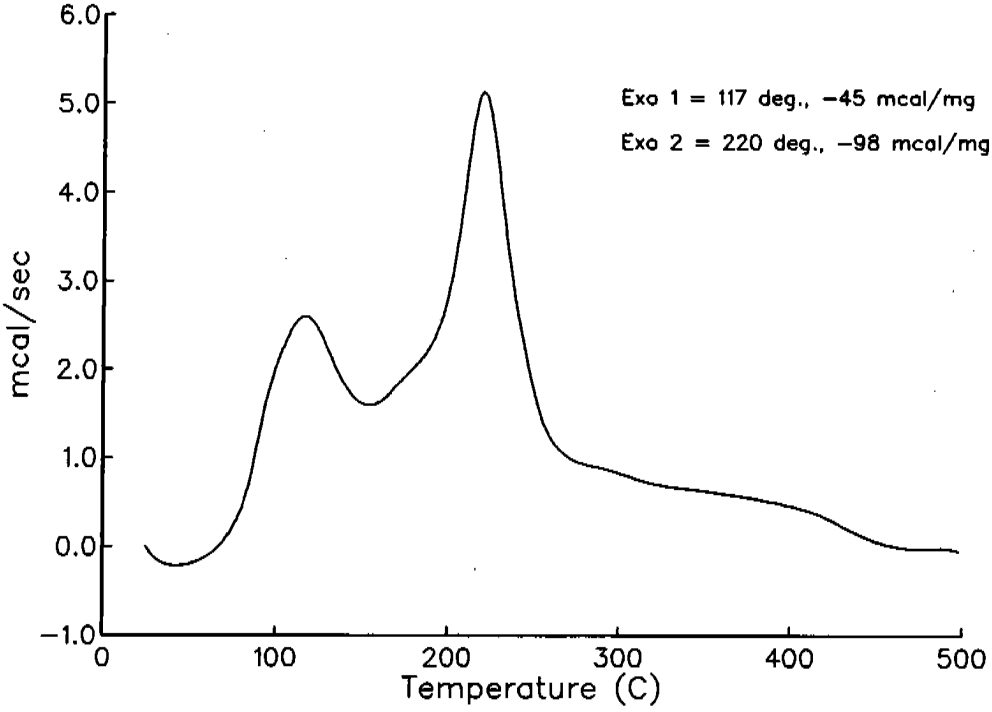

Figure 58
DSC of Residue from Solvent Rinse of RCS S/N 467 P_c Tube, 10 msec Fuel Lead, After Exposure to Gaseous NTO

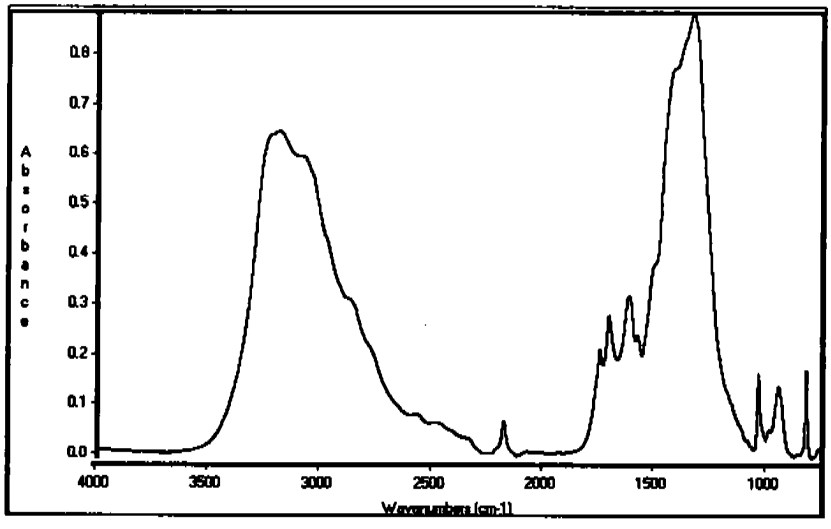

Figure 59
FTIR of Residue from Solvent Rinse of RCS S/N 467 P_c Tube, 10 msec Fuel Lead, After Exposure to Liquid NTO

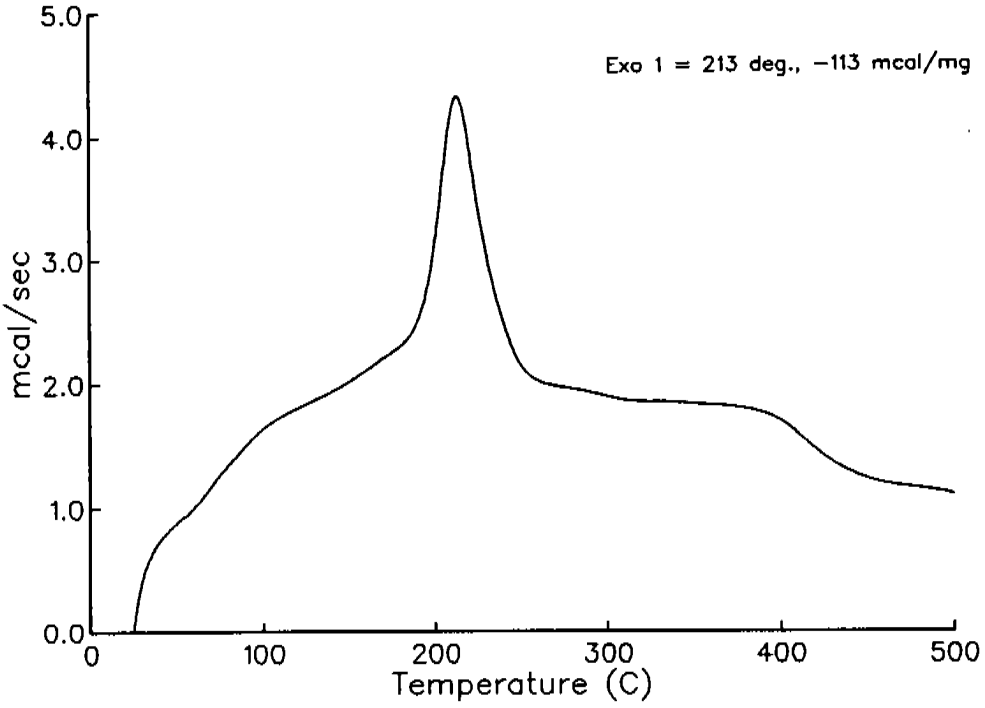

Figure 60
DSC of Residue from Solvent Rinse of RCS S/N 467 P_c Tube, 10 msec Fuel Lead, After Exposure to Liquid NTO

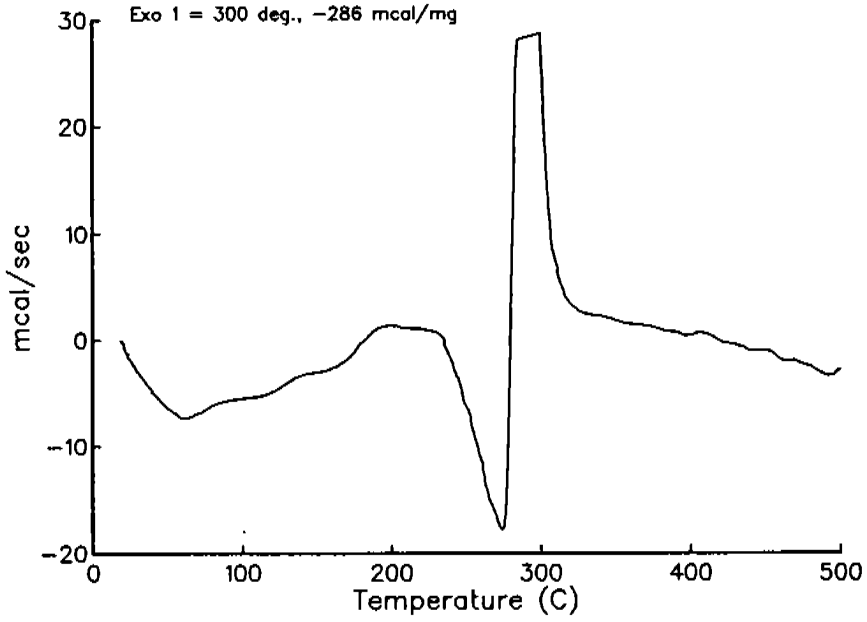

Figure 61
DSC of WSTF Laboratory-Synthesized FORP Batch 19

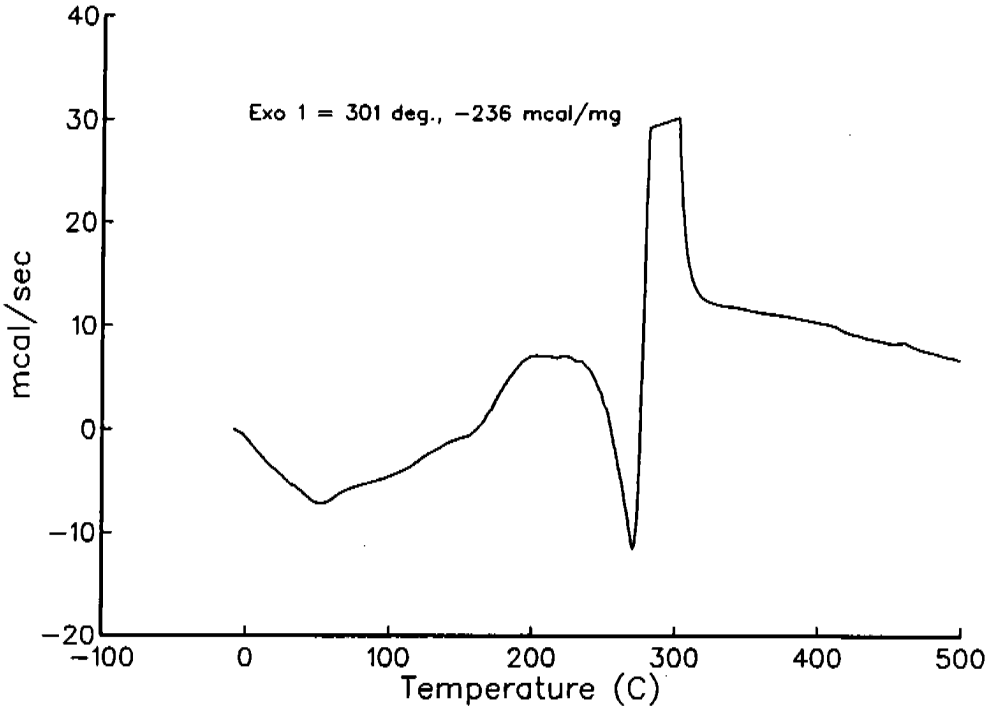

Figure 62
DSC of WSTF Laboratory-Synthesized FORP Batch 19' Containing 17% Titanium Powder

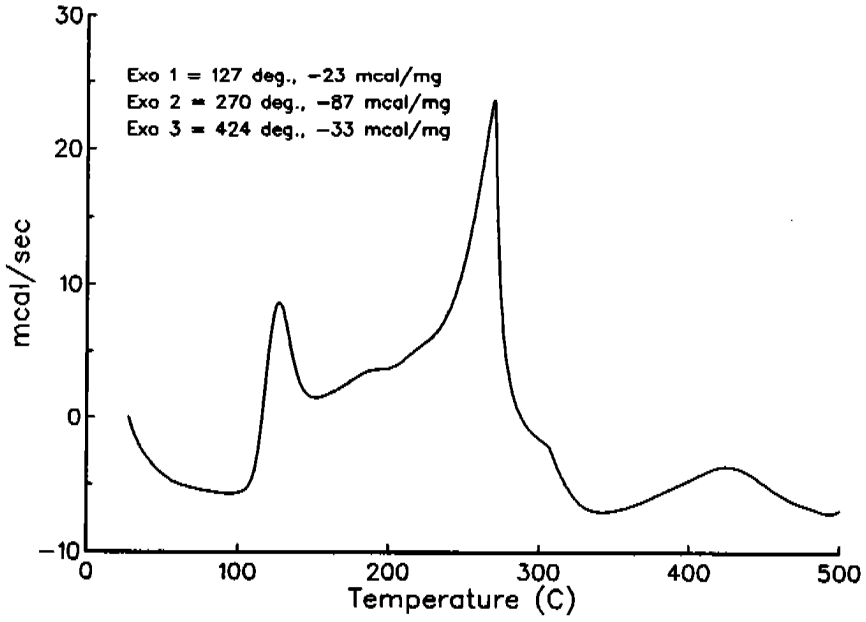

Figure 63
DSC of WSTF Laboratory-Synthesized FORP Batch 5 Treated with HNO_3 and Containing 4% Fe_2O_3

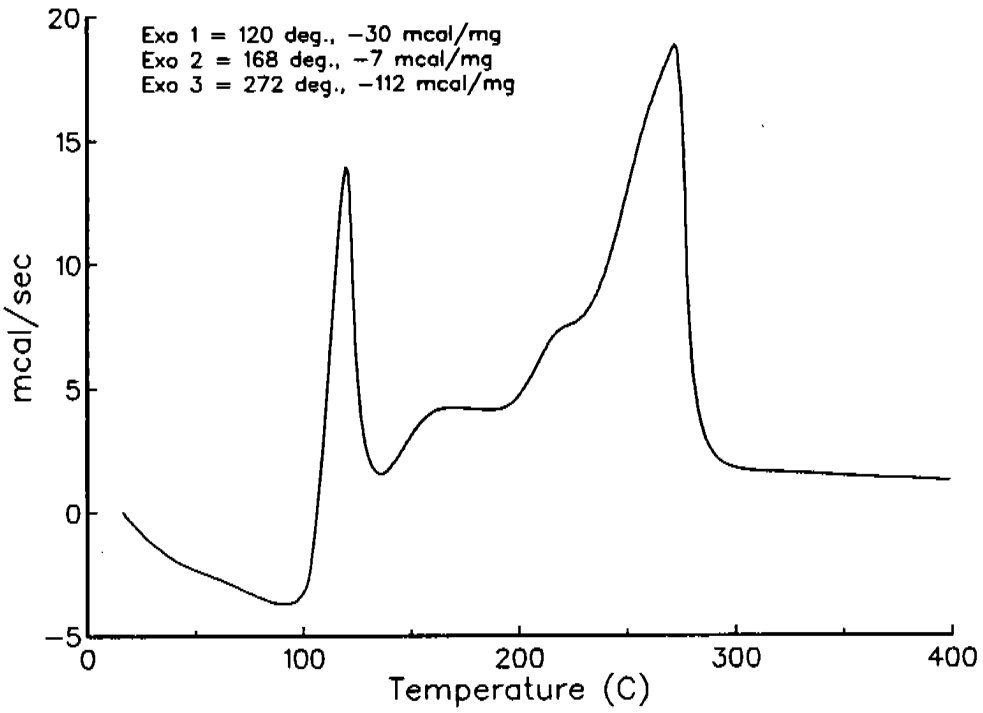

Figure 64
DSC of WSTF Laboratory-Synthesized FORP Combined Batches 578 Treated with HNO_3

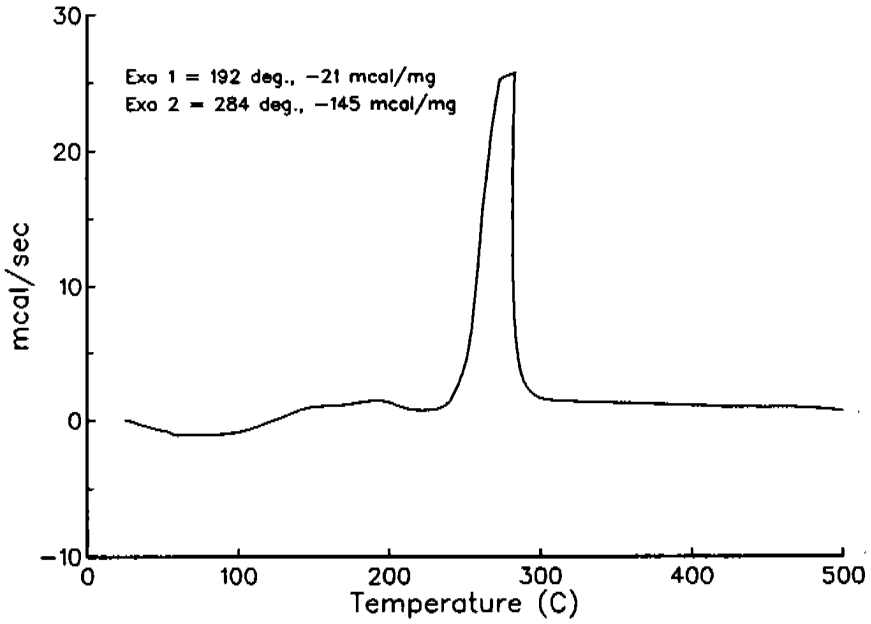

Figure 65
DSC of WSTF Laboratory-Synthesized FORP Combined Batches 578, Neat

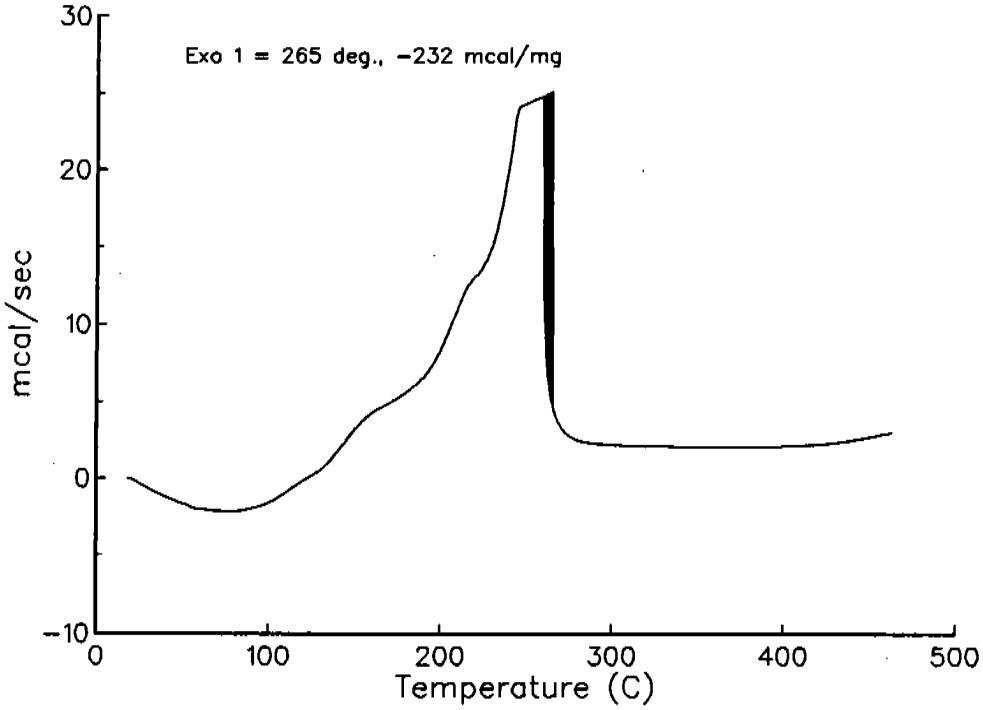

Figure 66
DSC of WSTF Laboratory-Synthesized FORP Combined Batches 578 Treated with HNO_3 and Containing 36% Inconel® 718 Filings

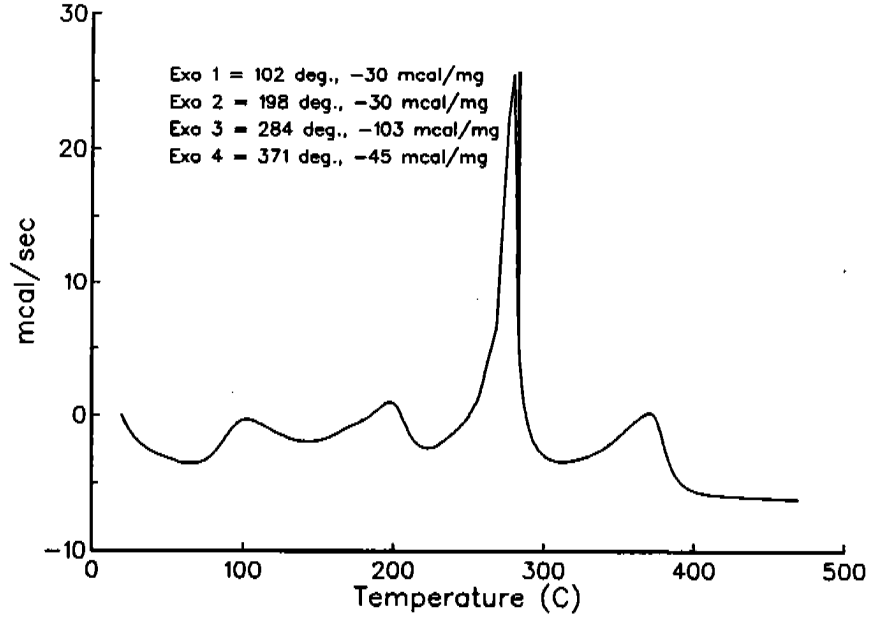

Figure 67
DSC of WSTF Laboratory-Synthesized FORP Combined Batches 578 Treated with HNO_3 and Containing 28% Nickel Powder

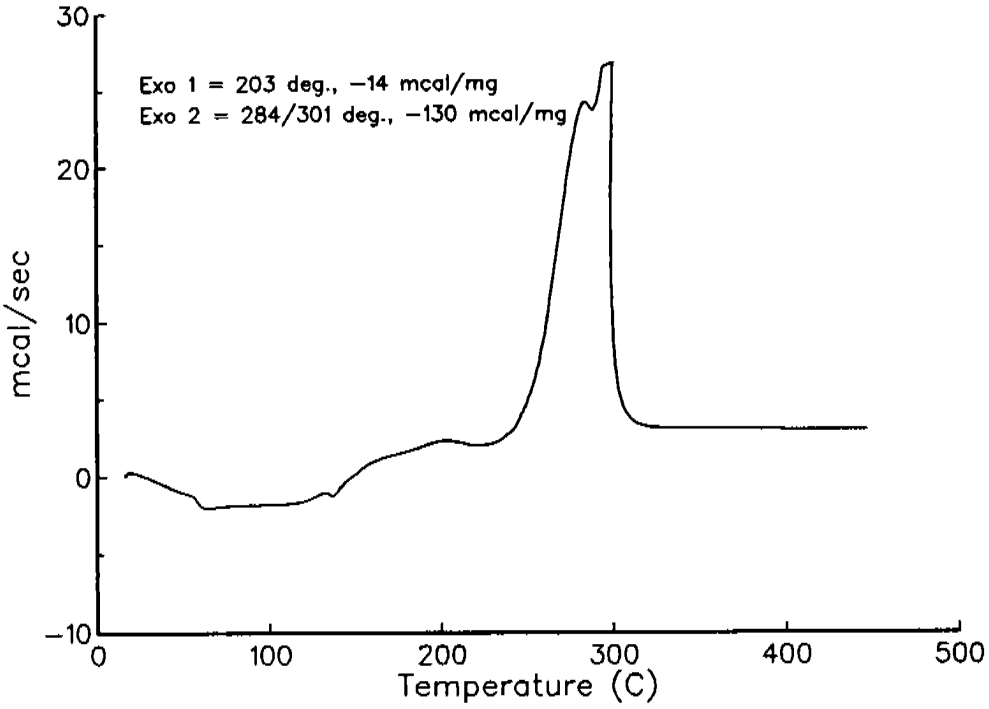

Figure 68
DSC of WSTF Laboratory-Synthesized FORP Combined Batches 578, Neat with 34% NH_4NO_3

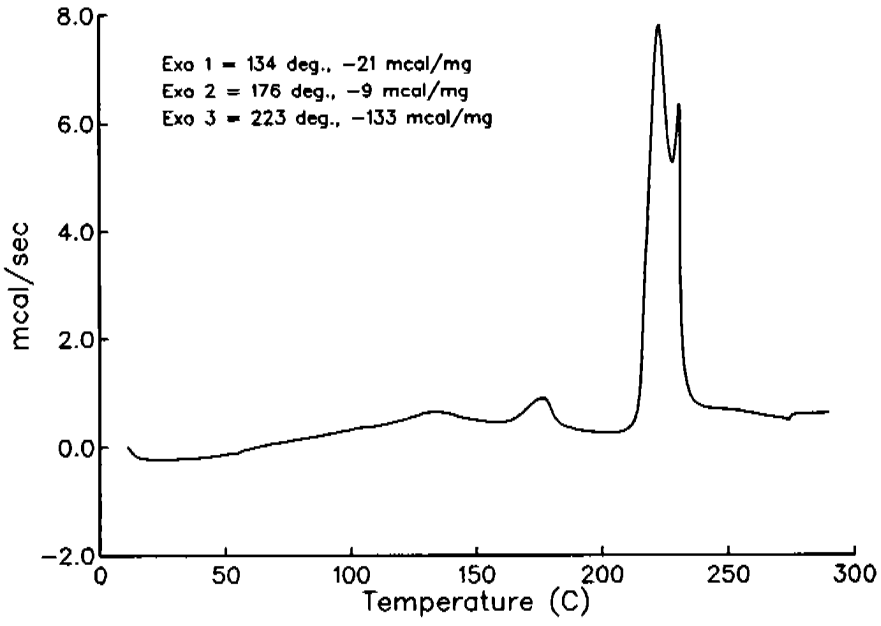

Figure 69
DSC of WSTF Laboratory-Synthesized FORP Batch 7, Neat with 21% $NaNO_2$

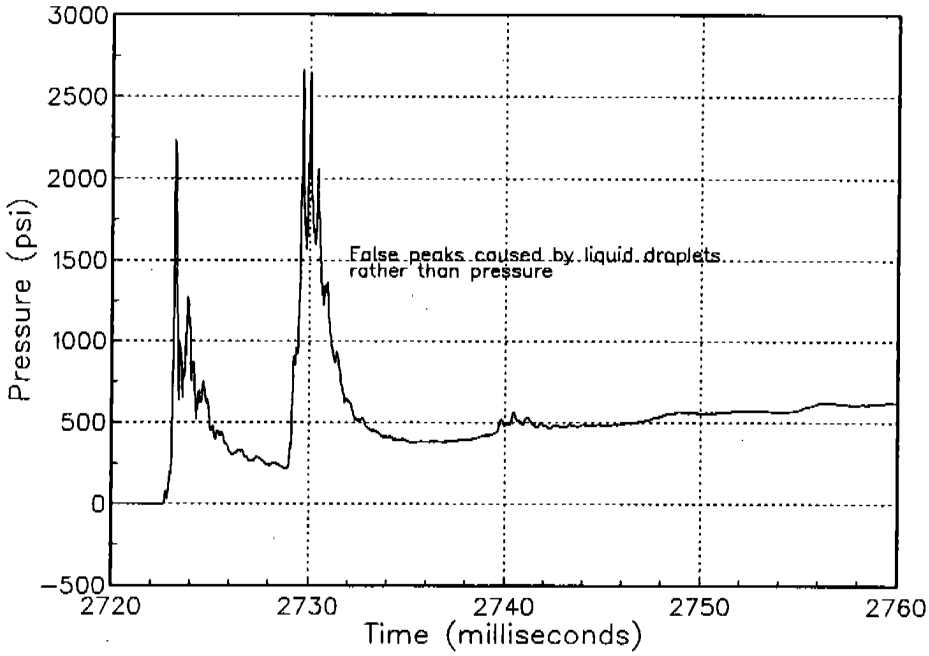

Figure 70
PCB Pressure Trace for Test 1

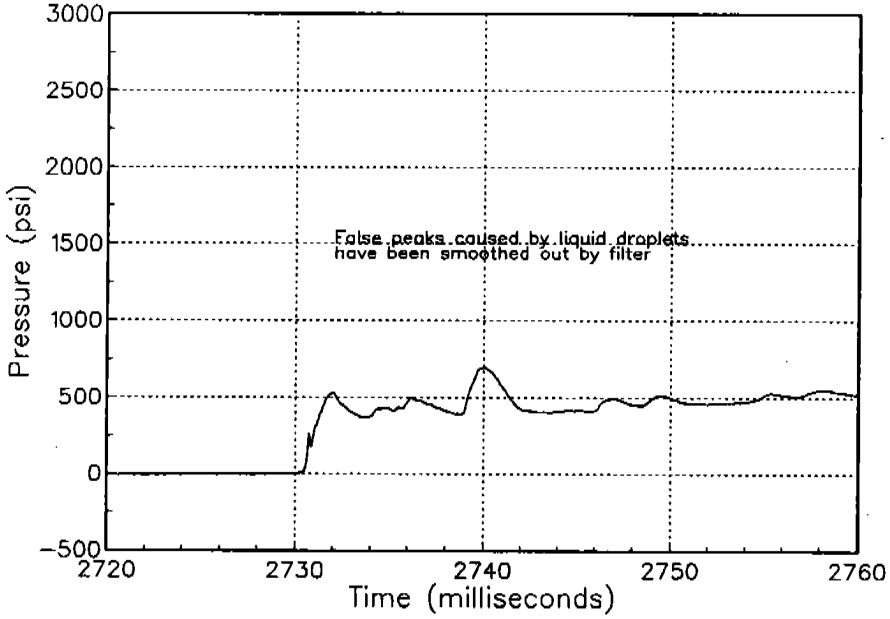

Figure 71
PCB Pressure Trace for Test 2

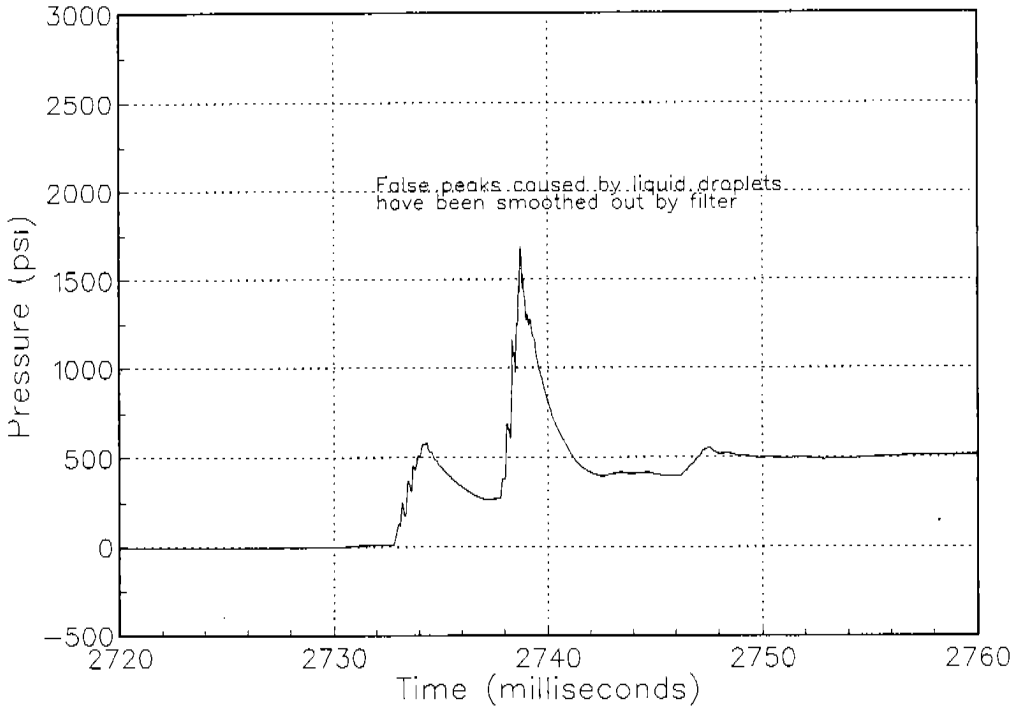

Figure 72
PCB Pressure Trace for Test 3

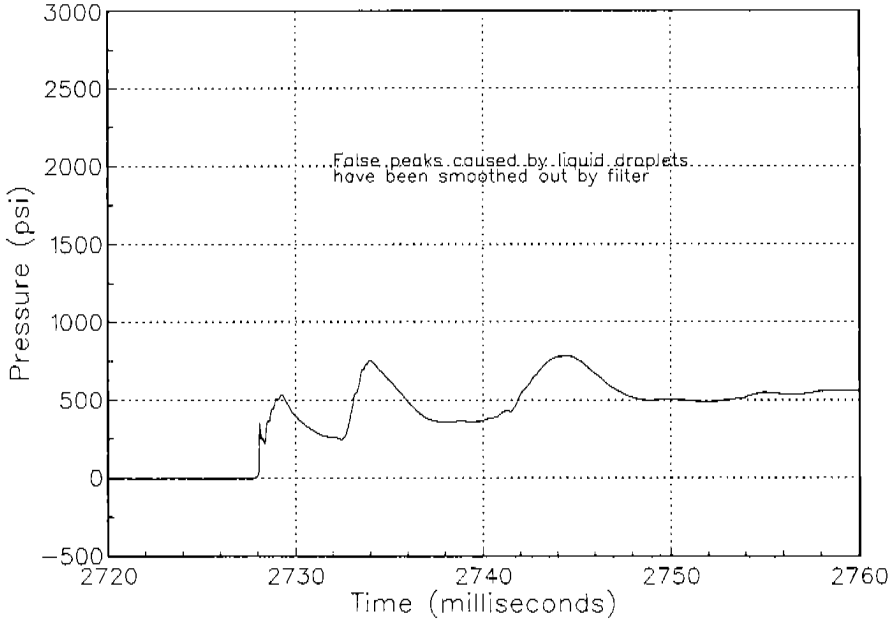

Figure 73
PCB Pressure Trace for Test 4

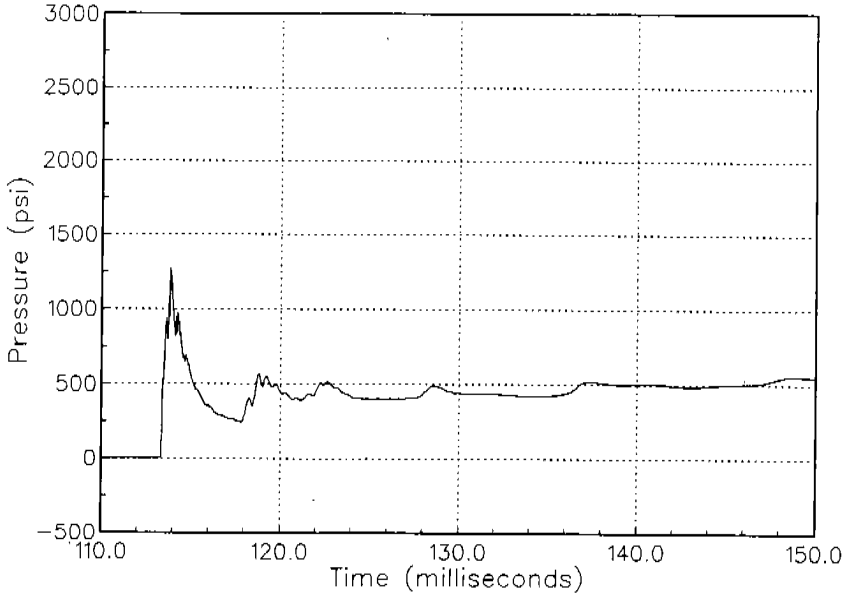

Figure 74
PCB Pressure Trace for Test 7

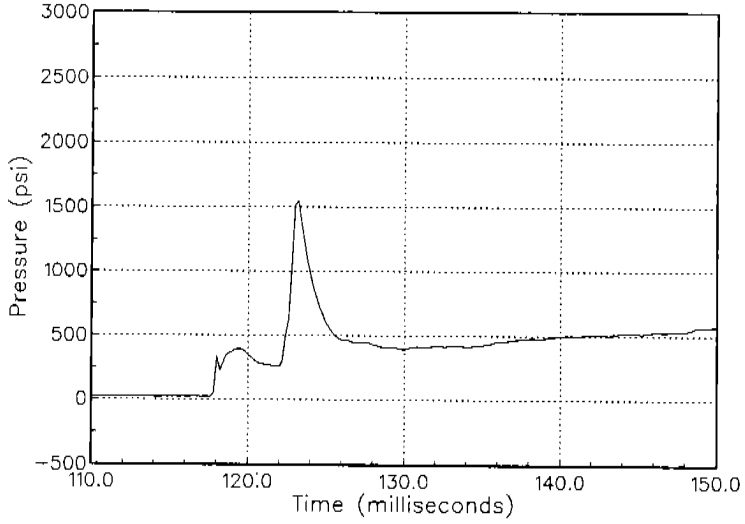

Figure 75
PCB Pressure Trace for Test 8

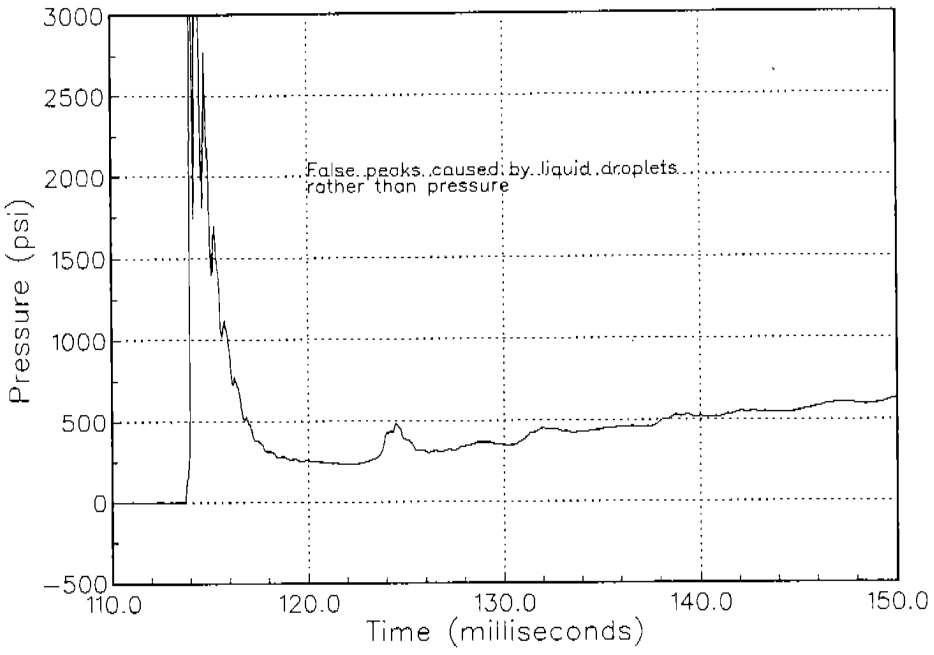

Figure 76
PCB Pressure Trace for Test 11

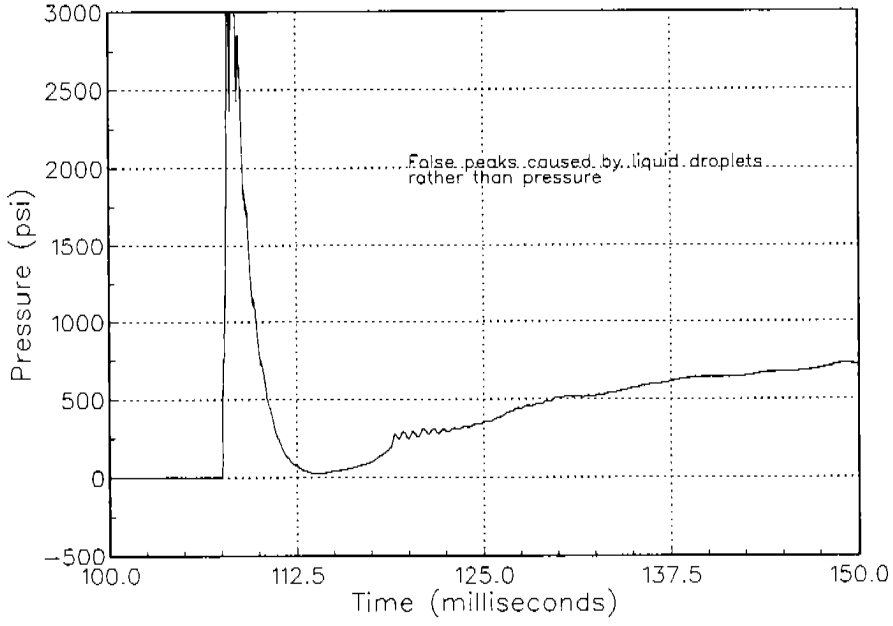

Figure 77
PCB Pressure Trace for Test 12

Figure 78
Reaction System PCB Pressure Transducer Face, Test 11

Figure 79
Reaction System Adapter, Test 11

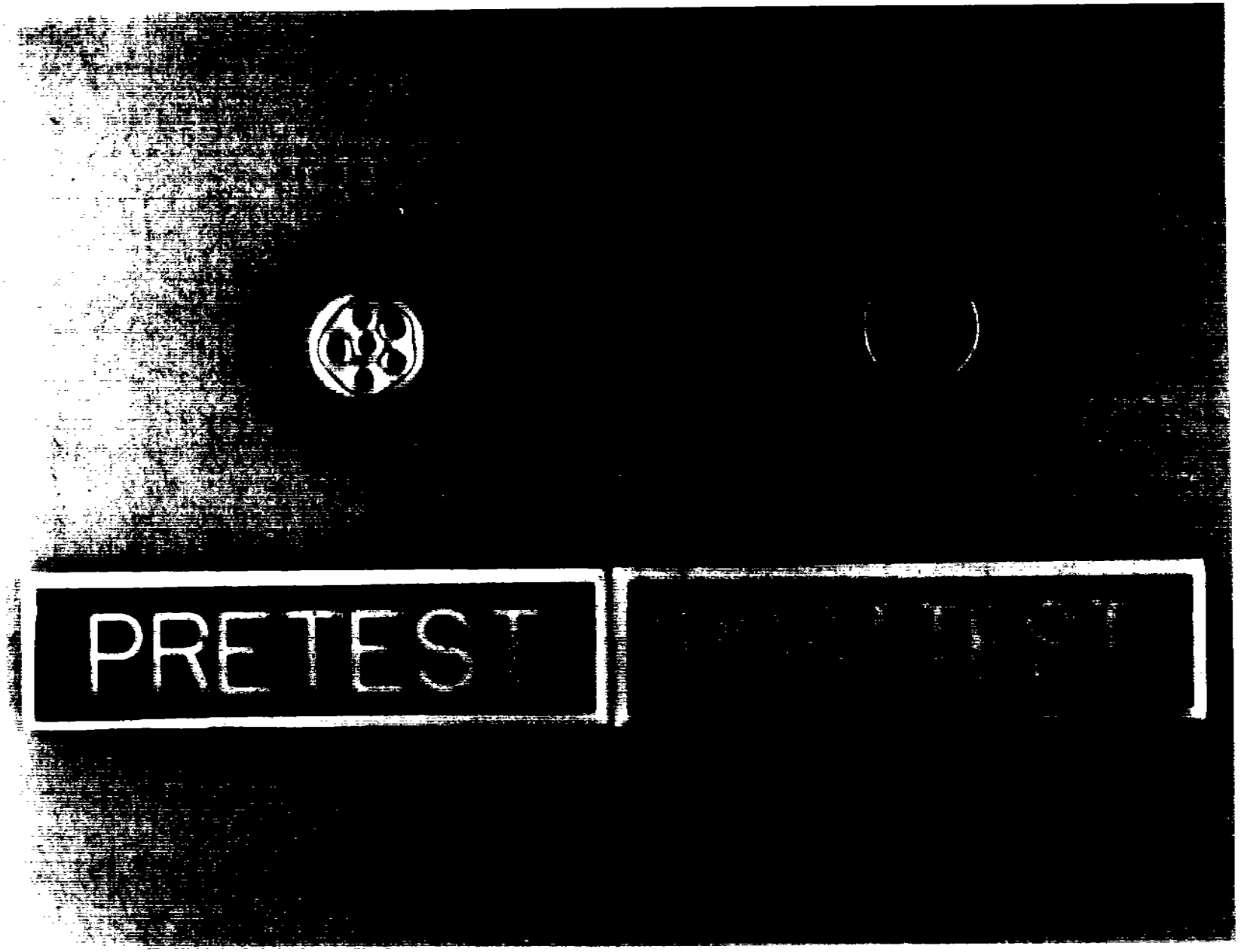

Figure 80
Reaction System Filter, Test 11

Figure 81
Reaction System PCB Pressure Transducer Face, Test 12

Figure 82
Reaction System Filter, Test 12

Figure 83
Reaction System Filter, Test 14

Figure 84
Reaction System Filter, Test 16

References

ASTM D2512-82. *Standard Test Method for Compatibility of Materials with Liquid Oxygen.* Vol. 15.03. Philadelphia, PA: American Society for Testing Materials, 1991.

Harris, G. (ed.). *Dictionary of Organic Compounds*. Fourth Edition, New York, NY: Oxford University Press, 1965.

Lawton, E. A. and C. M. Moran. "Methylhydrazinium Nitrate." *J. Chem. Eng. Data*, Vol. 29 (1984): pp. 357-58.

Miron, Y. and H. Perlee. *Hard Start Phenomena in Hypergolic Engines, Volume II.* Combustion Characteristics of Propellants and Propellant Combinations, Interim Report No. 1646, Bureau of Mines, Pittsburgh, PA, Mar. 22, 1974a.

Miron, Y., and H. Perlee. *Hard Start Phenomena in Hypergolic Engines, Volume IV.* The Chemistry of Hydrazine Fuels and Nitrogen Tetroxide Propellant Systems, Interim Report No. 1646, Bureau of Mines, Pittsburgh, PA, Mar. 22, 1974b.

Purlee, H., Y. Miron, H. James, and T. Christos. *Hypergolic Ignition and Combustion Phenomena in the Propellant System Aerozine-50/N_2O4.* Final Report No. 4019, Bureau of Mines, Pittsburgh, PA, Apr. 1, 1965 to Mar. 31, 1967.

Saad, M. A., M. B. Detweiler, and M. A. Sweeney. "Analysis of Reaction Products of Nitrogen Tetroxide with Hydrazines under Nonignition Conditions." *AIAA Journal*, Vol. 10, No. 8 (Aug. 1972): pp. 1073-78.

Takimoto, H. H. and G. C. Denault. *Combustion Residues from N_2O_4 - MMH Motors.* Aerospace Report No. TR-0066 (5210-10)-1, Air Force Report No. SAMSO-TR-69-373, Aerospace Corporation, El Segundo, CA, Sept. 15, 1969.

Tanner, P. *Vapor-Phase Reaction of Hydrazine or Monomethylhydrazine with MON-3 Nitrogen Tetroxide.* TR-600-001, NASA Johnson Space Center White Sands Test Facility, Las Cruces, NM, Oct. 6, 1989.

Acknowledgements

Of the many people who participated in this work, special acknowledgement is made to David L. Baker, Wade D. Bannister, Harold D. Beeson, Rafael H. Delgado, William A. Haney, Thomas P. Martinez, Mark B. McClure, and Keith D. Webb.